Title
Surveillance and Defense Mechanisms in Microbes

Author
Osuna, Beatriz Adriana

Publication Date
2019

Peer reviewed|Thesis/dissertation

Surveillance and Defense Mechanisms in Microbes

by
Beatriz Osuna

DISSERTATION
Submitted in partial satisfaction of the requirements for degree of
DOCTOR OF PHILOSOPHY

in

Biochemistry and Molecular Biology

in the

GRADUATE DIVISION
of the
UNIVERSITY OF CALIFORNIA, SAN FRANCISCO

Approved:

DocuSigned by:
Joseph Bondy-Denomy
D23522498F4247C...

Joseph Bondy-Denomy
Chair

DocuSigned by:
David Morgan
DocuSigned by:

David Morgan

DocuSigned by:

Seemay Chou

DocuSigned by:
Alexander Johnson
E2BBE6A63C2745B...

Alexander Johnson

Committee Members

Dedicated to Ali and Samir

ACKNOWLEDGEMENTS

When I embarked on this journey, I thought that science would pose the greatest challenges I'd ever encounter. Looking back, I'm proud to say that overcoming scientific challenges has actually been the most enjoyable and rewarding aspect of this journey. I am so grateful to be at this point now—a scientist through and through, confident that I can approach any scientific problem and enjoy the process of finding a solution. Much to my surprise, non-science obstacles were actually the most difficult. Nonetheless, even the non-science problems I couldn't troubleshoot helped me grow as a scientist and overall human. I'm beyond grateful to the incredible people that were there for me during this rollercoaster of an experience.

Thank you to my best friend, partner, and colleague: Jonathan Asfaha. I'm so lucky that we've gone through grad school together. You've always been my biggest source of support. You always see the best in me. You always enthusiastically talk through data and experiments with me. You always wholeheartedly and sincerely celebrate my wins and you always hype me up when I'm discouraged by the L's. Thank you for everything—I can't even begin to imagine what grad school would have been like without you.

Thank you to the mentors that changed my life and made me the scientist I am today: my eighth-grade math teacher, Samir Bolar, and my undergrad supervisor, Alison Frand. I can never thank you enough for genuinely investing in me and encouraging me to reach my potential. Thank you to my friends for all their love and support: Jairo Lopez, Paola Castro, Emma Powell, Terri Lee, and Nathan Gamarra. Thank you to the incredible women that have been influential friends and mentors, both scientifically and generally: Gabriela Monsalve, D'Anne Duncan, and Seemay Chou. Thank you to my little brother, Enrique Torres, for always having my back. Thank you to my SRTP students for inspiring me to be the best mentor and scientist I can be; and above all, for giving me the opportunity to feel like I made a difference in their scientific training and trajectories.

Of course, thank you to the scientists that advised my thesis work: David Weinberg and Joseph Bondy-Denomy. David—thank you for teaching me biochemistry and for inspiring me to become a fearless scientist. I am grateful that I had the opportunity to learn from an exceptional RNA biochemist that I truly respect and admire. Joe—thank you for welcoming me into your lab, for teaching me phage biology, and for giving me the freedom to grow immensely as a scientist. I feel so fortunate that I had the opportunity to work with the incredibly talented and brilliant group of scientists that comprise the JBD lab (including you, of course!). The strong work ethic and passion for science that's been cultivated in your lab never ceases to amaze me!

Thank you to David Morgan for being my advocate and mentor throughout the entirety of my thesis work. Thank you to Sandy Johnson for providing helpful scientific advice as part of my thesis committee. Thank you to the brilliant scientists that worked with me directly: Conor Howard, Shweta Karambelkar, Caroline Mahendra, and Samuel Kilcher. It was truly a pleasure collaborating with you and learning from all of you.

Thank you to my yoga teachers for keeping me sane during this final stretch of my PhD journey. Finally, thank you to my therapists Adam Frey and Colby Croft. Thank you for helping me learn so much about myself. Most of all, thank you for your kindness and support when I needed it most.

PUBLISHED WORK

Chapter 1 is adapted from:

Osuna, B.A., Howard, C.J., Kc, S., Frost, A., and Weinberg, D.E. (2017). *In vitro* analysis of RQC activities provides insights into the mechanism and function of CAT tailing. ELife *6*, e27949. DOI: 10.7554/eLife.27949

Chapter 2 is adapted from:

Osuna, B.A., Karambelkar, S., Mahendra, C., Christie, K.A., Garcia, B., Davidson, A.R., Kleinstiver, B.P., Kilcher, S., and Bondy-Denomy, J. (2019). *Listeria* phages induce Cas9 degradation to protect lysogenic genomes. BioRxiv 787200. DOI: https://doi.org/10.1101/787200

ABSTRACT

SURVEILLANCE AND DEFENSE MECHANISMS IN MICROBES

Beatriz A. Osuna

To survive the harsh conditions of their environment, microbes have evolved protection mechanisms that counteract the most lethal of threats: damage to essential biosynthetic machinery and infiltration by foreign invaders. Surveillance mechanisms monitor fundamental biosynthetic processes—including DNA replication, mRNA transcription, and protein translation—to ensure their accuracy and limit the accumulation of incorrectly synthesized macromolecules in the cell. Immunity mechanisms, on the other hand, prevent cellular infiltration by external invaders such as viruses. In the first half of this study, I investigated a surveillance pathway that detects ribosomes stalled during protein translation and marks the incomplete nascent proteins for degradation. In yeast, this pathway was known to involve Carboxy-terminal Alanine and Threonine (CAT) tailing: a non-canonical, mRNA-independent peptide synthesis mechanism. However, the mechanism of CAT tailing and its role in maintaining protein homeostasis was unknown. Here, I show that CAT tailing requires the catalytic activity of fragmented 60*S* ribosomes and charged tRNAs, but is otherwise distinct from canonical protein synthesis. Moreover, CAT tailing of the incomplete nascent protein exposes a lysine residue that is modified with ubiquitin, a tag for protein destruction. In the second half of this study, I investigated the bacterial CRISPR-Cas9 immune system in *Listeria monocytogenes*, which detects and destroys invading phage (virus) DNA. The phage protein, AcrIIA1, was known to inactivate CRISPR-Cas9 but its mechanism was uncharacterized. Here, I show that AcrIIA1 binds to Cas9 with high affinity via the catalytic HNH domain to induce Cas9 degradation, thereby protecting the *Listeria* genome during lysogeny but not during lytic growth. AcrIIA1 also directly represses transcription of the anti-CRISPR locus and is therefore required for optimal phage replication. Finally, bacterial hosts have co-opted AcrIIA1 homologs that potentially act as “anti-anti-CRISPRs” by blocking the deployment of phage anti-CRISPRs.

TABLE OF CONTENTS

LIST OF FIGURES

CHAPTER 1

CHAPTER 2

LIST OF TABLES

CHAPTER 1

CHAPTER 2

CHAPTER 1

In vitro analysis of RQC activities provides insights into the mechanism and function of CAT tailing

In vitro analysis of RQC activities provides insights into the mechanism and function of CAT tailing

Beatriz A. Osuna[1,2], Conor J. Howard[2,3,4], Subheksha KC[1],

Adam Frost[2,3,4,5,†], and David E. Weinberg[1,6,†]

[1] Department of Cellular and Molecular Pharmacology, University of California, San Francisco, San Francisco, CA 94158, USA

[2] Department of Biochemistry and Biophysics, University of California, San Francisco, San Francisco, CA 94158, USA

[3] California Institute for Quantitative Biomedical Research, San Francisco, CA 94158, USA

[4]Chan Zuckerberg Biohub, San Francisco, CA 94158, USA

[5] Department of Biochemistry, University of Utah, Salt Lake City, UT, 84112, USA

[6] Sandler Faculty Fellows Program, University of California, San Francisco, San Francisco, CA 94158, USA

ABSTRACT

Ribosomes can stall during translation due to defects in the mRNA template or translation machinery, leading to the production of incomplete proteins. The Ribosome-associated Quality control Complex (RQC) engages stalled ribosomes and targets nascent polypeptides for proteasomal degradation. However, how each RQC component contributes to this process remains unclear. Here we demonstrate that key RQC activities—Ltn1p-dependent ubiquitination and Rqc2p-mediated Carboxy-terminal Alanine and Threonine (CAT) tail elongation—can be recapitulated *in vitro* with a yeast cell-free system. Using this approach, we determined that CAT tailing is mechanistically distinct from canonical translation, that Ltn1p-mediated ubiquitination depends on the poorly characterized RQC component Rqc1p, and that the process of CAT tailing enables robust ubiquitination of the nascent polypeptide. These findings establish a novel system to study the RQC and provide a framework for understanding how RQC factors coordinate their activities to facilitate clearance of incompletely synthesized proteins.

INTRODUCTION

Eukaryotic cells contain several cotranslational quality-control pathways that limit the production of aberrant proteins and thereby maintain protein homeostasis. One such pathway is activated when a ribosome fails to complete translation, leading to the recruitment of specialized factors that disassemble the stalled ribosome and facilitate degradation of the nascent protein (Brandman and Hegde, 2016; Shoemaker and Green, 2012). A key effector of this process is the highly conserved Ribosome-associated Quality control Complex (RQC), which in budding yeast comprises the E3 ubiquitin ligase Ltn1p, the ATPase Cdc48p, and the poorly characterized proteins Rqc1p and Rqc2p (Brandman et al., 2012; Defenouillère et al., 2013; Verma et al., 2013)—the human homologs of which are Listerin, VCP/p97, TCF25, and NEMF, respectively. The stalled translation complex is first separated into subunits by ribosome splitting factors, allowing the small ribosomal subunit (40*S*) and mRNA to be released. The RQC then recognizes and assembles on the large ribosomal subunit (60*S*) that still contains a nascent polypeptide linked to a tRNA molecule (60*S*:peptidyl–tRNA). Ltn1p facilitates ubiquitination of the nascent chain while on the 60*S* subunit, marking the incompletely synthesized protein for proteasomal degradation (Bengtson and Joazeiro, 2010; Shao et al., 2013). Additionally, Rqc2p recruits charged tRNAs to the 60*S* subunit to direct elongation of the nascent protein with a Carboxy-terminal Alanine and Threonine extension, or CAT tail (Shen et al., 2015).

Structural analysis of the yeast RQC, identification of the tRNA molecules that co-purify with the RQC, and biochemical characterization of failed nascent chains suggested that CAT tailing occurs on the 60*S* subunit by a unique mechanism that does not require an mRNA template or the 40*S* subunit (Shen et al., 2015). However, many questions about the mechanism of CAT-tail synthesis and the consequences of elongating nascent polypeptides with CAT tails remain unanswered. Recent studies have suggested that one function of CAT tails is to facilitate aggregation of nascent polypeptides that fail to be ubiquitinated by Ltn1p (due

to either disruptions in *LTN1* or the absence of a suitable ubiquitin acceptor). CAT tail-driven aggregation may limit the otherwise toxic effects of incomplete translation products accumulating in the cytoplasm (Choe et al., 2016; Defenouillère et al., 2016; Yonashiro et al., 2016). However, our understanding of the functions of CAT tails in the context of an intact RQC or of the process of CAT tailing itself remains incomplete.

Previous studies have analyzed the RQC *in vitro* by using cell-free translation systems based on rabbit reticulocyte lysates (Shao et al., 2013) or *Neurospora crassa* extracts (Doamekpor et al., 2016). In the presence of a suitable mRNA substrate, both cell-free systems recapitulate Ltn1p-dependent ubiquitination and thereby provide valuable insight into the mechanism by which Ltn1p orthologs discriminate between elongating and stalled ribosomes (Shao et al., 2013) and the role of the N-terminal domain of Ltn1p in binding the 60*S* subunit (Doamekpor et al., 2016). However, neither system recapitulates Rcq2p-dependent CAT tailing, leaving important unanswered questions about how CAT tails are synthesized and whether the two principal activities of the RQC—ubiquitination by Ltn1p and CAT tailing by Rqc2p—are functionally related.

Although many studies have identified Rqc1p/TCF25 as a core component of the yeast and mammalian RQC required for nascent-chain degradation (Brandman et al., 2012; Defenouillère et al., 2013; Shao and Hegde, 2014), Rqc1p's precise structural and functional roles in the complex remain unclear. Previous work in yeast suggested that Rqc1p acts after Ltn1p to promote nascent-chain degradation. This hypothesis emerged from two lines of evidence: The presence of polyubiquitinated proteins in purified RQC depends on Ltn1p (and to a lesser extent on Rqc2p) but not on Rqc1p or Cdc48p (Brandman and Hegde, 2016; Brandman et al., 2012); and recruitment of Cdc48p to the 60*S* subunit requires Rqc1p and nascent-chain ubiquitination (Defenouillère et al., 2013). However, these studies did not determine whether Rqc1p is necessary for ubiquitination of the nascent chain itself or whether recruitment of

Cdc48p requires a direct interaction with Rqc1p. Therefore, the mechanism by which Rqc1p promotes nascent-chain degradation *in vivo* has remained unclear.

In this study, we provide an *in vitro* characterization of the RQC in a budding-yeast extract that uniquely recapitulates ubiquitination by Ltn1p and CAT tailing by Rqc2p, providing new insights into RQC action in promoting degradation of stalled translation products.

RESULTS

A cell-free system that recapitulates Rqc2p-mediated nascent-chain elongation

Because CAT tails have thus far only been observed in *S. cerevisiae* (Choe et al., 2016; Defenouillère et al., 2016; Shen et al., 2015; Yonashiro et al., 2016), we used *S. cerevisiae* extracts to recapitulate Rqc2p-mediated elongation *in vitro*. Although *S. cerevisiae* has long been used for *in vitro* translation (Hussain and Leibowitz, 1986; Iizuka et al., 1994; Rojas-Duran and Gilbert, 2012; Tarun and Sachs, 1995), these reactions are notoriously inefficient. Further exacerbating this problem, we aimed to program these reactions with truncated mRNA substrates that trigger quality control, which are translated less efficiently because they lack poly(A) tails that normally enhance translation. Thus, we found it necessary to first establish an optimized protocol that could reproducibly generate translation products that were detectable by immunoblotting (see Materials and methods). Critical aspects of our protocol included: 1) lysing cells with a freezer mill under cryogenic conditions rather than by bead beating in the cold; 2) minimizing the number of lysis cycles; 3) removing small molecules by dialysis rather than by size-exclusion chromatography; and 4) programming translation reactions with an mRNA encoding a small protein (i.e., 23-kDa NanoLuc luciferase), which is translated more efficiently than an mRNA encoding a larger protein (e.g., 62-kDa firefly luciferase).

To produce a substrate for the RQC, we used a truncated reporter mRNA that terminates with a sense codon (i.e., does not contain a stop codon, 3′–untranslated region (3′-UTR), or poly(A) tail). This mRNA substrate has been shown previously to generate a ribosome–nascent chain complex stalled at the 3′ end of the message (Becker et al., 2011; Shao et al., 2013). Our reporter mRNA encodes a NanoLuc luciferase (NL) protein in which the seven native lysine residues have been mutated to arginine to avoid potential confounding effects of lysine ubiquitination. The protein also includes an N-terminal 3xHA tag (which is naturally devoid of lysines) to allow detection of translation products by immunoblotting.

Programming *S. cerevisiae in vitro* translation (ScIVT) reactions with a full-length control mRNA that contains a stop codon, 3′-UTR, and 50-nucleotide poly(A) tail resulted in the time-dependent accumulation of a 23-kDa product corresponding to 3xHA-NL (Figure 1-1A, left). In contrast, ScIVT of a truncated mRNA initially produced a ~43-kDa mass-shifted product not observed in control reactions (Figure 1-1A, right), which we hypothesized corresponded to a peptidyl–tRNA intermediate. Remarkably, as the reaction proceeded we observed the disappearance of the initial ~43-kDa product and concomitant accumulation of smaller mass-shifted products ranging from 23 kDa to 43 kDa (Figure 1-1A, right). These mass-shifted products were reminiscent of CAT-tailed species previously observed *in vivo* (Choe et al., 2016; Defenouillère et al., 2016; Shen et al., 2015; Yonashiro et al., 2016).

To further characterize the mass-shifted species, we added a sequence encoding a TEV protease cleavage site (TCS) at the 3′ end of our mRNA substrate (Shen et al., 2015) and determined the susceptibility of the mass-shifted species to TEV protease and RNase. We reasoned that a nascent polypeptide with its C-terminus covalently linked to a tRNA molecule would be liberated by either TEV protease or RNase. In contrast, a nascent polypeptide containing an untemplated C-terminal amino-acid extension (e.g., a CAT tail) would be cleaved by TEV protease but not RNase, and a protein containing additional mass due to modifications anywhere except the C-terminus would be unaffected by either treatment. When treated with either RNase or TEV protease, the ~45-kDa intermediate observed at early time points was converted to a 25-kDa species, corresponding to the molecular weight of 3xHA-NL-TCS (Figure 1-1B). Given that the average molecular weight of a tRNA is ~20 kDa, these results suggest that the ~45-kDa species contained a tRNA covalently linked to the C-terminus of 3xHA-NL-TCS (“peptidyl–tRNA”)—which has previously been characterized as an intermediate of the quality-control pathway (Shao et al., 2013; Shoemaker et al., 2010; Tsuboi et al., 2012). In contrast, the heterogeneous collection of ~25–45-kDa products that accumulated at later time points were only affected by TEV protease, converting them to a discrete 25-kDa species (Figure 1-1B), as

expected if the products originally contained additional mass downstream of the TCS (i.e., appended to the C-terminus of 3xHA-NL-TCS). Because the truncated mRNA substrate used for ScIVT contained no sequences downstream of the TCS, this additional mass was necessarily untemplated and therefore consistent with CAT tails. Notably, the prominent peptidyl–tRNA species that accumulated at early time points was largely absent after 60 minutes of translation (Figure 1-1A and 1-1B), presumably due to peptidyl–tRNA hydrolysis that occurred after untemplated elongation of the nascent chain.

In addition to being C-terminal and untemplated, another known feature of CAT tails is that their synthesis is strictly dependent on Rqc2p but not on Ltn1p or Rqc1p (Choe et al., 2016; Defenouillère et al., 2016; Shen et al., 2015; Yonashiro et al., 2016). To determine if the ~23–43-kDa mass-shifted species share this property, we took advantage of the genetic tractability of *S. cerevisiae* and non-essential nature of the RQC by performing ScIVT using extracts prepared from *ltn1Δ*, *rqc1Δ*, and *rqc2Δ* strains. While reactions using *ltn1Δ* and *rqc1Δ* extracts yielded all of the mass-shifted products observed when using wild-type (WT) extracts (Figure 1-1C), reactions using *rqc2Δ* extracts did not (Figure 1-1D), consistent with those species corresponding to CAT-tailed protein. However, rather than producing the expected 23-kDa 3xHA-NL protein, reactions lacking Rqc2p generated a relatively stable 43-kDa peptidyl–tRNA species, indicating a defect in peptidyl–tRNA hydrolysis. This finding suggests that in addition to facilitating the incorporation of untemplated amino acids, Rqc2p may also be involved in promoting hydrolysis of the final peptidyl–tRNA bond and thereby liberating the nascent polypeptide.

Previous biochemical and structural studies have suggested that Rqc2p engagement and subsequent CAT tailing must be preceded by ribosome splitting, which exposes the P-site tRNA and the surface of the Sarcin-Ricin loop (SRL) that are recognized by Rqc2p/NEMF (Lyumkis et al., 2014; Shao et al., 2015; Shen et al., 2015). In the case of truncated mRNAs that generate a ribosome stalled at the mRNA 3′ end with an empty A site, ribosome splitting is

effected by the release-factor mimics Hbs1p and Dom34p (Shao et al., 2013; Shoemaker et al., 2010). Accordingly, ScIVT of a truncated mRNA in *hbs1Δ* or *dom34Δ* extracts generated only the ~43-kDa product corresponding to an especially stable peptidyl–tRNA (Figure 1-1E), which is presumably protected within a stalled but intact 80*S* ribosome. Collectively, these data demonstrate that ScIVT of a truncated mRNA generates polypeptides containing untemplated Rqc2p-dependent C-terminal extensions. Although we have not been able to confirm that these extensions are composed of alanine and threonine residues (for technical reasons), we suspect that this is the case and therefore refer to the extensions as CAT tails for simplicity.

The lack of CAT-tailing activity in *rqc2Δ* extracts (Figure 1-1D) is consistent with previous observations that CAT tails are absent from *rqc2Δ* strains *in vivo* (Choe et al., 2016; Defenouillère et al., 2016; Shen et al., 2015; Yonashiro et al., 2016), which could reflect either a direct role for Rqc2p in CAT tailing (as suggested by structural studies) or indirect effects of *RQC2* disruption on CAT tailing. To distinguish between these possibilities, we tested whether the absence of CAT-tailing activity in *rqc2Δ* extracts could be rescued by adding purified Rqc2p to ScIVT reactions already in progress. Remarkably, the addition of exogenous Rqc2p (Figure 1-S1) to *rqc2Δ* extracts restored both CAT-tail synthesis and peptidyl–tRNA hydrolysis, whereas the addition of a CAT-tailing-deficient Rqc2p mutant containing the D98A substitution (Shen et al., 2015; Yonashiro et al., 2016) did not promote either CAT-tail synthesis or robust peptidyl–tRNA hydrolysis (Figure 1-1F). These results provide direct evidence that Rqc2p is biochemically required for CAT tailing, consistent with its proposed role in recruiting alanine- and threonine-charged tRNAs to the 60*S* subunit (Shen et al., 2015). Also, our ability to temporally separate CAT tailing from canonical translation *in vitro* (by the addition of exogenous Rqc2p to *rqc2Δ* extracts) provided an experimental strategy for specifically testing the requirements of CAT-tail elongation.

Mechanistic differences between CAT-tail synthesis and canonical translation

Though previous structural studies of the RQC were instrumental in discovering CAT tailing and suggested a direct role for Rqc2p in the process (Shen et al., 2015), the mechanism of CAT tailing has only been inferred from these data and otherwise remains poorly characterized. In particular, no published studies have investigated the extent to which CAT tailing by the 60*S* subunit is mechanistically similar to canonical elongation by the 80*S* ribosome. To address this question, we sought to examine the sensitivity of *in vitro* CAT tailing to a collection of well-characterized chemical inhibitors that target different sites of the ribosome or elongation factors (Figure 1-2A) and thereby interfere with canonical translation. Importantly, because canonical translation is required to generate the substrate for the RQC (i.e., a stalled ribosome at the post-splitting stage), it was necessary to temporally separate canonical translation from CAT tailing to isolate the effects of these inhibitors on the latter reaction. To do so, we first translated a truncated mRNA in *rqc2Δ* extracts in the absence of any inhibitors for 20 minutes to generate a pool of RQC substrate (60*S*:peptidyl–tRNA). We then supplemented the reactions with one of the inhibitors (at a concentration that completely inhibited canonical translation *in vitro*; Figure 1-S2A) and purified Rqc2p (Figure 1-S2B) (or a buffer-only control) to initiate CAT-tail synthesis. Finally, we allowed the reactions to proceed for an additional 40 minutes before analyzing the products by immunoblotting.

As predicted by the structural analyses, treatment with drugs that target the peptidyl-transferase center (PTC) of the 60*S* subunit (anisomycin and the chain terminator puromycin) completely prevented CAT-tail synthesis, providing direct evidence that the catalytic activity of the ribosome is required for CAT tailing (Figure 1-2B and C). Puromycin treatment also resulted in a complete collapse of the 43-kDa mass-shifted species to 23 kDa, confirming the identity of this larger species as peptidyl–tRNA (Figure 1-2B). In contrast to the dramatic effects of PTC inhibitors, inhibitors that target the 40*S* subunit (emetine and G418) did not inhibit CAT-tail synthesis (Figure 1-2B), consistent with the proposed 40*S* subunit–independent mechanism of

CAT tailing. Surprisingly, cycloheximide—which binds in the E site of the 60*S* subunit and sterically clashes with the 3′ end of the deacylated tRNA during canonical translation—did not inhibit CAT tailing (Figure 1-2B). Cycloheximide insensitivity identifies an unanticipated feature of CAT-tail elongation that may reflect a distinct mechanism of deacylated-tRNA displacement in the absence of mRNA and the 40*S* subunit.

It was previously proposed that specific Rqc2p–tRNA interactions impart selectivity for alanine- and threonine-tRNAs to CAT-tail elongation (Shen et al., 2015). However, it is not known if the translation elongation factors eEF1a and eEF2—which deliver aminoacyl-tRNAs to the ribosome and promote translocation, respectively—collaborate with Rqc2p to facilitate CAT-tail synthesis. Strikingly, we found that drugs targeting either eEF1a or eEF2 (didemnin variants (Carelli et al., 2015) or sordarin (Justice et al., 1998), respectively) had no effect on CAT tailing (Figure 1-2C). Because many canonical translation factors are GTPases, including eEF1a and eEF2, we also examined whether CAT tailing requires GTP hydrolysis. We tested for inhibition by the non-hydrolyzable GTP analog GMP-PCP, using a similar approach as before except that at the time of Rqc2p addition we stopped translation by adding emetine to prevent ongoing translation in the GTP control reaction. Consistent with the above differences between CAT-tail elongation and translation, treatment with GMP-PCP had no impact on CAT tailing (Figure 1-2D), indicating that this mRNA-independent elongation mechanism does not require energy from GTP hydrolysis or the canonical activities of the translational GTPases eEF1a and eEF2. Collectively, these findings provide direct evidence that CAT tailing is a 40*S* subunit–independent, PTC-catalyzed reaction and identify key differences from canonical translation that suggest an entirely different elongation cycle.

Ltn1p- and Rqc1p-dependent ubiquitination in the yeast cell-free system

The ability of ScIVT to recapitulate Rqc2p-dependent CAT tailing (Figure 1-1) led us to explore whether this system also recapitulates the other key activity of the RQC, Ltn1p-dependent nascent-chain ubiquitination. Initial experiments comparing a lysine-containing

truncated reporter mRNA to a lysine-free version revealed a faint smear of high-molecular-weight (HMW) products (~50–115 kDa) unique to the lysine-containing reporter (Figure 1-3A, compare lanes 1 and 4). We reasoned that these HMW products were likely ubiquitinated proteins because lysine residues are the canonical ubiquitination sites (Pickart, 2001). However, because ScIVT extracts contain many ubiquitin ligase activities and a finite pool of endogenous ubiquitin, we suspected that Ltn1p-dependent ubiquitination of the reporter protein (which occurs late in the reactions) might have been limited by the amount of ubiquitin available to Ltn1p. Indeed, supplementing ScIVT reactions with exogenous ubiquitin resulted in enhanced accumulation of the lysine-dependent HMW products (Figure 1-3A). Treatment of ubiquitin-supplemented reactions with TEV protease or RNase did not fully collapse the HMW species as it did for CAT-tailed species (Figure 1-3B), consistent with the HMW species containing ubiquitin-modified residues rather than simply having exceptionally long CAT tails. To directly demonstrate that these HMW species contained ubiquitin, we translated truncated mRNAs (with or without lysines) in the presence of exogenous Myc-tagged ubiquitin and purified the reporter protein under denaturing conditions, followed by immunoblotting to detect Myc-tagged ubiquitin. In reactions conducted with WT extracts, we readily detected Myc-tagged ubiquitin within the purified HMW species (Figure 1-3C, fourth lanes in left and right panels).

As expected, we did not observe ubiquitination of the reporter protein in reactions performed with *ltn1Δ* extracts (Figure 1-3C and Figure 1-4A), consistent with Ltn1p being the responsible E3 ubiquitin ligase. The addition of purified Ltn1p to *ltn1Δ* extracts restored ubiquitination, while the addition of purified Ltn1p containing the W1542E substitution—a RING domain mutant that does not support protein turnover *in vivo* (Bengtson and Joazeiro, 2010)—did not (Figure 1-4A and Figure 1-S3). These results demonstrate that the lack of ubiquitination in *ltn1Δ* extracts is a direct consequence of the absence of Ltn1p rather than an indirect effect. Collectively, these results demonstrate that in addition to Rqc2p-dependent CAT tailing the ScIVT system we established also recapitulates Ltn1p-dependent ubiquitination, as previously

shown for lysates derived from *N. crassa* and rabbit reticulocytes (Doamekpor et al., 2016; Shao et al., 2013).

Unexpectedly, we did not detect any Ltn1p-dependent ubiquitination of the reporter protein in *rqc1Δ* extracts (Figure 1-3C). The addition of purified Rqc1p (Figure 1-S3), however, fully rescued ubiquitination in *rqc1Δ* extracts (Figure 1-3C and Figure 1-4B). Increasing the concentration of Ltn1p in the reaction did not bypass the requirement for Rqc1p in ubiquitination (Figure 1-S4). These observations suggest that Rqc1p is directly involved in nascent-chain ubiquitination. Such a role is consistent with the fact that *LTN1* deletion phenocopies *RQC1* deletion in both the accumulation of stalling reporters *in vivo* and, more broadly, in their correlated set of genetic interactions (Brandman et al., 2012; Defenouillère et al., 2013). Although TCF25/Rqc1p was previously reported to be dispensable for Listerin/Ltn1p-mediated ubiquitination of purified 60*S*-bound stalled nascent chains (Shao and Hegde, 2014), the stringent purification of ribosome–nascent chain complexes in that study might have removed factors that otherwise impose a requirement for Rqc1p/TCF25 (e.g., chaperones that protect the nascent chain). Our results support a model in which Rqc1p directly promotes Ltn1p-mediated ubiquitination of the nascent chain via a mechanism that remains to be determined.

Interplay between CAT tailing and ubiquitination

Previous studies have shown that a CAT-tailing-deficient mutant of Rqc2p preserves degradation of stalled nascent chains (Shen et al., 2015) and that *in vitro* reconstitution of Listerin/Ltn1p-mediated ubiquitination does not strictly require NEMF/Rqc2p (Shao and Hegde, 2014; Shao et al., 2013). Together, these studies suggested that CAT tailing is dispensable for degradation of the assayed reporter constructs. Based on these results and structural data, it was proposed that Rqc2p indirectly contributes to ubiquitination by recognizing the aberrant 60*S*:peptidyl–tRNA complex, stabilizing Ltn1p on the 60*S* subunit, and sterically preventing the 40*S* subunit from rejoining (Shao et al., 2015). Together with the minimal impact of *LTN1* disruption on CAT tailing *in vivo* (Choe et al., 2016; Defenouillère et al., 2016; Shen et al., 2015;

Yonashiro et al., 2016) and *in vitro* (Figure 1-1), these studies led to a model in which ubiquitination by Ltn1p and CAT tailing by Rqc2p are independent activities of the RQC (Inada, 2017).

The unique ability of our ScIVT system to recapitulate both activities of the RQC, combined with its genetic tractability, allowed us to directly test this model *in vitro.* Consistent with the proposed scaffolding function of Rqc2p in ubiquitination, disruption of *RQC2* abrogated nascent-chain ubiquitination by Ltn1p (Figure 1-3C and Figure 1-4C), and addition of wild-type Rqc2p rescued ubiquitination (Figure 1-4C and Figure 1-S1). Unexpectedly, however, the addition of CAT-tailing-deficient (D98A) Rqc2p to *rqc2Δ* extracts only partially rescued ubiquitination (Figure 1-4C). Similarly, reactions using extracts containing endogenously expressed Rqc2p(D98A) as the only *RQC2* gene product yielded minimal ubiquitinated protein (Figure 1-3C). To rule out the possibility that the effect of the D98A substitution on ubiquitination was due to disruption of the known scaffolding function of Rqc2p, we took an alternative approach to inhibit CAT tailing in the context of wild-type Rqc2p. As observed in the Rqc2p(D98A) experiments, preventing CAT tailing of stalled nascent chains—in this case with anisomycin treatment (Figure 1-2C)—substantially reduced ubiquitination (Figure 1-4D and Figure 1-S5). These results suggest that Rqc2p not only provides structural support for Ltn1p but also that CAT tailing directly enhances Ltn1p-dependent ubiquitination of at least some substrates (see Discussion). Collectively, our *in vitro* analyses reveal that all three components of the RQC—Ltn1p/Listerin, Rqc1p/TCF25, and Rqc2p/NEMF—contribute to ubiquitination of the nascent chain.

Structural studies of full-length Listerin on the 60*S* subunit localized its active-site-containing RING domain near the ribosomal exit tunnel (Shao et al., 2015), poised to facilitate ubiquitination of lysine residues recently emerged from the tunnel. At the same time, the implied physical tethering of the RING domain to the ribosome suggests that the active site may not be able to access more distantly positioned lysines in the nascent polypeptide, nor can the most

recently translated lysines—contained within the 30–60-amino-acid long exit tunnel (Kramer et al., 2009)—be accessed by Ltn1p until their emergence. Collectively, these physical constraints suggest that only a limited subset of lysines in stalled nascent chains are accessible to the active site of Ltn1p, with other lysines either being either too far from the RING domain or buried in the ribosomal exit tunnel. We reasoned that CAT tailing could therefore expose the latter class of "hidden" lysine residues to the RING domain of Ltn1p.

To evaluate this model of CAT-tailing-dependent ubiquitination, we used the aforementioned denaturing purification assay (Figure 1-3) to compare the extent of nascent-chain ubiquitination in the absence versus the presence of CAT tailing (i.e., ScIVT extracts containing Rqc2p(D98A) versus Rqc2p) across a set of truncated mRNAs encoding lysine residues at different positions (Figure 1-5A) . In the absence of CAT tailing, only two of the lysine-containing nascent chains were efficiently ubiquitinated by Ltn1p (Figure 1-5B, top left panel), consistent with the limited reach of the Ltn1p RING domain in the context of a fixed nascent chain. In both substrates, multiple lysines were located ~30–50 residues from the stalling site—a distance predicted to naturally position the lysines proximal to the exit tunnel near the Ltn1p active site. Remarkably, however, all of the lysine-containing nascent chains could be detectably ubiquitinated above background in the presence of CAT tailing (Figure 1-5B, top left panel), demonstrating that CAT tailing can greatly expand the range of suitable Ltn1p substrates. Most notably, nascent chains containing one (Figure 1-5A, reporter E) or three lysine residues (Figure 1-S6A, reporters L and M) that upon stalling should be hidden in the exit tunnel (i.e., 0-30 amino acids from the C terminus) were ubiquitinated in a CAT-tailing-dependent manner, albeit weakly (but consistently above background levels seen in a lysine-free reporter) (Figure 1-5B, top left panel, compare reporter B to E; Figure 1-S6B, compare reporter I to L and M). These data demonstrate that the range of Ltn1p-accessible lysine residues is limited by spatial constraints, and that these constraints are relaxed by CAT-tailing-dependent exposure of lysines.

We then asked if the enhancement of ubiquitination by CAT tailing observed *in vitro* has functional consequences on protein turnover *in vivo*. The few nascent chain RQC substrates previously studied *in vivo* were shown to be degraded in a CAT-tailing-independent manner (Shen et al., 2015), which we reasoned might have been due to native lysines being fortuitously positioned proximal to the Ltn1p RING domain. To explore the relationship between lysine positioning and Ltn1p-dependent protein degradation *in vivo*, we generated ribosome-stalling reporters encoding the analogous RQC substrates from our *in vitro* studies (see Materials and Methods) and assessed their steady-state levels in living budding-yeast cells. Consistent with our *in vitro* analyses (Figure 1-5B and 1-S6B) and previous studies using a native (i.e., lysine-containing) GFP reporter (Shen et al., 2015), substrates predicted to contain exposed lysines near the exit tunnel did not accumulate in either WT or CAT-tailing-deficient cells (Figure 1-S6C, top left panel, reporters H′ and K′), indicative of efficient ubiquitination and proteasomal degradation. By contrast, substrates in which there were no lysines near or within the exit tunnel showed no evidence of RQC-dependent degradation, providing *in vivo* evidence for the limited reach of Ltn1p (Figure 1-S6C, top left panel, lanes I′ and J′). Finally, substrates that contained lysines within the exit tunnel were more abundant in Rqc2(D98A) cells than in WT cells, suggesting that for these substrates CAT tails exposed hidden lysines to Ltn1p for ubiquitination and subsequent degradation (Figure 1-S6C, top left panel, lanes L′ and M′). These results reveal that CAT tailing is required for nascent-chain ubiquitination when lysines are not conveniently located proximal to the Ltn1p RING domain. Additionally, in cells lacking intact *LTN1* or *RQC1*, all reporters accumulated at similar steady state levels regardless of lysine position, demonstrating that Ltn1p and Rqc1p are required for degradation of truncated NanoLuc nascent chains *in vivo* (Figure 1-S6C, top right and bottom left panels). Broadly, these findings establish that for many substrates CAT tailing and ubiquitination are coupled, rather than distinct, activities of the RQC and provide new insight into the physiological role of CAT tailing.

Because ribosomes could potentially stall anywhere on an mRNA during translation elongation, the RQC machinery would ideally be able to act on a wide range of possible nascent chains to facilitate degradation. However, the fact that the Ltn1p RING domain can only access a small window of amino acids outside the exit tunnel limits the set of suitable nascent chains that can be readily ubiquitinated. The ability of CAT tailing to expose lysine residues buried in the exit tunnel to Ltn1p would relieve this limitation, so long as the nascent chain contains a lysine hidden in the exit tunnel at the time of ribosome stalling. To evaluate the possible extent this phenomenon in *S. cerevisiae*, we performed a computational analysis to determine the fraction of all potential nascent polypeptides across the yeast proteome that encode a lysine predicted to be in the ribosome exit tunnel. Remarkably, we found that ~90% of all possible nascent polypeptides generated by a stalled ribosome would contain at least one lysine buried in the exit tunnel (85–96% for 30–60 amino acids of buried nascent chain as a function of potential secondary structure; Figure 1-5C). Moreover, non-stop mRNAs that lack a termination codon and are translated into the poly(A) tail (Bengtson and Joazeiro, 2010; Defenouillère et al., 2013; Ito-Harashima et al., 2007) would also generate nascent polypeptides with lysines (encoded by 'AAA' codons) hidden in the exit tunnel, which might be an important class of CAT-tailing-dependent ubiquitination substrates. Altogether, these results suggest that CAT tailing can facilitate ubiquitination of the vast majority of potential RQC substrates. For the remaining <15% of nascent polypeptides stalled on ribosomes without a lysine positioned near or within the exit tunnel, the CAT tail may facilitate protein aggregation as previously described (Choe et al., 2016; Yonashiro et al., 2016). However, rather than being the primary role of CAT tails, aggregation is more likely a backup pathway to mitigate the toxic effects of stalled polypeptides that cannot be immediately degraded.

DISCUSSION

We have shown that establishing a cell-free system that recapitulates both CAT tailing and ubiquitination opens new opportunities to explore how the fully functional RQC promotes clearance of aberrant translation products. Our analyses reveal that Rqc2p-mediated nascent-chain elongation is mechanistically distinct from canonical translation, that ubiquitination of the nascent polypeptide requires both Ltn1p and Rqc1p, and that the ubiquitination and CAT-tailing activities of the RQC are coupled through a mutual requirement for active Rqc2p (Figure 1-6).

The key benefit of an *in vitro* system to study CAT tailing is the ability to perform experiments that would be intractable *in vivo*. Indeed, a major difficulty in studying CAT tailing is that it utilizes some of the same machinery as canonical translation (i.e., the 60*S* subunit) and requires a substrate that is generated by canonical translation, making it difficult to perturb CAT tailing specifically. By temporally separating the translation- and CAT-tailing-phases of *in vitro* reactions, we overcame this obstacle and specifically tested the sensitivity of the CAT-tailing reaction to a wide range of well-characterized ribosome and translation inhibitors. These analyses revealed that aside from requiring the catalytic PTC of the ribosome, CAT tailing is otherwise fundamentally different from translation elongation in ways that could not have been fully anticipated from previous studies (Figure 1-2). In particular, our findings that CAT tailing does not require the canonical activities of the elongation factors or energy from GTP hydrolysis suggest a unique mechanism of elongation. Reexamining 60*S*:RQC structures (Shao et al., 2015; Shen et al., 2015), we noted that the network of interactions between Ltn1p/Rqc2p and the 60*S* subunit overlaps with the ribosome-binding sites of eEF1a (Shao et al., 2016) and eEF2 (Taylor et al., 2007). The overlap in binding sites indicates that either eEF1a/eEF2 are dispensable for CAT tailing, or that eEF1a/eEF2 and the RQC interact transiently with the 60*S* subunit during elongation. Our findings favor the former model and suggest that Rqc2p directly recruits charged tRNAs with its selective tRNA-binding activity (Shen et al., 2015), without the

involvement of eEF1a. Following peptide-bond formation by the 60*S* subunit, the A/P and P/E tRNAs may spontaneously translocate in the absence of interactions with an mRNA template or 40*S* subunit; whereas during canonical translation such interactions impose an energy requirement for translocation that is fulfilled by the GTPase activity of eEF2. Given that CAT tailing was proposed to occur on the 60*S* subunit (Shen et al., 2015), we predicted that all translation inhibitors that bind the 60*S* subunit would inhibit CAT-tail synthesis. However, we found that CAT tailing was not inhibited by cycloheximide, suggesting that the deacylated tRNA may rapidly dissociate from the 60*S* subunit following peptidyl transfer.

Together, these findings suggest that a minimal set of factors—a 60*S*:peptidyl–tRNA complex, charged alanine and threonine tRNAs, and Rqc2p—may be sufficient for CAT-tail synthesis. In 1969, Monro demonstrated that in the presence of certain alcohols, isolated bacterial 50*S* ribosomal subunits could catalyze polymerization from aminoacyl-tRNAs in the absence of an mRNA template and 30*S* subunits (Monro, 1969). Thus, it is conceivable that Rqc2p may stimulate nascent-chain elongation much as in Monro's minimal prokaryotic system. Many questions remain about Rqc2p dynamics during CAT tailing, including whether a single molecule of Rqc2p remains on the 60*S* subunit for successive cycles of peptide-bond formation or whether each cycle of elongation requires binding by a new Rqc2p–tRNA complex.

CAT-tail synthesis eventually terminates by hydrolysis of the peptidyl–tRNA linkage, which is presumably needed to release the CAT-tailed nascent chain from the 60*S* subunit for its destruction by the proteasome. Indeed, one critical function of CAT tailing might be to provide a mechanism of termination in the absence of a stop codon. The wide range of CAT-tail lengths observed both *in vivo* (Choe et al., 2016; Defenouillère et al., 2016; Shen et al., 2015; Yonashiro et al., 2016) and *in vitro* suggests that termination is a stochastic process. Furthermore, our finding that peptidyl–tRNA intermediates are relatively stable *in vitro* in the absence of Rqc2p (Figures 1-1D and 1-1F, Figure 1-2, and Figure 1-4C) indicates a potentially direct role of Rqc2p in the termination reaction. These observations lead to a model for CAT-tailing termination in

which Rqc2p recruits a termination factor to the 60*S* subunit in a stochastic manner during the process of elongation. Because Rqc2p interacts with A-site tRNAs at a site distant from the acceptor stem (Shen et al., 2015), it is possible that the “termination factor” is an uncharged alanine- or threonine-tRNA (Caskey et al., 1971; Zavialov et al., 2002). Alternatively, Rqc2p might interact with the canonical termination factor eRF1 or another protein with peptidyl–tRNA hydrolase activity to facilitate termination.

Taking advantage of the fact that our extracts also recapitulated Ltn1p-dependent ubiquitination, we found that Rqc1p plays a critical role in nascent-chain ubiquitination *in vitro* (Figure 1-3C and Figure 1-4B). This direct role of Rqc1p in ubiquitination contrasts with its previously suggested role in recruiting Cdc48p downstream of ubiquitination (Brandman et al., 2012; Defenouillère et al., 2013). Nevertheless, our discovery that ubiquitination *in vitro* is as dependent on Rqc1p as it is on the E3 ligase Ltn1p is consistent with the fact that yeast strains lacking Rqc1p and Ltn1p have very similar phenotypes and genetic interaction profiles, suggesting a similar molecular defect in these strains (Brandman et al., 2012). We speculate that Rqc1p may facilitate ubiquitination by positioning the nascent chain in proximity to the Ltn1p RING domain, by promoting binding of the E2 ubiquitin-conjugating enzyme, or by activating Ltn1p’s E3 ligase activity on the 60*S* subunit.

With a system that uniquely recapitulates both nascent-chain elongation by Rqc2p and ubiquitination by Ltn1p, we discovered that Rqc2p can elongate the nascent chain to enhance ubiquitination, rather than just providing structural support for Ltn1p binding to the 60*S* subunit (Figure 1-3C and Figure 1-4C). This finding was surprising given that previous studies have shown that a CAT-tailing-deficient mutant of Rqc2p preserves degradation of aberrant nascent chains in yeast cells (Shen et al., 2015) and that *in vitro* reconstitution of Listerin/Ltn1p-mediated ubiquitination does not strictly require NEMF/Rqc2p (Shao and Hegde, 2014). How can we reconcile these findings? Structural studies of full-length Listerin/Ltn1p on the 60*S* subunit localized its RING domain (which binds an E2 ubiquitin-conjugating enzyme) near the

ribosomal exit tunnel (Shao et al., 2015), poised to facilitate ubiquitination of lysine residues close to or recently emerged from the tunnel. The physical tethering of the RING domain near the exit tunnel suggests that Ltn1p may not be able to access more distantly positioned lysines in the nascent polypeptide, nor can the most recently translated lysines—contained within the 30–60-amino-acid long exit tunnel (Kramer et al., 2009)—be accessed by Ltn1p until their emergence. Our observations lead to a model in which Ltn1p can only ubiquitinate a spatially restricted set of lysines, while CAT tailing enables access to other lysines—as previously proposed (Brandman and Hegde, 2016; Simms et al., 2017). We reason that the few nascent chain RQC substrates previously studied *in vivo* could be degraded in a CAT-tailing-independent manner (Choe et al., 2016; Defenouillère et al., 2016; Shen et al., 2015; Yonashiro et al., 2016) due to native lysines being fortuitously positioned proximal to the Ltn1p RING domain.

Recent studies in budding yeast have demonstrated that CAT tails mediate formation of detergent-insoluble aggregates when the nascent chain cannot be degraded due to its limited ubiquitination potential or due to inactivation of Ltn1p (Choe et al., 2016; Defenouillère et al., 2016; Yonashiro et al., 2016). In the context of a fully intact RQC, however, our findings suggest that CAT tailing and ubiquitination are interdependent activities. Elongation of the nascent chain with CAT tails can result in two outcomes: positioning lysine residues proximal to the Ltn1p RING domain for efficient ubiquitination; or distancing lysine residues from the Ltn1p RING domain, making ubiquitination less efficient. Thus, CAT tailing and ubiquitination must be tightly coordinated to promote nascent-chain degradation and to avoid, where possible, aggregate formation and the detrimental sequestration of cytosolic chaperones. These studies collectively suggest that rather than being the primary role of CAT tails, aggregation is more likely a backup pathway to mitigate the toxic effects of stalled polypeptides that cannot be efficiently ubiquitinated and degraded (Figure 1-6). A notable distinction between the aggregation- and ubiquitination-promoting functions of CAT tails is that the former depends on the

alanine/threonine composition of the CAT tail (Choe et al., 2016), while the latter depends on the process of CAT tailing itself.

While CAT tailing has yet to be reported in metazoans, the conservation of Rqc1p/TCF25, Rqc2p/NEMF, and Ltn1p/Listerin—including critical residues that we mutated in this study—suggest that both RQC activities are conserved and together provide a means of protecting cells against the accumulation of faulty translation products. Ltn1p-dependent ubiquitination has been detected in rabbit reticulocyte extracts, so a CAT-tailing-dependent mechanism to facilitate ubiquitination of inaccessible lysine residues likely operates in metazoans as well. Underscoring the importance of this quality-control mechanism in maintaining proteostasis, mutations in the mammalian homologs of *HBS1* (Ishimura et al., 2014) and *LTN1* (Chu et al., 2009) cause neurodegeneration in mice.

With our newfound insights, the similarities between the bacterial tmRNA system and the eukaryotic RQC become even more striking than previously appreciated. In certain bacteria, a stalled ribosome is rescued by the recruitment of a hybrid tRNA/mRNA-like molecule (tmRNA) to the empty A-site of the ribosome, leading to translation of a tmRNA-encoded C-terminal degron that includes a dedicated stop codon (Moore and Sauer, 2007). In this way, stalled nascent chains are marked for degradation and translation can terminate even when the mRNA template lacks a stop codon. The RQC fulfills these same functions but in a different manner that is compatible with the ubiquitin-proteasome system: Stalled nascent chains are marked for degradation by ubiquitination (in certain cases facilitated by CAT tailing), and translation can terminate without a stop codon with the help of Rqc2p. Thus, both mechanisms involve a ribosome-catalyzed peptidyl-transferase reaction that adds a C-terminal extension that is not templated by the parent mRNA molecule. The addition of the C-terminal extension, moreover, facilitates peptidyl–tRNA hydrolysis and nascent-chain release either directly (tmRNA) or indirectly (RQC) to promote degradation. These functional similarities between the tmRNA system and the RQC—despite not sharing any related factors other than the ribosome—provide

a striking example of convergent evolution that emphasizes the physiological importance of discarding incompletely synthesized proteins and recycling the translation machinery.

AUTHOR CONTRIBUTIONS

B.A.O. and D.E.W. conceived and designed the study. B.A.O. and C.J.H. performed all experiments. A.F. and D.E.W. supervised experiments. All authors evaluated results. B.A.O. and D.E.W. wrote the manuscript with input from all authors.

ACKNOWLEDGEMENTS

We thank Soufiane Aboulhouda for initial work on yeast *in vitro* translation and David Morgan and Peter Shen for comments on the manuscript. We also thank members of the Weinberg and Frost labs, and Wendy Gilbert for insightful discussions, Jonathan Asfaha for experimental advice and reagents, and Jordan Carelli and Jack Taunton for eEF1a inhibitors. We also acknowledge Raul Andino, Keith Yamamoto, Alan Frankel, and David Agard for generously sharing equipment. This work was supported by an NSF Graduate Research Fellowship and a Moritz-Heyman Discovery Fellowship (B.A.O.), a Hillblom Graduate Research Fellowship (C.J.H.), the Searle Scholars Program 13SSP218 (A.F.), NIH grant 1DP2GM110772-01 (A.F.), an HHMI Faculty Scholar award (A.F.), the UCSF Program for Breakthrough Biomedical Research funded in part by the Sandler Foundation (A.F., D.E.W.), and an NIH Director's Early Independence Award DP5OD017895 (D.E.W.). A.F. is a Chan Zuckerberg Biohub Investigator.

MATERIALS AND METHODS

Yeast Strain Construction

Saccharomyces cerevisiae strains used in this study were derived from BY4741 (*MATa his3Δ1 leu2Δ0 met15Δ0 ura3Δ0*) and are listed in Supplementary file 1. Yeast transformations were performed using the PEG–lithium acetate method (Gietz and Woods, 2006). To generate gene knockouts, the entire coding sequence of the gene of interest was replaced with the *URA3* cassette of pRS416. Strains containing point mutations at endogenous loci were generated from *URA3*-disrupted strains by transformation with PCR fragments encoding the mutant gene of interest and 5-FOA counterselection (Boeke et al., 1987). Transformants were screened by PCR to identify integrants, which were subsequently verified by PCR and Sanger sequencing of the entire integrated cassette.

Preparation of mRNA for *In Vitro* Translation

pcDNA3.1(+) (Thermo Fisher Scientific, Waltham, MA) was modified using Gibson Assembly Master Mix (New England Biolabs, Ipswich, MA) and appropriate DNA fragments according to the Gibson assembly method (Gibson et al., 2009) to generate pBAO1124, which contains (in order): T7 promoter, 46-nt 5′-UTR lacking any AUG or near-AUG codons (i.e., NUG, ANG, or AUN, where N is any nucleotide), 3xHA-NanoLuc luciferase ORF, 56-nt 3′-UTR, and 50-nt poly(A) sequence. RNAs were generated by run-off transcription with T7 RNA Polymerase using the MEGAscript T7 Transcription Kit (Thermo Fisher Scientific) according to the manufacturer's instructions using PCR-amplified DNA templates derived from pBAO1124 or its variants. Transcription reactions were terminated by addition of ammonium acetate stop solution. RNA was extracted with neutral phenol:chloroform:isoamyl alcohol (25:24:1) (Sigma, St. Louis, MO), precipitated with ethanol, and resuspended in nuclease-free water. A 5′-7-methylguanosine cap was added to RNA post-transcriptionally using the Vaccinia Capping

System (New England Biolabs). Capping reactions were desalted using Micro Bio-Spin Columns with Bio-Gel P-30 (Bio-Rad, Hercules, CA) before RNA was extracted with phenol, precipitated with ethanol, and resuspended in nuclease-free water.

S. cerevisiae In Vitro Translation Extract Preparation

S. cerevisiae strains were grown overnight to saturation in rich YPAD media, diluted the next morning to OD_{600} 0.2 in a total volume of 1 L YPAD, and harvested at OD_{600} 1.4–1.8 by centrifugation at 3500 rpm for 6 min at 4°C. The cell pellet was washed with water and resuspended in lysis buffer A (30 mM HEPES-KOH pH 7.4, 100 mM KOAc, 2 mM $Mg(OAc)_2$, 2mM DTT, and cOmplete mini EDTA-free protease inhibitor cocktail [Roche, Switzerland]) using 1 ml per 6 g of wet cell pellet. The cell slurry was dripped into liquid nitrogen to produce frozen pellets, which were then pulverized using a 6970EFM Freezer/Mill (SPEX SamplePrep, Metuchen, NJ) by three cycles of 12 Hz agitation for 1.5 min with cooling for 2 min after each cycle. The resulting "grindate" was combined with an equal volume of pre-chilled lysis buffer A (i.e., 1 ml per 1 g of grindate) and allowed to thaw on ice. Cell debris was cleared by sequential centrifugation at 4°C at 1000*g* for 5 min, 1350*g* for 5 min, 14000*g* for 30 min, and finally 14000*g* for an additional 10 min. The clarified lysate was dialyzed twice for 2 hr against 250 ml lysis buffer A (except without protease inhibitor cocktail) using 3500 MWCO cassettes (Thermo Fisher Scientific #87722). After dialysis, lysates were flash frozen in 50 µl aliquots in liquid nitrogen and stored at –80°C.

S. cerevisiae In Vitro Translation

Endogenous mRNAs in thawed extracts were degraded by treatment with 0.3 U/µl micrococcal nuclease (MNase) and 480 µM $CaCl_2$ for 10 min at room temperature, followed by addition of 2 mM EGTA and transfer to ice. ScIVT reactions were initiated by adding m^7G-capped RNA (40 ng per µl of reaction volume) to MNase-treated yeast extracts and incubating

at 25°C for up to 90 min. Final concentrations of reaction components were 48.67% (v/v) MNase-treated yeast extract, 22 mM HEPES-KOH (pH 7.4), 120 mM potassium acetate, 1.5 mM magnesium acetate, 0.75 mM ATP, 0.1 mM GTP, 0.04 mM each amino acid, 1.7 mM DTT, 25 mM creatine phosphate, 0.34 µg/µl creatine kinase, 0.14 U/µl SUPERase□In RNase Inhibitor (Thermo Fisher Scientific), and 0.16X cOmplete mini EDTA-free protease inhibitor cocktail (Roche). Where indicated, reactions also included 10 or 100 µM recombinant human ubiquitin or Myc-ubiquitin (Boston Biochem, Cambridge, MA). Reactions were halted by transferring to ice or by adding an equal volume of 2X Laemmli Sample Buffer (Bio-Rad). The results shown for all ScIVT experiments are representative of at least two technical replicates (i.e., experiments conducted with independently prepared reagents).

Denaturing Purification of ScIVT Products

30 µl ScIVT reactions were assembled with 1.2 µg 10xHis-3xHA-NL mRNAs and 10 µM recombinant Myc-ubiquitin (Boston Biochem) and incubated at 25°C for 1 hr. For input samples, 10 µl was removed and quenched in an equal volume of 2X Laemmli Sample Buffer. For Ni-NTA-purified samples, the remaining 20 µl was quenched by addition of denaturing buffer (6 M guanidine-HCl, 50 mM Tris pH 7.8, 300 mM KCl, 10 mM imidazole, 0.1% NP-40, 5 mM β-mercaptoethanol [βME]), and then incubated with 10 µl of pre-washed Ni-NTA Magnetic Agarose Beads (Qiagen, Germany) at 4°C overnight with end-over-end rotation. Beads were washed three times with wash buffer I (denaturing buffer except 500 mM KCl) and three times with wash buffer II (denaturing buffer except 50 mM KCl and no guanidine-HCl), each for 5 min at room temperature. Bound proteins were eluted from beads by adding 15 µl elution buffer (wash buffer II except 200 mM imidazole) and incubating at 22°C for 5 min with shaking at 1000 rpm. The elution step was repeated, and eluates were pooled and mixed with an equal volume of 2X Laemmli Sample Buffer. The results shown for all experiments that include a denaturing

purification of ScIVT products are representative of at least three technical replicates (i.e., experiments conducted with independently prepared reagents).

Immunoblotting

Protein samples were separated by SDS-PAGE using 12% Bolt Bis-Tris gels (Thermo Fisher Scientific) and transferred in 1X CAPS Buffer onto 0.22 micron PVDF membrane (Bio-Rad). Blots were probed with the following antibodies diluted 1:5000 in 1X TBS-T containing 5% nonfat dry milk: mouse anti-HA (RRID:AB_627809, Santa Cruz Biotechnology [Dallas, TX] sc-7392), rat anti-HA high sensitivity (RRID:AB_390918, Roche #11867423001), mouse anti-Myc (RRID:AB_331783, Cell Signaling Technology [Danvers, MA] #2276), HRP-conjugated goat anti-mouse IgG (RRID:AB_631736, Santa Cruz Biotechnology sc-2005), and HRP-conjugated goat anti-rat IgG (RRID:AB_631755, Santa Cruz Biotechnology sc-2032). Blots were developed using Clarity ECL Western Blotting Substrate (Bio-Rad), and chemiluminescence was detected on a ChemiDoc Imaging System (Bio-Rad).

Protein Purification

S. cerevisiae strain yRH101 (a gift from Stephen Bell, MIT) derived from ySC7 (Chen et al., 2007) containing a 2 μm P_{GAL1}-[protein]-10xHis plasmid (a gift from Bob Stroud, UCSF) was grown overnight in SC–His media containing 2% raffinose, diluted the next day, and grown for an additional night to early saturation. Protein expression was induced by adding an equal volume of Yeast-Peptone media containing 2% galactose, and cells were grown for 5 hr at 30°C. Cells were harvested by centrifugation at 3500 rpm for 6 min at 4°C, and the cell pellet was washed with water before resuspending in Lysis Buffer (20 mM HEPES-KOH pH 7.4, 500 mM KCl, 20 mM imidazole; 2 mM βME and cOmplete EDTA-free protease inhibitor cocktail [Roche] added just prior to use) at a ratio of 1 ml per gram of cell pellet. The resulting cell slurry was dripped into liquid nitrogen to produce frozen pellets, which were pulverized using a

6970EFM Freezer/Mill (SPEX SamplePrep) by three cycles of 12 Hz agitation for 1.67 min with 2 min cooling after each cycle. The resulting powder was briefly thawed before adding Lysis Buffer (1 mL per 1 g of powder) supplemented with additional protease inhibitors (292 μM Pepstatin, 8.4 mM Leupeptin, 1.23 mM Aprotinin, 1 mM Phenylmethylsulfonyl fluoride [PMSF]). Cell debris was cleared by sequential centrifugation at 4000 rpm at 4°C for 10 min and then 30 min, followed by sequential filtration through 2.7 and 1.6 μm Whatman GD/X filters (GE Healthcare Life Sciences, Marlborough, MA). His-tagged proteins were purified from lysate using Ni-NTA Sepharose beads (Qiagen) as follows. Beads (~1 ml 50% slurry per 1 L yeast culture) were washed with water and equilibrated in Lysis Buffer. Lysate was added to semi-dry beads and rotated at 4°C for 2 hr. Beads were collected by centrifugation at 800 rpm for 3 min, resuspended in an equal volume of Lysis Buffer, loaded over a disposable Bio-Spin column (Bio-Rad), and washed once with 10 ml Lysis Buffer. The column was then washed as follows: once with 10 ml Wash Buffer (20 mM HEPES-KOH pH 7.4, 500 mM KCl, 10% glycerol, 2 mM βME) containing 20 mM imidazole and 1 mM PMSF; once with 10 ml Wash Buffer containing 20 mM imidazole; and twice with 10 ml Wash Buffer containing 50 mM imidazole. Proteins were sequentially eluted from the beads by gravity rinses as follows: once with 250 μl Wash Buffer containing 250 mM imidazole; twice with 500 μl Wash Buffer containing 250 mM imidazole; and twice with 500 μl Wash Buffer containing 500 mM imidazole. Elution fractions were analyzed by SDS-PAGE and staining with Coomassie Brilliant Blue R-250 to identify those containing the protein of interest, which were then pooled and concentrated to ~500 μl before overnight dialysis into Rqc2p/Ltn1p Storage Buffer (50 mM HEPES-KOH pH 7.4, 300 mM KOAc, 5% glycerol, 2 mM DTT) or Rqc1p Storage Buffer (20 mM HEPES-KOH pH 7.4, 500 mM KOAc, 10% glycerol, 2 mM DTT). Dialyzed protein was passed through a 0.1 μm centrifugal filter (EMD Millipore [Hayward, CA] #UFC30VV00) before flash freezing in liquid nitrogen. Protein concentration was determined by both spectrophotometry using a Nanodrop 2000 (Thermo Fisher Scientific) and Coomassie staining against BSA standards.

REFERENCES

1. Becker, T., Armache, J.-P., Jarasch, A., Anger, A.M., Villa, E., Sieber, H., Motaal, B.A., Mielke, T., Berninghausen, O., and Beckmann, R. (2011). Structure of the no-go mRNA decay complex Dom34–Hbs1 bound to a stalled 80S ribosome. Nat. Struct. Mol. Biol. *18*, 715–720.

2. Bengtson, M.H., and Joazeiro, C.A.P. (2010). Role of a ribosome-associated E3 ubiquitin ligase in protein quality control. Nature *467*, 470–473.

3. Boeke, J.D., Trueheart, J., Natsoulis, G., and Fink, G.R. (1987). [10] 5-Fluoroorotic acid as a selective agent in yeast molecular genetics. B.-M. in Enzymology, ed. (Academic Press), pp. 164–175.

4. Brandman, O., and Hegde, R.S. (2016). Ribosome-associated protein quality control. Nat. Struct. Mol. Biol. *23*, 7–15.

5. Brandman, O., Stewart-Ornstein, J., Wong, D., Larson, A., Williams, C.C., Li, G.-W., Zhou, S., King, D., Shen, P.S., Weibezahn, J., et al. (2012). A Ribosome-Bound Quality Control Complex Triggers Degradation of Nascent Peptides and Signals Translation Stress. Cell *151*, 1042–1054.

6. Carelli, J.D., Sethofer, S.G., Smith, G.A., Miller, H.R., Simard, J.L., Merrick, W.C., Jain, R.K., Ross, N.T., and Taunton, J. (2015). Ternatin and improved synthetic variants kill cancer cells by targeting the elongation factor-1A ternary complex. eLife *4*, e10222.

7. Caskey, C.T., Beaudet, A.L., Scolnick, E.M., and Rosman, M. (1971). Hydrolysis of fMet-tRNA by Peptidyl Transferase. Proc. Natl. Acad. Sci. U. S. A. *68*, 3163–3167.

8. Chen, S., de Vries, M.A., and Bell, S.P. (2007). Orc6 is required for dynamic recruitment of Cdt1 during repeated Mcm2–7 loading. Genes Dev. *21*, 2897–2907.

9. Choe, Y.-J., Park, S.-H., Hassemer, T., Körner, R., Vincenz-Donnelly, L., Hayer-Hartl, M., and Hartl, F.U. (2016). Failure of RQC machinery causes protein aggregation and proteotoxic stress. Nature *531*, 191–195.

10. Chu, J., Hong, N.A., Masuda, C.A., Jenkins, B.V., Nelms, K.A., Goodnow, C.C., Glynne, R.J., Wu, H., Masliah, E., Joazeiro, C.A.P., et al. (2009). A mouse forward genetics screen identifies LISTERIN as an E3 ubiquitin ligase involved in neurodegeneration. Proc. Natl. Acad. Sci. *106*, 2097–2103.

11. Defenouillère, Q., Yao, Y., Mouaikel, J., Namane, A., Galopier, A., Decourty, L., Doyen, A., Malabat, C., Saveanu, C., Jacquier, A., et al. (2013). Cdc48-associated complex bound to 60S particles is required for the clearance of aberrant translation products. ResearchGate *110*.

12. Defenouillère, Q., Zhang, E., Namane, A., Mouaikel, J., Jacquier, A., and Fromont-Racine, M. (2016). Rqc1 and Ltn1 Prevent C-terminal Alanine-Threonine Tail (CAT-tail)-induced Protein Aggregation by Efficient Recruitment of Cdc48 on Stalled 60S Subunits. J. Biol. Chem. *291*, 12245–12253.

13. Doamekpor, S.K., Lee, J.-W., Hepowit, N.L., Wu, C., Charenton, C., Leonard, M., Bengtson, M.H., Rajashankar, K.R., Sachs, M.S., Lima, C.D., et al. (2016). Structure and function of the yeast listerin (Ltn1) conserved N-terminal domain in binding to stalled 60S ribosomal subunits. Proc. Natl. Acad. Sci. *113*, E4151–E4160.

14. Gibson, D.G., Young, L., Chuang, R.-Y., Venter, J.C., Hutchison, C.A., and Smith, H.O. (2009). Enzymatic assembly of DNA molecules up to several hundred kilobases. Nat. Methods *6*, 343–345.

15. Gietz, R.D., and Woods, R. (2006). Yeast Transformation by the LiAc/SS Carrier DNA/PEG Method. In Yeast Protocol, W. Xiao, ed. (Humana Press), pp. 107–120.

16. Hussain, I., and Leibowitz, M.J. (1986). Translation of homologous and heterologous messenger RNAs in a yeast cell-free system. Gene *46*, 13–23.

17. Iizuka, N., Najita, L., Franzusoff, A., and Sarnow, P. (1994). Cap-dependent and cap-independent translation by internal initiation of mRNAs in cell extracts prepared from Saccharomyces cerevisiae. Mol. Cell. Biol. *14*, 7322–7330.

18. Inada, T. (2017). The Ribosome as a Platform for mRNA and Nascent Polypeptide Quality Control. Trends Biochem. Sci. *42*, 5–15.

19. Ishimura, R., Nagy, G., Dotu, I., Zhou, H., Yang, X.-L., Schimmel, P., Senju, S., Nishimura, Y., Chuang, J.H., and Ackerman, S.L. (2014). Ribosome stalling induced by mutation of a CNS-specific tRNA causes neurodegeneration. Science *345*, 455–459.

20. Justice, M.C., Hsu, M.-J., Tse, B., Ku, T., Balkovec, J., Schmatz, D., and Nielsen, J. (1998). Elongation Factor 2 as a Novel Target for Selective Inhibition of Fungal Protein Synthesis. J. Biol. Chem. *273*, 3148–3151.

21. Kostova, K.K., Hickey, K.L., Osuna, B.A., Hussmann, J.A., Frost, A., Weinberg, D.E., and Weissman, J.S. (2017). CAT-tailing as a fail-safe mechanism for efficient degradation of stalled nascent polypeptides. Science *in press*.

22. Kramer, G., Boehringer, D., Ban, N., and Bukau, B. (2009). The ribosome as a platform for co-translational processing, folding and targeting of newly synthesized proteins. Nat. Struct. Mol. Biol. *16*, 589–597.

23. Lyumkis, D., Passos, D.O. dos, Tahara, E.B., Webb, K., Bennett, E.J., Vinterbo, S., Potter, C.S., Carragher, B., and Joazeiro, C.A.P. (2014). Structural basis for translational surveillance by the large ribosomal subunit-associated protein quality control complex. Proc. Natl. Acad. Sci. *111*, 15981–15986.

24. Monro, R.E. (1969). Protein Synthesis: Uncoupling of Polymerization from Template Control. Nature *223*, 903–905.

25. Moore, S.D., and Sauer, R.T. (2007). The tmRNA System for Translational Surveillance and Ribosome Rescue. Annu. Rev. Biochem. *76*, 101–124.

26. Pickart, C.M. (2001). Mechanisms Underlying Ubiquitination. Annu. Rev. Biochem. *70*, 503–533.

27. Rojas-Duran, M.F., and Gilbert, W.V. (2012). Alternative transcription start site selection leads to large differences in translation activity in yeast. RNA *18*, 2299–2305.

28. Shao, S., and Hegde, R.S. (2014). Reconstitution of a Minimal Ribosome-Associated Ubiquitination Pathway with Purified Factors. Mol. Cell *55*, 880–890.

29. Shao, S., von der Malsburg, K., and Hegde, R.S. (2013). Listerin-Dependent Nascent Protein Ubiquitination Relies on Ribosome Subunit Dissociation. Mol. Cell *50*, 637–648.

30. Shao, S., Brown, A., Santhanam, B., and Hegde, R.S. (2015). Structure and Assembly Pathway of the Ribosome Quality Control Complex. Mol. Cell *57*, 433–444.

31. Shao, S., Murray, J., Brown, A., Taunton, J., Ramakrishnan, V., and Hegde, R.S. (2016). Decoding Mammalian Ribosome-mRNA States by Translational GTPase Complexes. Cell *167*, 1229–1240.e15.

32. Shen, P.S., Park, J., Qin, Y., Li, X., Parsawar, K., Larson, M.H., Cox, J., Cheng, Y., Lambowitz, A.M., Weissman, J.S., et al. (2015). Rqc2p and 60S ribosomal subunits mediate mRNA-independent elongation of nascent chains. Science *347*, 75–78.

33. Shoemaker, C.J., and Green, R. (2012). Translation drives mRNA quality control. Nat. Struct. Mol. Biol. *19*, 594–601.

34. Shoemaker, C.J., Eyler, D.E., and Green, R. (2010). Dom34:Hbs1 promotes subunit dissociation and peptidyl-tRNA drop off to initiate no-go decay. Science *330*, 369–372.

35. Simms, C.L., Thomas, E.N., and Zaher, H.S. (2017). Ribosome-based quality control of mRNA and nascent peptides. Wiley Interdiscip. Rev. RNA *8*, n/a-n/a.

36. Tarun, S.Z., and Sachs, A.B. (1995). A common function for mRNA 5'and 3'ends in translation initiation in yeast. Genes Dev. *9*, 2997–3007.

37. Taylor, D.J., Nilsson, J., Merrill, A.R., Andersen, G.R., Nissen, P., and Frank, J. (2007). Structures of modified eEF2·80S ribosome complexes reveal the role of GTP hydrolysis in translocation. EMBO J. *26*, 2421–2431.

38. Tsuboi, T., Kuroha, K., Kudo, K., Makino, S., Inoue, E., Kashima, I., and Inada, T. (2012). Dom34:Hbs1 Plays a General Role in Quality-Control Systems by Dissociation of a Stalled Ribosome at the 3′ End of Aberrant mRNA. Mol. Cell *46*, 518–529.

39. Verma, R., Oania, R.S., Kolawa, N.J., and Deshaies, R.J. (2013). Cdc48/p97 promotes degradation of aberrant nascent polypeptides bound to the ribosome. eLife *2*, e00308.

40. Yonashiro, R., Tahara, E.B., Bengtson, M.H., Khokhrina, M., Lorenz, H., Chen, K.-C., Kigoshi-Tansho, Y., Savas, J.N., Iii, J.R.Y., Kay, S.A., et al. (2016). The Rqc2/Tae2 subunit of the ribosome-associated quality control (RQC) complex marks ribosome-stalled nascent polypeptide chains for aggregation. eLife *5*, e11794.

41. Zavialov, A.V., Mora, L., Buckingham, R.H., and Ehrenberg, M. (2002). Release of Peptide Promoted by the GGQ Motif of Class 1 Release Factors Regulates the GTPase Activity of RF3. Mol. Cell *10*, 789–798.

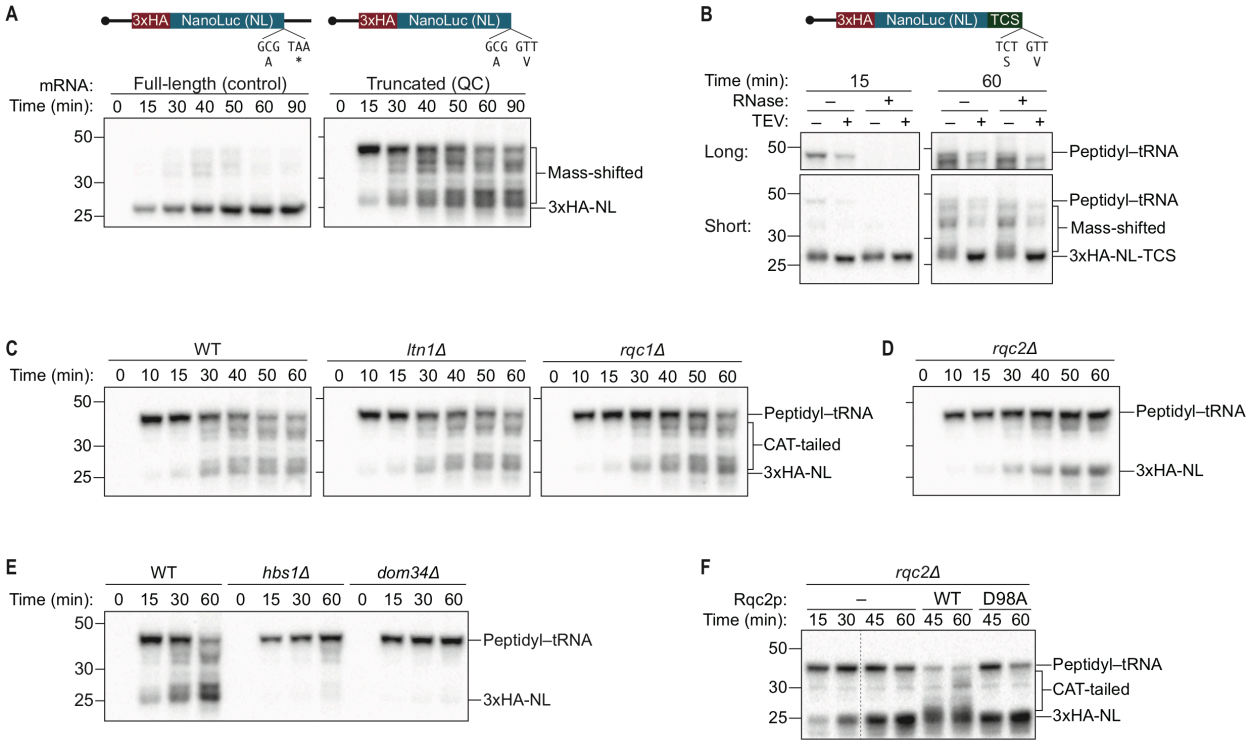

Figure 1-1. An *S. cerevisiae in vitro* translation system recapitulates synthesis of Rqc2p-dependent polypeptide extensions.

(A) Time courses of *S. cerevisiae in vitro* translation (ScIVT) reactions. ScIVT reactions were prepared using wild-type (WT) extracts and 1 µg of either a full-length (left; includes a stop codon and 3′-UTR) or truncated (right; encodes a terminal valine residue) mRNA encoding lysine-free 3xHA-NanoLuc (3xHA-NL). At the indicated time points, aliquots of the reactions were quenched in 2X Laemmli Sample Buffer. Proteins were separated by SDS-PAGE, and HA-tagged translation products were visualized by immunoblotting. 'Long' and 'Short' refer to exposure times of the blots. (B) Analyses of mass-shifted products. An ScIVT reaction was prepared using WT extracts and a lysine-free truncated mRNA substrate that also encodes a TEV cleavage site (TCS). Translation was halted after 15 or 60 minutes by addition of 20 mM EDTA, after which reactions were treated without (–) or with (+) TEV and/or RNase A/T1 cocktail for 60 minutes. Translation products were analyzed by immunoblotting as in (A). (C–E) Genetic analysis of mass-shifted products. ScIVT reactions were prepared using extracts from strains of the indicated genotypes and a lysine-free truncated mRNA substrate. Reactions were performed and analyzed as in (A) but with less mRNA (480 ng). The species that migrate just below the peptidyl–tRNA in *rqc2Δ* extracts in (D) represent peptidyl–tRNA degradation products that arise due to prolonged incubation in the absence of Rqc2p. (F) Rescuing Rqc2p deficiency *in vitro*. ScIVT reactions were prepared using *rqc2Δ* extracts and a lysine-free truncated mRNA substrate. After 30 min of translation, reactions were supplemented with either protein storage buffer (–) or purified Rqc2p (WT or CAT-tailing deficient D98A at 420 nM final concentration) and indicated time points were analyzed by SDS-PAGE and immunoblotting. Dashed lines indicate where intervening lanes were removed for clarity.

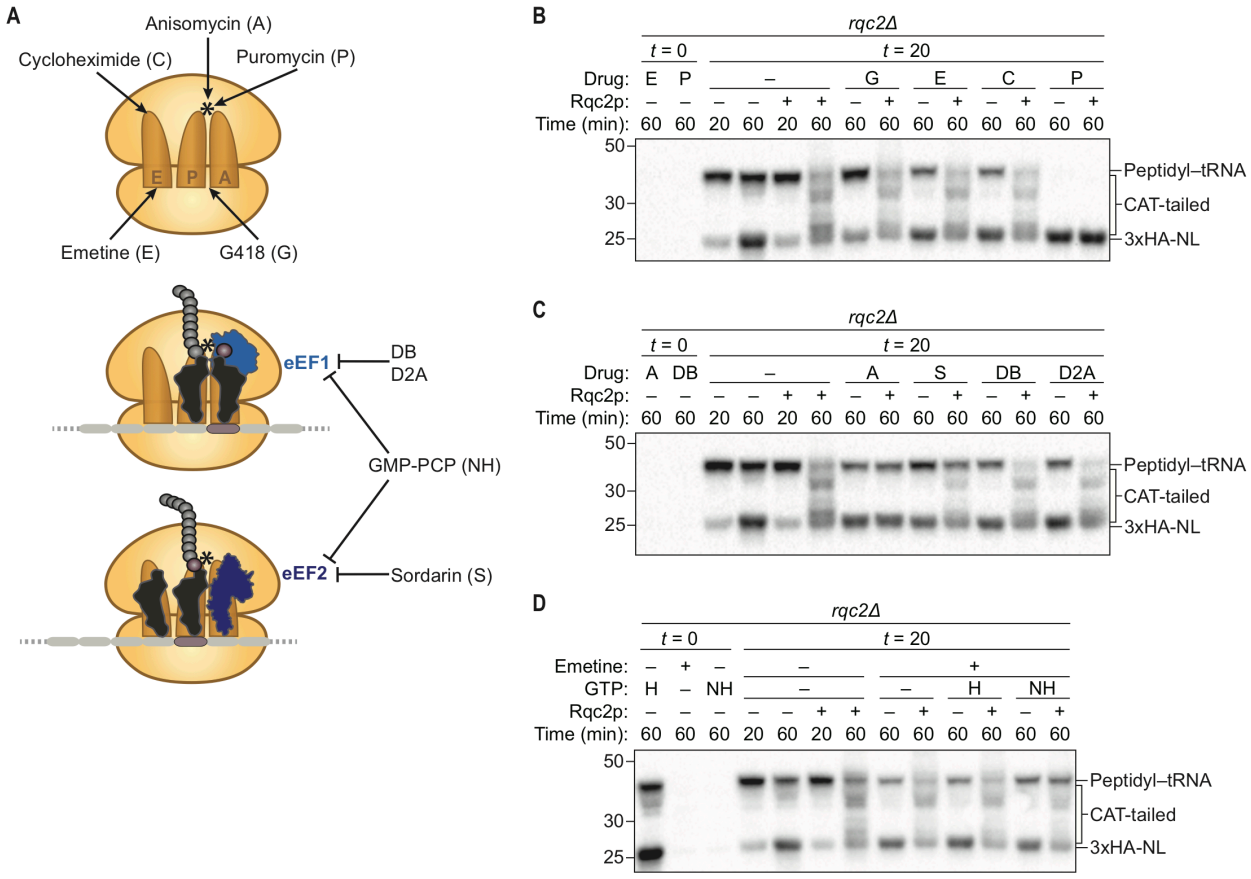

Figure 1-2. CAT-tail synthesis is mechanistically distinct from canonical translation.

(A) Schematics of small-molecule inhibitors that directly bind the ribosome (top) or that target the translation elongation factors eEF1a or eEF2 (bottom). Inhibitors: (A) anisomycin; (C) cycloheximide; (D2A) didemnin 2A; (DB) didemnin B; (E) emetine; (G) G418; (H) hydrolyzable GTP; (NH) non-hydrolyzable GTP-analog GMP-PCP; (P) puromycin; (S) sordarin. (*) Denotes the peptidyl-transferase center of the 60*S* subunit. (B–D) Effects of small-molecule inhibitors on CAT tailing. ScIVT reactions were prepared using *rqc2Δ* extracts and a lysine-free truncated mRNA substrate. After 0 min (*t*=0) or 20 min (*t*=20) of translation, reactions were supplemented with either protein storage buffer (–) or purified Rqc2p at 670 nM final concentration (+) and the indicated inhibitor(s). Indicated time points ("Time (min)") were analyzed by SDS-PAGE and immunoblotting. Additional *t*=0 controls for the remaining inhibitors can be found in Figure 1-S2.

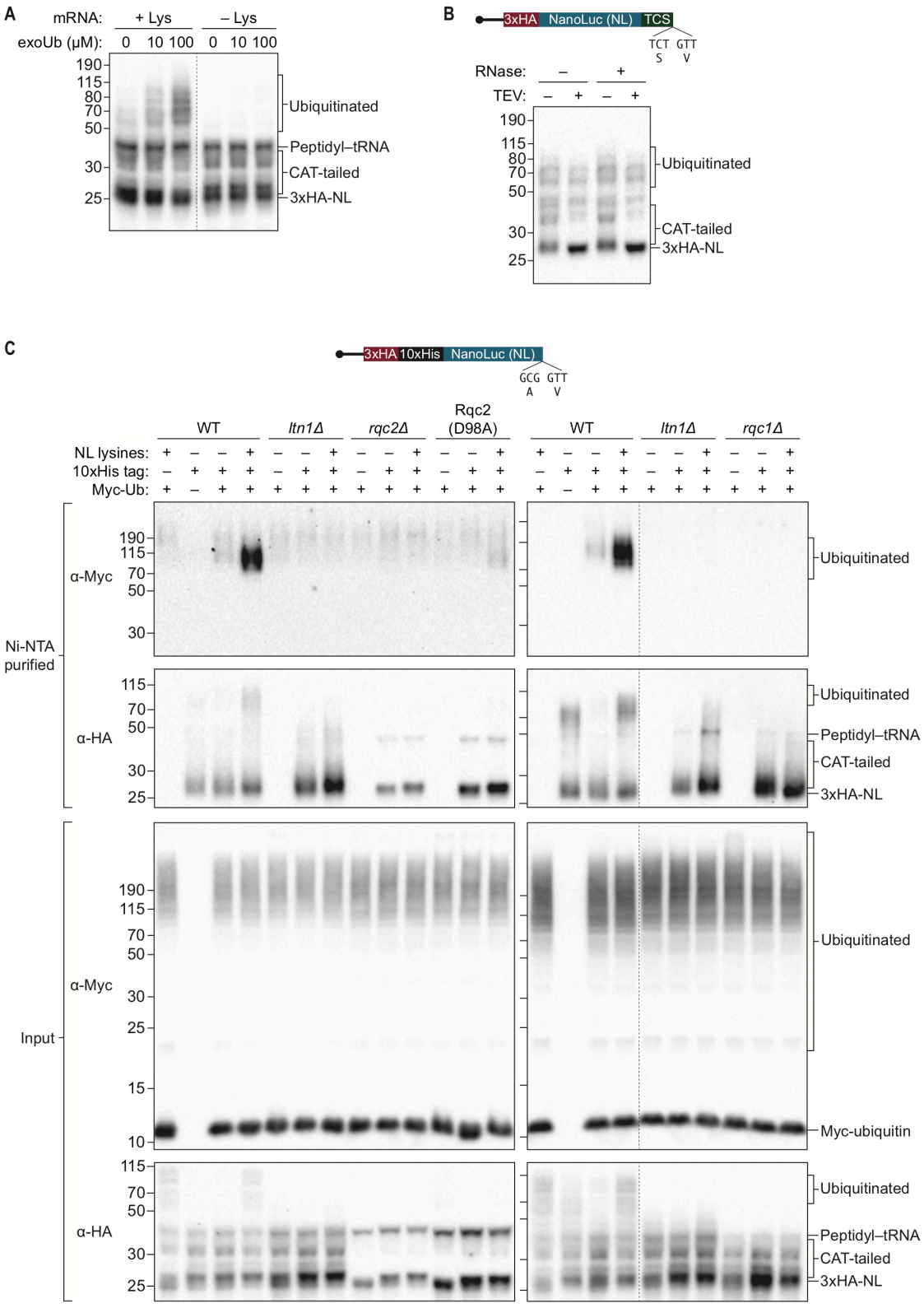

Figure 1-3. *S. cerevisiae in vitro* translation recapitulates Ltn1p-mediated ubiquitination.

(A) Effects of adding exogenous ubiquitin to ScIVT reactions. ScIVT reactions conducted in WT extracts with lysine-containing (+Lys) or lysine-free (–Lys) truncated mRNA were supplemented with the

indicated concentrations of recombinant ubiquitin, incubated for 60 minutes, and then analyzed by SDS-PAGE and immunoblotting. Dashed line indicates where intervening lanes were removed for clarity. (B) Analysis of high-molecular-weight smears. RNase A/T1 and TEV protease treatment of ScIVT reactions programmed with lysine-containing truncated mRNA encoding a TEV cleavage site (TCS) in WT extracts supplemented with 100 μM recombinant ubiquitin. Translation was halted after 60 minutes by addition of 20 mM EDTA, after which reactions were treated without (–) or with (+) TEV and/or RNase A/T1 for 60 minutes, and then analyzed by SDS-PAGE and immunoblotting. Note that due to long incubations (120 mins), very little peptidyl–tRNA persists in these reactions. (C) Isolation and detection of ubiquitinated ScIVT products. ScIVT reactions were conducted with 1.2 μg of truncated mRNA (3xHA-10xHis-NanoLuc, with or without lysines or His tag as indicated) in extracts prepared from strains of the indicated genotypes and supplemented with 10 μM recombinant Myc-ubiquitin. For input samples (bottom panels), one-third of the ScIVT reaction was quenched with 2X Laemmli Sample Buffer. For Ni-NTA-purified samples (top panels), two-thirds of the ScIVT reaction was quenched with 6 M guanidine-HCl. For SDS-PAGE, 30% of input samples and 100% of Ni-NTA-purified samples were separated on 12% NuPAGE gels and translation products were visualized by immunoblotting with antibodies indicated at left. Dashed lines indicate where intervening lanes were removed for clarity.

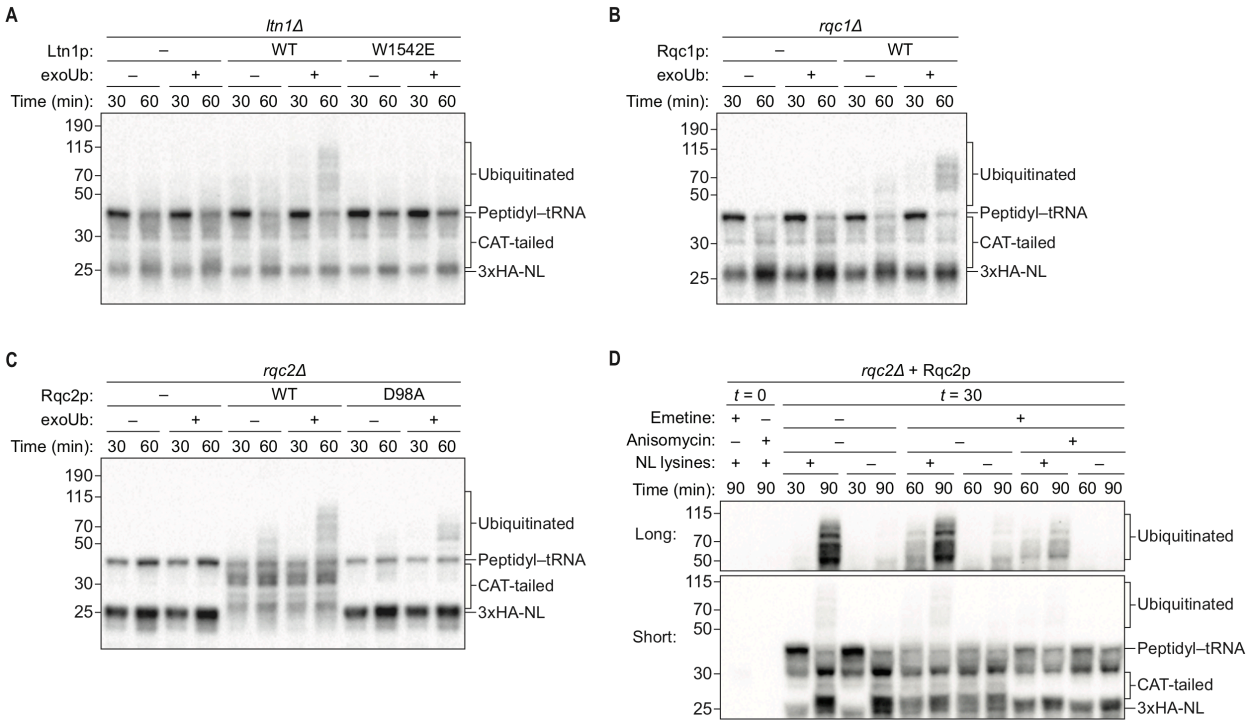

Figure 1-4. Rqc1p and CAT tailing contribute to Ltn1p-dependent ubiquitination.

(A–C) Genetic analysis of RQC-mediated ubiquitination in ScIVT. ScIVT reactions were prepared using extracts from strains of the indicated genotype, a lysine-containing truncated mRNA substrate, ubiquitin storage buffer (–) or 100 μM recombinant ubiquitin (+), and either protein storage buffer (–) or the indicated purified proteins (+): Ltn1p at 130 nM, Rqc1p at 70 nM, and Rqc2p at 420 nM final concentration. (D) ScIVT reactions were conducted using *rqc2Δ* extracts, a lysine-free or lysine-containing truncated mRNA substrate, and 100 μM exogenous ubiquitin. After 0 min (*t*=0) or 30 min (*t*=30) of translation, all reactions were supplemented with an equal volume of 'mock ScIVT' (i.e., without mRNA) containing 1.34 μM purified Rqc2p, 100 μM exogenous ubiquitin, and the indicated inhibitor(s). Indicated time points ("Time (min)") were analyzed by SDS-PAGE and immunoblotting. 'Long' and 'Short' refer to exposure times of the blots.

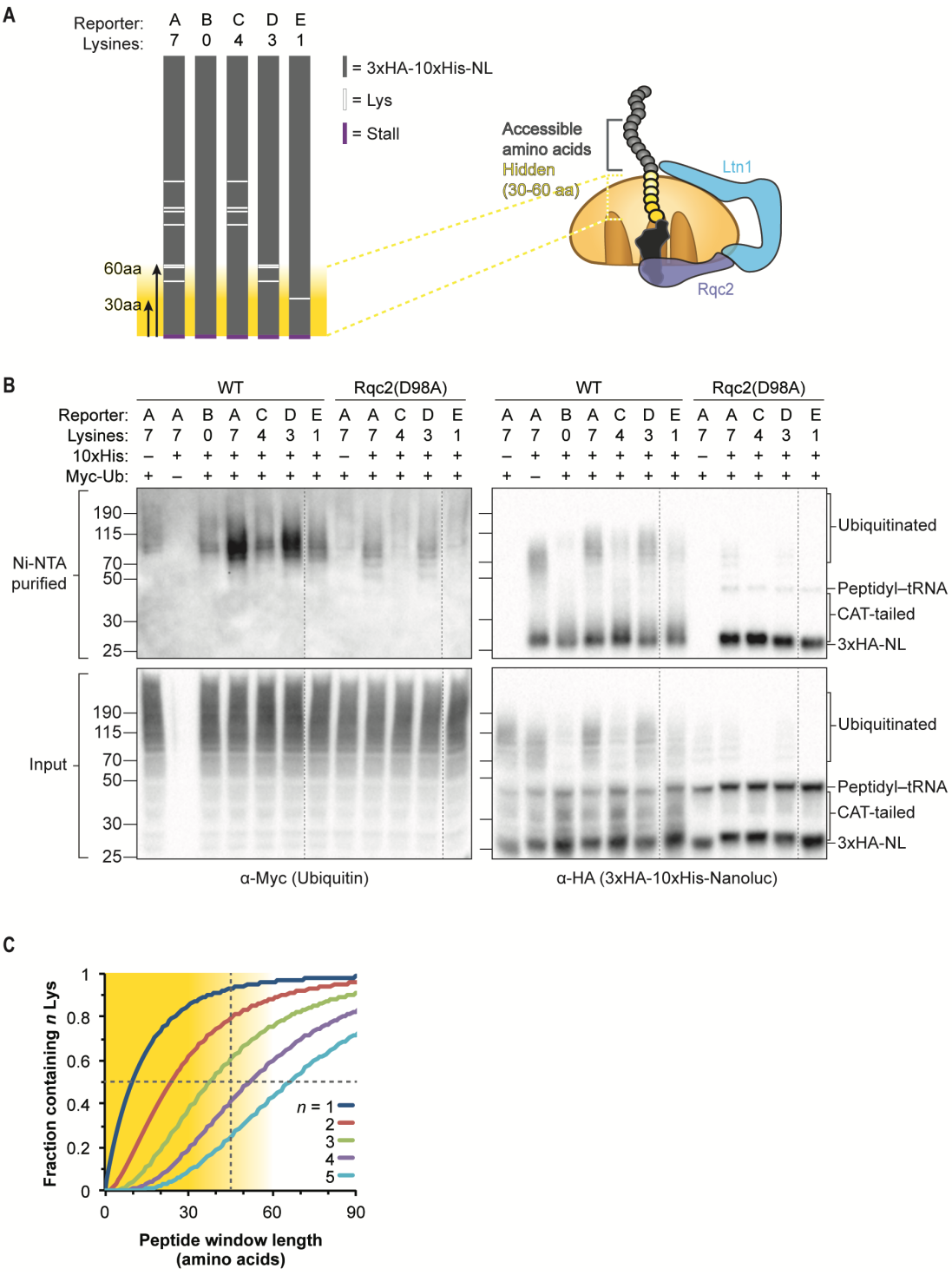

Figure 1-5. CAT tailing alters the availability of lysine residues for Ltn1p-mediated ubiquitination.

(A) Schematic of reporter mRNAs encoding RQC substrates with 0–7 lysine residues (white lines) at different positions. Approximately 30–60 residues can be buried in the ribosome exit tunnel (yellow gradient). (B) Isolation and detection of ubiquitinated ScIVT products. ScIVT reactions were conducted with 1.2 µg of truncated mRNA in extracts prepared from strains of the indicated genotypes and supplemented with 100 µM recombinant Myc-ubiquitin. For input samples, one-third of the ScIVT reaction was quenched with 2x Laemmli Sample Buffer. For immunoprecipitation samples, two-thirds of the ScIVT

reaction was quenched with 6 M guanidine-HCl. For SDS-PAGE, 30% of input samples and 100% of immunoprecipitated samples were loaded onto 12% NuPAGE gels and translation products were visualized by immunoblotting. Dashed lines indicate that lanes were removed from the original image. (C) Computational analysis of the fraction of potential nascent polypeptides across the yeast proteome that encode a lysine in or around the ribosome exit tunnel.

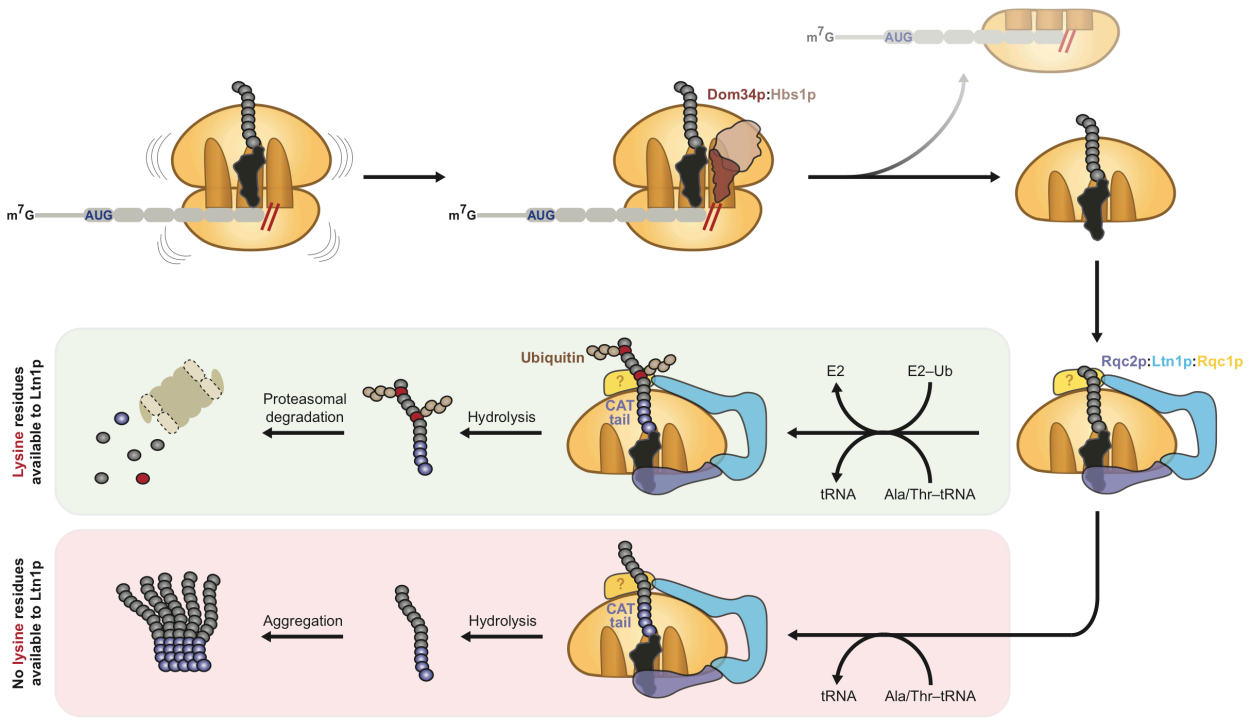

Figure 1-6. Model for CAT tailing and ubiquitination of stalled nascent chains.

When an 80*S* ribosome stalls during translation, splitting factors recognize the stalled translation complex to facilitate dissociation of the 40*S* subunit and mRNA. Ltn1p, Rqc2p, and Rqc1p (unknown location indicated by "?") bind the resulting 60*S*:peptidyl–tRNA complex. Together with the peptidyl-transferase center of the 60*S* subunit, Rqc2p facilitates elongation of the stalled nascent chain with a CAT tail by recruiting alanine- and threonine-charged tRNAs to the A site. If the nascent chain contains a lysine residue (red circle) located within the vicinity of the Ltn1p RING domain (or potentially hidden inside the ribosome exit tunnel), CAT tailing and Rqc1p enhance or facilitate Ltn1p-mediated ubiquitination of the nascent chain, respectively, for subsequent proteasomal degradation (green box). If the nascent chain does not contain any lysine residues (or contains lysine residues that are too distant from the Ltn1p RING domain), CAT tails may promote aggregation of incompletely synthesized proteins (red box). In both instances, Rqc2p activity promotes hydrolysis of the peptidyl–tRNA linkage and liberation from the 60*S* subunit.

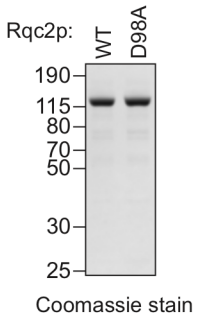

Figure 1-S1. Purified wild-type and mutant Rqc2p.

C-terminal polyhistidine-tagged Rqc2p (WT and D98A mutant) were purified as described in Materials and methods and analyzed by SDS-PAGE and Coomassie staining. 1/10th volume of the corresponding purified protein was added to ScIVT reactions.

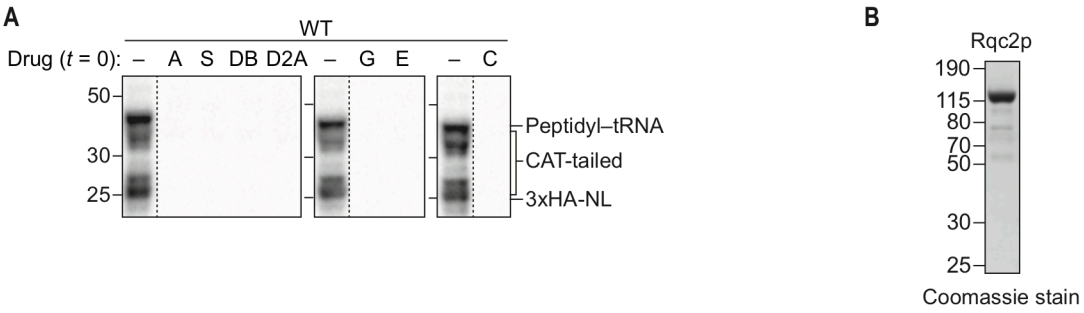

Figure 1-S2. Inhibitors and purified Rqc2p used to dissect the mechanism of CAT-tail synthesis.

(A) Effects of small-molecule inhibitors on translation. ScIVT reactions were prepared using WT extracts and a truncated mRNA substrate, supplemented without (–) or with (+) the indicated inhibitors after 0 min (*t=0*) of translation, and analyzed by SDS-PAGE and immunoblotting. Inhibitors: (A) anisomycin; (C) cycloheximide; (D2A) didemnin 2A; (DB) didemnin B; (E) emetine; (G) G418; (S) sordarin. Dashed lines indicate where intervening lanes were removed for clarity. (B) C-terminal polyhistidine-tagged Rqc2p was purified as described in Materials and methods and analyzed by SDS-PAGE and Coomassie staining. 1/10th volume of purified protein was added to ScIVT reactions. Note that this stock of protein was expressed and purified independently from the stock in Figure 1-S1.

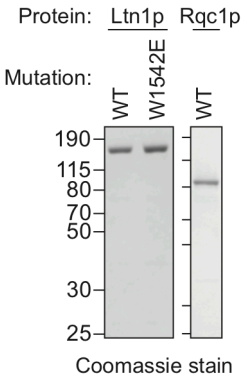

Figure 1-S3. Purified Ltn1p and Rqc1p.

C-terminal polyhistidine-tagged Ltn1p (WT and W1542E mutant) and Rqc1p were purified as described in Materials and methods and analyzed by SDS-PAGE and Coomassie staining. 1/10th volume of the corresponding purified protein was added to ScIVT reactions.

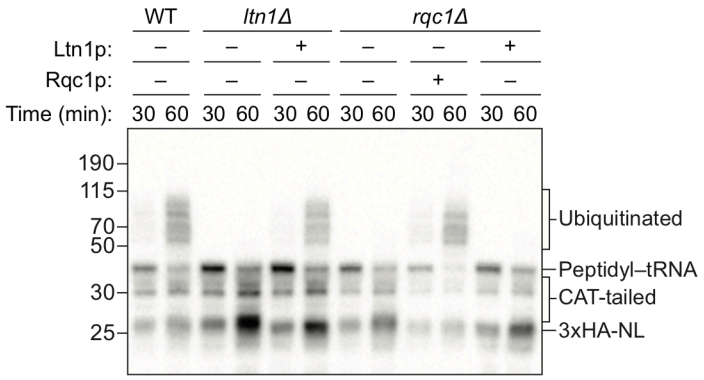

Figure 1-S4. Impact of excess Ltn1p on ubiquitination in *rqc1Δ* extracts.

ScIVT reactions were conducted as in Figure 1-4A to 1-4C except that 100 μM exogenous ubiquitin was present in all reactions.

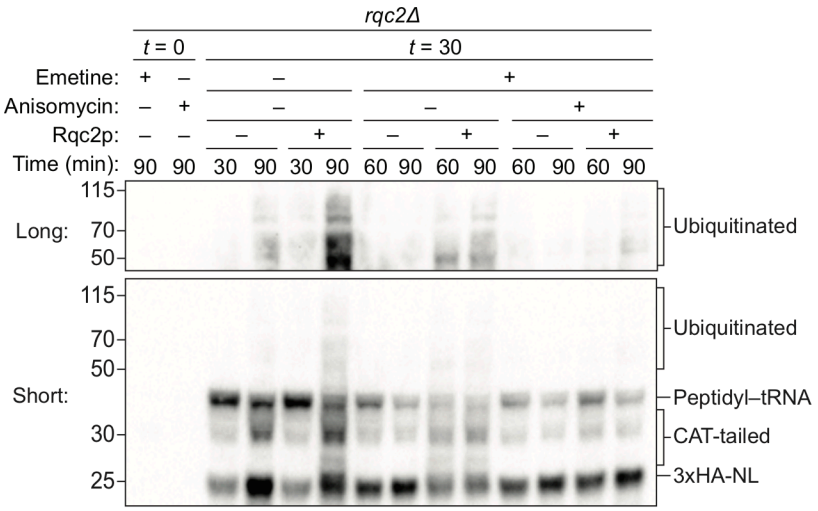

Figure 1-S5. Impact of CAT-tailing inhibition on ubiquitination.

ScIVT reactions were conducted as in Figure 1-4D, except all reactions were performed with lysine-containing mRNA and 'mock ScIVT' containing either protein storage buffer (–) or 1.34 μM purified Rqc2p (+).

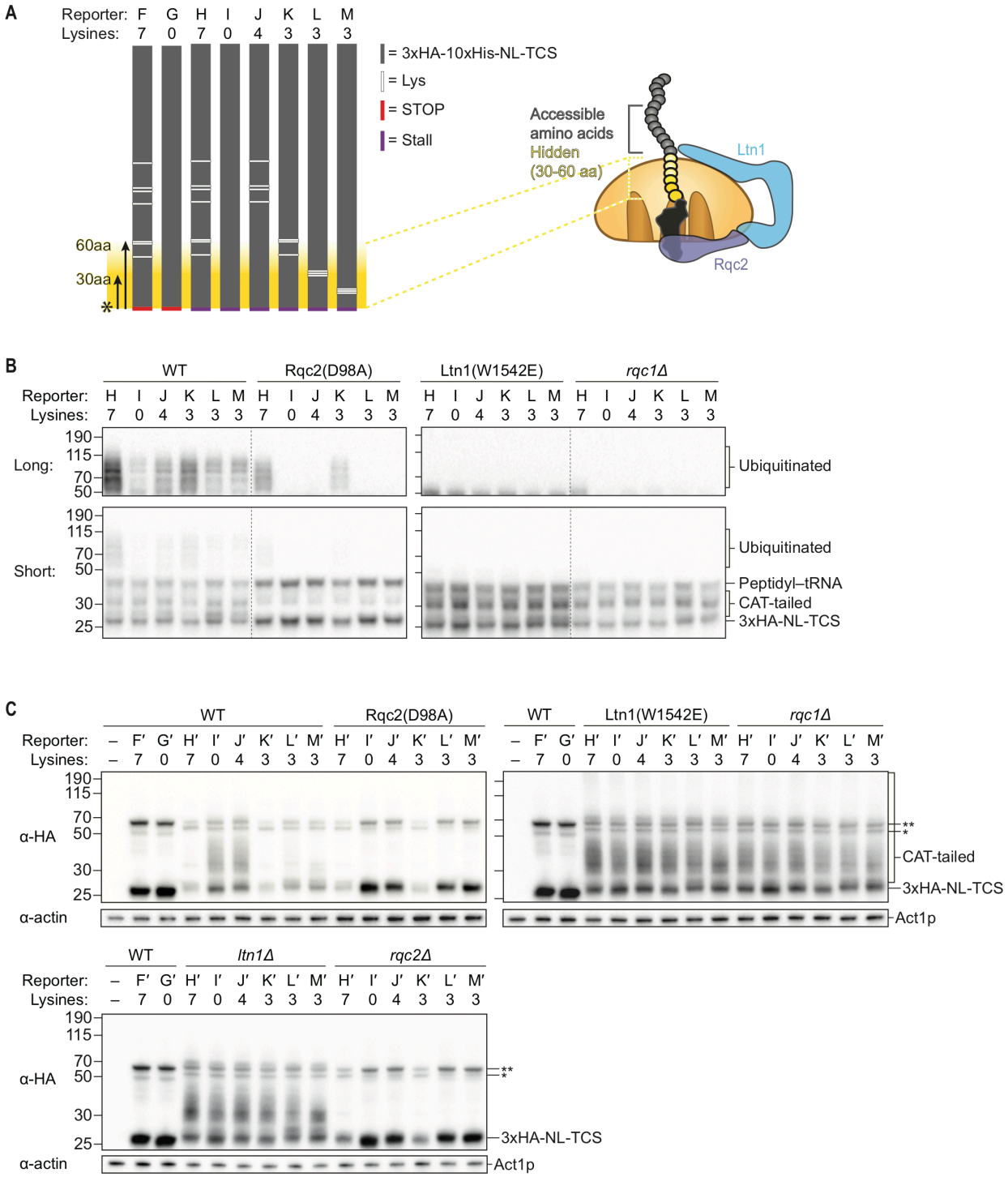

Figure 1-S6. CAT tailing exposes lysines to the Ltn1p RING domain for ubiquitination and subsequent degradation.

(A) Schematic of reporter mRNAs encoding RQC substrates with 0–7 lysines (white lines) at different positions (reporters H-M) and control substrates (reporters F-G). Approximately 30–60 residues can be buried in the ribosome exit tunnel (yellow gradient)—i.e.: Reporters F, H, K and L, M encode lysines located just outside or inside of the ribosome exit tunnel, respectively. (B) Effects of Rqc2p-dependent polypeptide extensions on ubiquitination *in vitro*. ScIVT reactions were conducted with extracts

prepared from strains of the indicated genotypes and supplemented with 100uM ubiquitin. The top panel was exposed longer to amplify detection of ubiquitinated species. Dashed lines indicate that lanes were removed from the original image. (C) Effects of CAT tailing on steady-state protein levels *in vivo*. (′) Denotes *in vivo* equivalent of *in vitro* reporters. RQC reporters encoding different lysine positions and an R12 ribosome-stalling sequence were transformed into strains of the indicated genotypes. Proteins were extracted from mid-log-phase cultures and analyzed for HA-tagged proteins by immunoblotting. (*) Denotes a reporter product generated from read-through of the R12 stalling sequence and (**) denotes an uncleaved product generated due to inefficient 2A activity and read-through of the R12 stalling sequence (refer to Materials and Methods).

Table 1-S1. *S. cerevisiae* strains used in this study.

The names, genetic backgrounds, and protein expression plasmids of the strains generated and used in this study are listed in this table.

Strain	Background	Plasmid
yBAO2112	BY4741	
yBAO2116	BY4741 *ltn1Δ::ura3*	
yBAO2117	BY4741 *rqc1Δ::ura3*	
yBAO2118	BY4741 *rqc2Δ::ura3*	
yBAO2125	BY4741 *hbs1Δ::ura3*	
yBAO2126	BY4741 *dom34Δ::ura3*	
yBAO2128	BY4741 Rqc2p(D98A)	
yBAO2142	W303 *Δbar1 lys2::HisG pep4::KanMX*	pGAL1-Rqc2p-10xHis, HIS3 marker
yBAO2633	W303 *Δbar1 lys2::HisG pep4::KanMX*	pGAL1-Rqc2p(D98A)-10xHis, HIS3 marker
yBAO2634	W303 *Δbar1 lys2::HisG pep4::KanMX*	pGAL1-Ltn1p-10xHis, HIS3 marker
yBAO2635	W303 *Δbar1 lys2::HisG pep4::KanMX*	pGAL1-Ltn1p(W1542E)-10xHis, HIS3 marker
yBAO2636	W303 *Δbar1 lys2::HisG pep4::KanMX*	pGAL1-Rqc1p-10xHis, HIS3 marker

Table 1-S2. DNA sequences of the mRNAs used in this study.

T7 promoter is underlined, 5'- and 3'-UTRs (if any) are in bold, TEV cleavage site (TCS) is in lower case.

mRNA	Sequence 5′ - 3′	Length (bp)
Full-length 3xHA-NL (without lysines):	TAATACGACTCACTATA**GGGAGACCCAAGCTAGCTAGCGTTTAAACTTAAGCTAGGTACCGAGACC**ATGGCCGTTTA CCCATACGATGTTCCTGACTATGCGGGCTATCCCTATGACGTCCCGGACTATGCAGGCTCCTATCCATATGACGTTCC AGATTACGCTGGATCTGGCGTCTTCACACTCGAAGATTTCGTTGGGGACTGGCGACAGACAGCCGGCTACAACCTGG ACCAAGTCCTTGAACAGGGAGGTGTGTCCAGTTTGTTTCAGAATCTCGGGGTGTCCGTAACTCCGATCCAAAGGATTG TCCTGAGCGGTGAAAATGGGCTGCGGATCGACATCCATGTCATCATCCCGTATGAAGGTCTGAGCGGCGACCAAATG GGCCAGATCGAAAGGATTTTTAGAGTGGTGTACCCTGTGGATGATCATCACTTTCGCGTGATCCTGCACTATGGCACA CTGGTAATCGACGGGGTTACGCCGAACATGATCGACTATTTCGGACGGCCGTATGAAGGCATCGCCGTGTTCGACGG CAGACGCATCACTGTAACAGGGACCCTGTGGAACGGCAACAGGATTATCGACGAGCGCCTGATCAACCCCGACGGCT CCCTGCTGTTCCGAGTAACCATCAACGGAGTGACCGGCTGGCGGCTGTGCGAACGCATTCTGGCGTAA**ACTAGTCCA GTGTGGTGGAATTCTGCAGATATCCAGCACAGTGGCGGCCGCTCGAG**	743
Truncated 3xHA-NL (without lysines):	TAATACGACTCACTATA**GGGAGACCCAAGCTAGCTAGCGTTTAAACTTAAGCTAGGTACCGAGACC**ATGGCCGTTTA CCCATACGATGTTCCTGACTATGCGGGCTATCCCTATGACGTCCCGGACTATGCAGGCTCCTATCCATATGACGTTCC AGATTACGCTGGATCTGGCGTCTTCACACTCGAAGATTTCGTTGGGGACTGGCGACAGACAGCCGGCTACAACCTGG ACCAAGTCCTTGAACAGGGAGGTGTGTCCAGTTTGTTTCAGAATCTCGGGGTGTCCGTAACTCCGATCCAAAGGATTG TCCTGAGCGGTGAAAATGGGCTGCGGATCGACATCCATGTCATCATCCCGTATGAAGGTCTGAGCGGCGACCAAATG GGCCAGATCGAAAGGATTTTTAGAGTGGTGTACCCTGTGGATGATCATCACTTTCGCGTGATCCTGCACTATGGCACA CTGGTAATCGACGGGGTTACGCCGAACATGATCGACTATTTCGGACGGCCGTATGAAGGCATCGCCGTGTTCGACGG CAGACGCATCACTGTAACAGGGACCCTGTGGAACGGCAACAGGATTATCGACGAGCGCCTGATCAACCCCGACGGCT CCCTGCTGTTCCGAGTAACCATCAACGGAGTGACCGGCTGGCGGCTGTGCGAACGCATTCTGGCGGTT	687
Truncated 3xHA-NL (with lysines):	TAATACGACTCACTATA**GGGAGACCCAAGCTAGCTAGCGTTTAAACTTAAGCTAGGTACCGAGACC**ATGGCCGTTTA CCCATACGATGTTCCTGACTATGCGGGCTATCCCTATGACGTCCCGGACTATGCAGGCTCCTATCCATATGACGTTCC AGATTACGCTGGATCTGGCGTCTTCACACTCGAAGATTTCGTTGGGGACTGGCGACAGACAGCCGGCTACAACCTGG ACCAAGTCCTTGAACAGGGAGGTGTGTCCAGTTTGTTTCAGAATCTCGGGGTGTCCGTAACTCCGATCCAAAGGATTG TCCTGAGCGGTGAAAATGGGCTGAAGATCGACATCCATGTCATCATCCCGTATGAAGGTCTGAGCGGCGACCAAATG GGCCAGATCGAAAAAATTTTTAAGGTGGTGTACCCTGTGGATGATCATCACTTTAAGGTGATCCTGCACTATGGCACA CTGGTAATCGACGGGGTTACGCCGAACATGATCGACTATTTCGGACGGCCGTATGAAGGCATCGCCGTGTTCGACGG CAAAAAGATCACTGTAACAGGGACCCTGTGGAACGGCAACAAAATTATCGACGAGCGCCTGATCAACCCCGACGGCT CCCTGCTGTTCCGAGTAACCATCAACGGAGTGACCGGCTGGCGGCTGTGCGAACGCATTCTGGCGGTT	687
Truncated 3xHA-NL-TCS (without lysines):	TAATACGACTCACTATA**GGGAGACCCAAGCTAGCTAGCGTTTAAACTTAAGCTAGGTACCGAGACC**ATGGCCGTTTA CCCATACGATGTTCCTGACTATGCGGGCTATCCCTATGACGTCCCGGACTATGCAGGCTCCTATCCATATGACGTTCC AGATTACGCTGGATCTGGCGTCTTCACACTCGAAGATTTCGTTGGGGACTGGCGACAGACAGCCGGCTACAACCTGG ACCAAGTCCTTGAACAGGGAGGTGTGTCCAGTTTGTTTCAGAATCTCGGGGTGTCCGTAACTCCGATCCAAAGGATTG TCCTGAGCGGTGAAAATGGGCTGCGGATCGACATCCATGTCATCATCCCGTATGAAGGTCTGAGCGGCGACCAAATG GGCCAGATCGAAAGGATTTTTAGAGTGGTGTACCCTGTGGATGATCATCACTTTCGCGTGATCCTGCACTATGGCACA CTGGTAATCGACGGGGTTACGCCGAACATGATCGACTATTTCGGACGGCCGTATGAAGGCATCGCCGTGTTCGACGG CAGACGCATCACTGTAACAGGGACCCTGTGGAACGGCAACAGGATTATCGACGAGCGCCTGATCAACCCCGACGGCT CCCTGCTGTTCCGAGTAACCATCAACGGAGTGACCGGCTGGCGGCTGTGCGAACGCATTCTGGCGggaggttcaggttcagg tgaaaatttgtattttcaatctGTT	726
Truncated 3xHA-NL-TCS (with lysines):	TAATACGACTCACTATA**GGGAGACCCAAGCTAGCTAGCGTTTAAACTTAAGCTAGGTACCGAGACC**ATGGCCGTTTA CCCATACGATGTTCCTGACTATGCGGGCTATCCCTATGACGTCCCGGACTATGCAGGCTCCTATCCATATGACGTTCC AGATTACGCTGGATCTGGCGTCTTCACACTCGAAGATTTCGTTGGGGACTGGCGACAGACAGCCGGCTACAACCTGG ACCAAGTCCTTGAACAGGGAGGTGTGTCCAGTTTGTTTCAGAATCTCGGGGTGTCCGTAACTCCGATCCAAAGGATTG TCCTGAGCGGTGAAAATGGGCTGAAGATCGACATCCATGTCATCATCCCGTATGAAGGTCTGAGCGGCGACCAAATG GGCCAGATCGAAAAAATTTTTAAGGTGGTGTACCCTGTGGATGATCATCACTTTAAGGTGATCCTGCACTATGGCACA CTGGTAATCGACGGGGTTACGCCGAACATGATCGACTATTTCGGACGGCCGTATGAAGGCATCGCCGTGTTCGACGG CAAAAAGATCACTGTAACAGGGACCCTGTGGAACGGCAACAAAATTATCGACGAGCGCCTGATCAACCCCGACGGCT CCCTGCTGTTCCGAGTAACCATCAACGGAGTGACCGGCTGGCGGCTGTGCGAACGCATTCTGGCGggaggttcaggttcagg tgaaaatttgtattttcaatctGTT	726
Truncated 3xHA-10xHis-NL (without lysines):	TAATACGACTCACTATA**GGGAGACCCAAGCTAGCTAGCGTTTAAACTTAAGCTAGGTACCGAGACC**ATGGCCGTTTA CCCATACGATGTTCCTGACTATGCGGGCTATCCCTATGACGTCCCGGACTATGCAGGCTCCTATCCATATGACGTTCC AGATTACGCTGGATCTGGCCATCACCATCATCACCATCACCATCATCACGGATCTGGCGTCTTCACACTCGAAGATTT CGTTGGGGACTGGCGACAGACAGCCGGCTACAACCTGGACCAAGTCCTTGAACAGGGAGGTGTGTCCAGTTTGTTTC AGAATCTCGGGGTGTCCGTAACTCCGATCCAAAGGATTGTCCTGAGCGGTGAAAATGGGCTGCGGATCGACATCCAT GTCATCATCCCGTATGAAGGTCTGAGCGGCGACCAAATGGGCCAGATCGAAAGGATTTTTAGAGTGGTGTACCCTGT GGATGATCATCACTTTCGCGTGATCCTGCACTATGGCACACTGGTAATCGACGGGGTTACGCCGAACATGATCGACTA TTTCGGACGGCCGTATGAAGGCATCGCCGTGTTCGACGGCAGACGCATCACTGTAACAGGGACCCTGTGGAACGGC AACAGGATTATCGACGAGCGCCTGATCAACCCCGACGGCTCCCTGCTGTTCCGAGTAACCATCAACGGAGTGACCGG CTGGCGGCTGTGCGAACGCATTCTGGCGGTT	726
Truncated 3xHA-10xHis-NL (with lysines):	TAATACGACTCACTATA**GGGAGACCCAAGCTAGCTAGCGTTTAAACTTAAGCTAGGTACCGAGACC**ATGGCCGTTTA CCCATACGATGTTCCTGACTATGCGGGCTATCCCTATGACGTCCCGGACTATGCAGGCTCCTATCCATATGACGTTCC AGATTACGCTGGATCTGGCcatCACCATCATCACCATCACCATCATCACGGATCTGGCGTCTTCACACTCGAAGATTTC GTTGGGGACTGGCGACAGACAGCCGGCTACAACCTGGACCAAGTCCTTGAACAGGGAGGTGTGTCCAGTTTGTTTCA GAATCTCGGGGTGTCCGTAACTCCGATCCAAAGGATTGTCCTGAGCGGTGAAGATCGACATCCATG TCATCATCCCGTATGAAGGTCTGAGCGGCGACCAAATGGGCCAGATCGAAAAAATTTTTAAGGTGGTGTACCCTGTGG ATGATCATCACTTTAAGGTGATCCTGCACTATGGCACACTGGTAATCGACGGGGTTACGCCGAACATGATCGACTATT TCGGACGGCCGTATGAAGGCATCGCCGTGTTCGACGGCAAAAAGATCACTGTAACAGGGACCCTGTGGAACGGCAA CAAAATTATCGACGAGCGCCTGATCAACCCCGACGGCTCCCTGCTGTTCCGAGTAACCATCAACGGAGTGACCGGCT GGCGGCTGTGCGAACGCATTCTGGCGGTT	726

CHAPTER 2

Listeria phages induce Cas9 degradation to protect lysogenic genomes

Listeria phages induce Cas9 degradation to protect lysogenic genomes

Beatriz A. Osuna[1], Shweta Karambelkar[1], Caroline Mahendra[1], Kathleen A. Christie[2,3,4], Bianca Garcia[5], Alan R. Davidson[5,6], Benjamin P. Kleinstiver[2,3,4], Samuel Kilcher[7], Joseph Bondy-Denomy[1,8,9,*]

[1] Department of Microbiology and Immunology, University of California, San Francisco, San Francisco, CA 94158, USA
[2] Center for Genomic Medicine, Massachusetts General Hospital, Boston, MA 02114, USA
[3] Department of Pathology, Massachusetts General Hospital, Boston, MA 02114, USA
[4] Department of Pathology, Harvard Medical School, Boston, MA 02115, USA
[5] Department of Molecular Genetics, University of Toronto, Toronto, ON M5G 1M1, Canada
[6] Department of Biochemistry, University of Toronto, Toronto, ON M5G 1M1, Canada
[7] Institute of Food, Nutrition, and Health, ETH Zurich, Zurich CH 8092, Switzerland
[8] Quantitative Biosciences Institute, University of California, San Francisco, San Francisco, CA 94158, USA

This work was posted to bioRxiv as a preprint: doi.org/10.1101/787200

ABSTRACT

Bacterial CRISPR-Cas systems employ RNA-guided nucleases to destroy foreign DNA. Bacteriophages, in turn, have evolved diverse “anti-CRISPR” proteins (Acrs) to counteract acquired immunity. In *Listeria monocytogenes*, prophages encode 2-3 distinct anti-Cas9 proteins, with *acrIIA1* always present; however, its mechanism is unknown. Here, we report that AcrIIA1 binds with high affinity to Cas9 via the catalytic HNH domain and, in *Listeria*, triggers Cas9 degradation. AcrIIA1 displays broad-spectrum inhibition of Type II-A and II-C Cas9s, including an additional highly-diverged *Listeria* Cas9. During lytic infection, AcrIIA1 is insufficient for rapid Cas9 inactivation, thus phages require an additional “partner” Acr that rapidly blocks Cas9-DNA-binding. The AcrIIA1 N-terminal domain (AcrIIA1^{NTD}) is dispensable for anti-CRISPR activity; instead it is required for optimal phage replication through direct transcriptional repression of the anti-CRISPR locus. AcrIIA1^{NTD} is widespread amongst *Firmicutes*, can repress anti-CRISPR deployment by other phages, and has been co-opted by hosts potentially as an “anti-anti-CRISPR.” In summary, *Listeria* phages utilize narrow-spectrum inhibitors of DNA binding to rapidly inactivate Cas9 in lytic growth and the broad-spectrum AcrIIA1 to stimulate Cas9 degradation for protection of the *Listeria* genome in lysogeny.

INTRODUCTION

All cells must combat viral infections to survive. Bacteria have evolved innate and adaptive defense mechanisms against bacterial viruses (phages), which constantly pose a risk of infection. One such defense mechanism is CRISPR-Cas, a common and diverse adaptive immune system in prokaryotes that encompasses two distinct classes and six types (I-VI) (Koonin et al., 2017; Makarova et al., 2015). The CRISPR array maintains a genetic record of past viral infections with phage DNA fragments (spacers) retained between clustered regularly interspaced short palindromic repeats (CRISPR) (Mojica et al., 2005). These phage-derived spacers are transcribed into CRISPR RNAs (crRNAs) that complex with Cas nucleases to guide the sequence-specific destruction of invading nucleic acids (Brouns et al., 2008; Garneau et al., 2010). The CRISPR-associated (cas) genes typically neighbor the CRISPR array and encode proteins that facilitate spacer acquisition into the CRISPR array (Nuñez et al., 2014; Yosef et al., 2012), generate mature crRNAs (Deltcheva et al., 2011; Haurwitz et al., 2010), and cleave invading genomes (Garneau et al., 2010).

To counteract bacterial immunity, phages have evolved multiple mechanisms of CRISPR-Cas evasion (Borges et al., 2017). Phage-encoded anti-CRISPR proteins that directly inhibit type I-C, I-D, I-E, I-F, II-A, II-C, and V-A CRISPR-Cas systems have been identified (Hwang and Maxwell, 2019; Trasanidou et al., 2019). These anti-CRISPRs have distinct protein sequences, structures, and mechanisms of inactivation. Some anti-CRISPRs block CRISPR-Cas target DNA binding by steric occlusion and DNA mimicry (Bondy-Denomy et al., 2015; Dong et al., 2017; Jiang et al., 2019; Liu et al., 2019; Shin et al., 2017; Yang and Patel, 2017), guide-RNA loading interference (Thavalingam et al., 2019; Zhu et al., 2019), and effector dimerization (Fuchsbauer et al., 2019; Harrington et al., 2017; Zhu et al., 2019). Other anti-CRISPRs prevent DNA cleavage by interacting with the catalytic domain of Cas nucleases (Bondy-Denomy et al., 2015; Harrington et al., 2017). Anti-CRISPRs that inactivate Type II

CRISPR-Cas systems, which are widely utilized for genome editing applications, have been extensively characterized in biochemical and heterologous cell-based systems (Bondy-Denomy, 2018; Yao et al., 2018). However, few studies have examined anti-CRISPR functions in the natural context of phage-bacteria warfare (Hynes et al., 2017, 2018).

In the lytic cycle, phage replication causes host cell lysis, whereas in lysogeny, temperate phages integrate into the bacterial chromosome and become prophages. The bacterial host and prophage replicate together during lysogeny and prophages can contribute novel genes that provide fitness benefits or even serve as regulatory switches (Argov et al., 2017; Bondy-Denomy et al., 2016; Borges et al., 2017; Chen et al., 2005; Feiner et al., 2015). In *Listeria monocytogenes,* some prophages employ "active lysogeny" during mammalian cell infection, wherein temporary prophage excision from the bacterial chromosome allows expression of the *comK* gene required for *Listeria* replication in macrophages (Rabinovich et al., 2012). Prophages also inactivate CRISPR-Cas in *L. monocytogenes* through the expression of anti-CRISPR proteins (Rauch et al., 2017). In lysogens with CRISPR arrays encoding spacers that target the prophage (i.e. self-targeting), anti-CRISPRs are essential for host and prophage survival. Whether anti-CRISPRs play distinct roles during lysogeny or lytic growth when expressed by temperate phages is unknown.

Here, we show that the *Listeria* phage protein AcrIIA1 selectively triggers degradation of catalytically active Cas9*,* through a direct interaction between the AcrIIA1^{CTD} (C-terminal domain) unstructured loop and Cas9 HNH domain. AcrIIA1 is sufficient to stabilize CRISPR-targeted prophages, but is ineffective during lytic replication. This inactivity necessitates the co-existence of AcrIIA1 with an anti-CRISPR (e.g. AcrIIA2, AcrIIA4, or AcrIIA12, identified here) that rapidly blocks Cas9 during lytic infection. While highly conserved across AcrIIA1 homologs, the AcrIIA1^{NTD} (N-terminal domain) is completely dispensable for anti-CRISPR activity and is instead a crucial repressor of *acr* locus transcription, a requirement for optimal phage fitness.

RESULTS

AcrIIA1 interacts with Cas9 and triggers its degradation

To determine the AcrIIA1 mechanism of action, we first attempted to immunoprecipitate Cas9 from *L. monocytogenes* (*Lmo*10403s) strains, where AcrIIA1 was expressed from one of three prophages (ΦA006, ΦA118, and ΦJ0161a). Surprisingly, upon immunoblotting for Cas9 protein, we observed highly reduced Cas9 levels in these lysogens (Figure 2-1A). Transcriptional and translational reporters revealed that transcript levels were unaffected, while the protein reporter levels decreased by ~70% (Figure 2-1A). RT-qPCR experiments confirmed Cas9 mRNA levels were unaffected in each lysogen (Figure 2-S1A). AcrIIA1 alone, but not AcrIIA4, was sufficient to mediate decreased Cas9 levels in both reporter and western blot assays (Figure 2-1B). The well-studied orthologue, SpyCas9 (53% amino acid identity to LmoCas9), displayed the same post-transcriptional AcrIIA1-dependent loss of Cas9 when introduced into *L. monocytogenes* (Figure 2-1B).

To assay for a direct interaction *in vitro*, AcrIIA1 and SpyCas9 were purified (LmoCas9 was insoluble). AcrIIA1 and the SpyCas9-gRNA complex interacted with high affinity (K_D = 23 ± 15 nM) by microscale thermophoresis (MST), comparable to AcrIIA2b.3 (K_D = 20 ± 11 nM), a well-characterized Cas9-interactor (Jiang et al., 2019; Liu et al., 2019) (Figure 2-1C). Additionally, AcrIIA1 interacted with ApoCas9, unlike AcrIIA2b.3, suggesting a unique binding mechanism (Figure 2-S1B). Neither binding event was sufficient to degrade Cas9 *in vitro,* nor was the protein destabilized when subjected to limited proteolysis (Figure 2-S1C). We therefore considered whether the cellular environment of *L. monocytogenes* stimulates Cas9 degradation when bound by AcrIIA1. Indeed, we observed an accelerated decay of SpyCas9 protein upon induction of AcrIIA1 compared to treatment with a translation inhibitor, gentamicin (Figures 2-1D and 2-S1D). In contrast, SpyCas9 protein increased over time when AcrIIA1 was not induced; similar to strains expressing AcrIIA4 or lacking an anti-CRISPR (Figures 2-1D and 2-S1D).

However, we paradoxically observed that AcrIIA1 did not inhibit catalytically-dead Cas9 (dCas9) in a CRISPRi assay using Lmo- or Spy- dCas9 engineered to repress RFP expression (Figures 2-1E and 2-S1F), but did inhibit active Cas9 in an isogenic self-targeting strain (Figure 2-1F). Consistent with these findings, lysogens expressing AcrIIA1 or AcrIIA4 alone or together also revealed no significant decrease in dCas9 levels (Figures 2-1G and 2-S1H), whereas active Cas9 protein diminished by ~70% in all AcrIIA1-expressing lysogens (Figures 2-1G, 2-S1G and 2-S1H). Therefore, AcrIIA1 has a mechanism to detect catalytically active Cas9 protein and trigger its degradation.

Given the discrepant outcomes between Cas9 and dCas9, the ability of AcrIIA1 to bind these proteins *in vitro* was assessed. AcrIIA1 interacted with dCas9-gRNA ~40-fold weaker (K_D = 905 ± 874 nM) than with Cas9-gRNA (Figures 2-1C, 2-1H and 2-S1I). Only two residues differ between catalytically active Cas9 and dCas9 (D10A and H840A). AcrIIA1 binding to Cas9(D10A) (K_D = ~38 nM) was similar to wild-type Cas9 (K_D = ~23, Figure 2-1), whereas binding to Cas9(H840A) was ~80-fold weaker (K_D = 2 ± 4 μM) (Figures 2-1H and 2-S1I). AcrIIA2b.3, which binds the PAM-interacting domain, displayed no difference in binding affinity to the four Cas9 variants (K_D = 18 – 38 nM) (Figures 2-1H and 2-S1I). Therefore, we conclude that AcrIIA1 triggers the degradation of catalytically active Cas9 in *L. monocytogenes* through a direct interaction with the Cas9 HNH domain (where H840 resides).

AcrIIA1 protects CRISPR-targeted prophages but fails during lytic replication

Given that AcrIIA1 triggers Cas9 degradation, a mechanism not previously observed for any anti-CRISPR, we sought to determine when this activity manifests in the phage life cycle. Isogenic ΦA006 phages were engineered to encode no anti-CRISPR, *acrIIA1*, *acrIIA4*, or *acrIIA1* and *acrIIA4* together, and assessed along with wild-type (WT) phages, during lytic and lysogenic infection. When infecting *Lmo*10403s expressing Cas9 and a native ΦA006-targeting spacer sequence, phages encoding only *acrIIA1* surprisingly failed to replicate, similar to a Δ*acr* phage (efficiency of plaquing, EOP ≤ $3x10^{-5}$, Figures 2-2A and 2-S2A). Phages encoding

acrIIA4 replicated well (EOP = 0.1 – 0.7, depending *on acrIIA4* expression strength), similar to WT ΦA006 (EOP ≥ 0.7), with no added benefit derived from *acrIIA1* (Figures 2-2A and 2-S2A). In contrast, during lysogeny, ΦA006 prophages encoding *acrIIA1* completely prevented self-targeting upon Cas9 induction, whereas lysogens lacking an anti-CRISPR (Δ*acr*) died (Figure 2-2B). The remarkable difference in AcrIIA1 efficacy during lytic and lysogenic growth bolsters a conclusion that the Cas9 degradative mechanism is optimal for the lysogenic lifestyle, but not fast enough for inactivation during lytic replication.

Given the inability of AcrIIA1 to inhibit Cas9 during lytic infection, phages may need additional Cas9 inhibitors. Indeed, in 119 *Listeria* prophage genomes analyzed, 77% encode *acrIIA1* with at least one additional *acrIIA* gene (i.e. *acrIIA2-A4*), 13% possess *acrIIA1* without a known *acrIIA* neighbor (including WT ΦA006), and 10% encode *orfD* (a distant *acrIIA1* orthologue), along with other uncharacterized ORFs (Rauch et al., 2017). The WT ΦA006 phage, which has *acrIIA1* and no other known *acr*, replicated far better (EOP ≥ 0.7) than a phage encoding *acrIIA1* alone, suggesting an additional Cas9 inhibitor in this phage (Figures 2-2A and 2-S2A). Engineered phages encoding the gene adjacent to *acrIIA1* restored phage lytic replication (EOP ≥ 0.5) and revealed a new anti-CRISPR, AcrIIA12, which also inhibited Lmo (but not Spy) dCas9-based CRISPRi (Figures 2-2A, 2-S2A and 2-S2B). Notably, we observed the presence of *acrIIA12* in every *acr* locus previously reported to encode only *acrIIA1,* indicating that prophages do not encode *acrIIA1* alone. Therefore, *Listeria* prophages most commonly encode *acrIIA1,* which triggers Cas9 degradation to ensure stable lysogeny, in combination with a Cas9 interactor that blocks DNA binding (AcrIIA2, AcrIIA4, or AcrIIA12) for successful lytic replication.

AcrIIA1 utilizes an unstructured C-terminal loop to inactivate Cas9

The AcrIIA1 crystal structure revealed a two-domain architecture, with a helix-turn-helix (HTH)-containing AcrIIA1^{NTD} similar to known transcriptional repressors and an extended AcrIIA1^{CTD} of unknown function (Ka et al., 2018). Surprisingly, the AcrIIA1^{CTD} was sufficient for

anti-CRISPR function, protection from self-targeting, and triggering Cas9 protein degradation, while the AcrIIA1^{NTD} displayed no evidence of Cas9 regulation (Figures 2-S2C and 2-S2D). To identify AcrIIA1 residues required for anti-CRISPR function, we conducted multi-sequence alignments and used our previously developed heterologous *P. aeruginosa* anti-SpyCas9 screening platform (Jiang et al., 2019). AcrIIA1 homologs were identified in mobile genetic elements of *Listeria, Enterococcus, Lactobacillus,* and *Leuconostoc* species, ranging from 22% to 77% protein sequence identity (Figures 2-2C and 2-S4D). Homology was driven by obvious sequence similarity in the NTD, with CTD conservation in only a subset of proteins. AcrIIA1 homologs with conserved CTDs displayed anti-SpyCas9 activity (except AcrIIA1$_{LMO10}$), whereas the three proteins with highly diverged CTDs (including *orfD*) did not (Figures 2-2D and 2-S3A). Alanine scanning mutagenesis of the conserved amino acids present in AcrIIA1 homologs identified a stretch of aromatic and charged residues in an unstructured region of the AcrIIA1^{CTD} (P112 to R117) that were required for complete anti-CRISPR activity (Figures 2-2E and 2-S3A). Expression levels of each mutant protein were unperturbed relative to WT AcrIIA1 (Figure 2-S3B). The F115A mutation completely abolished anti-CRISPR function (Figures 2-2E and 2-S3A) and the interaction with Cas9 (Figures 2-2F, 2-S2F and 2-S2G). In *Listeria,* AcrIIA1(F115A) and AcrIIA1(T114A/F115A) mutants failed to protect cells from genomic self-targeting (Figure 2-S2C) and these mutations either completely (T114A/F115A) or partially (F115A) restored Cas9 protein levels (Figure 2-S2E).

When verifying expression of AcrIIA1 mutants, we observed that AcrIIA1-mediated inhibition does not trigger Cas9 degradation in *P. aeruginosa* (Figure 2-S3B). Yet, similar to in *Listeria,* AcrIIA1 still displayed robust anti-CRISPR activity, inactivating Cas9 in phage-targeting and self-targeting experiments, while not interfering with CRISPRi (Figures 2-S3A and 2-S3C). Since AcrIIA1 can apparently inhibit Cas9 without causing degradation, we immunoprecipitated Cas9 bound to AcrIIA1 or the control AcrIIA4 from *P. aeruginosa* (Figures 2-2F and 2-S2F) and assessed DNA cleavage activity *in vitro*. Cas9 was functional when immunoprecipitated alone

but inhibited when co-purified with AcrIIA1 or AcrIIA4 (Figure 2-2G and 2-S2H). The AcrIIA1 mutants (F115A and T114A/F115A) interacted with Cas9 very weakly (Figures 2-2F, 2-S2F and 2-S2G) and had little impact on DNA cleavage (Figure 2-S2H). Interestingly, *in vitro* experiments with individually purified proteins revealed that AcrIIA1 is not sufficient to inhibit Cas9-mediated DNA cleavage (Figure 2-S2I), despite its strong binding affinity, suggesting an additional cellular factor is required to inactivate Cas9. This putative multi-step process may explain why inhibition does not manifest immediately during lytic growth. Therefore, AcrIIA1 utilizes conserved residues in its CTD to interact with the Cas9 HNH domain, blocking DNA cleavage and triggering Cas9 protein degradation in *Listeria*. In a foreign host potentially lacking the Cas9-degrading pathway, DNA cleavage inhibition manifests.

AcrIIA1 is a broad-spectrum Cas9 inhibitor

Given the ability of AcrIIA1 to inactivate Cas9 via recognition of a highly conserved catalytic residue, we assessed inhibition of diverged Cas9 orthologues. In *Escherichia coli* strains expressing Type II-A, II-B, and II-C Cas9 proteins (Figure 2-3A) targeting phage Mu, AcrIIA1 intermediately or completely inhibited four Type II-C (Boe, Hpa, Cje, and Geo) and two Type II-A (Sau and Spy) Cas9s (Figures 2-3B and 2-S3D). In contrast, AcrIIA2 only weakly inhibited Hpa and SpyCas9, while AcrIIA4 only inactivated SpyCas9 (Figure 2-3B). Considering the biological driver of broad-spectrum Cas9 inhibition by AcrIIA1, a smaller Type II-A Cas9 (1,078 a.a.) was recently discovered in *L. ivanovii* (LivCas9) (Hupfeld et al., 2018) with similarities to other small Cas9 proteins (e.g. SauCas9) and Type II-C orthologues (Figure 2-3A). In *Listeria* strains expressing the small LivCas9 variant programmed to target phage ΦP35 or ΦA511, AcrIIA1 inhibited LivCas9 (Figures 2-3C and 2-S3E). Thus, AcrIIA1 displays broad-spectrum activity against diverged Cas9 nucleases, whereas the well-characterized DNA binding inhibitors, AcrIIA2 and AcrIIA4, are much narrower in their inhibitory spectrum. This broad-spectrum inhibition also likely explains the utility of AcrIIA1 to phages infecting *Listeria,* where two distinct Cas9 orthologues are encountered.

The robust AcrIIA1 activity observed in various heterologous hosts led us to assess inhibition of Cas9 gene editing in human cells. We employed a deep sequencing-based approach to improve the dynamic range of edit detection, in comparison to our previous GFP-disruption assay (Rauch et al., 2017). HEK 293T cells were co-transfected with plasmids encoding *acrIIA1, cas9,* and sgRNAs targeting endogenous human sequences and editing efficacy was evaluated after 3 days. AcrIIA1 blocked the gene editing activity of SpyCas9 by 50-70% and of CjeCas9, SauCas9, St3Cas9, and NmeCas9 moderately, whereas AcrIIA4 only inhibited SpyCas9 (Figures 2-3D and 2-S3E). Thus, AcrIIA1 inactivates diverse Cas9 orthologues in many heterologous systems, including bacteria (*L. monocytogenes, P. aeruginosa, E. coli*), yeast (Nakamura et al., 2019), and human cells, providing a genome editing modulator that specifically prevents Cas9 DNA cleavage. Future work is needed to enhance its efficiency, however.

acr locus repression by AcrIIA1^{NTD} promotes general lytic growth and prophage induction

While interrogating the requirements for anti-CRISPR function, we observed that two engineered phages with deletions in their anti-CRISPR locus (ΦA006Δ*acr* and ΦJ0161aΔ*acrIIA1-2*) displayed a Cas9-independent lytic growth defect (Figure 2-4A). This defect was rescued by the provision of *acrIIA1^{NTD}* in *trans* or by engineering an ΦA006 phage to express only the *acrIIA1^{NTD}* (Figure 2-4A). Moreover, all engineered ΦA006 phages expressing an anti-CRISPR (e.g. *acrIIA1^{CTD}*, *acrIIA4, acrIIA12*) without the *acrIIA1^{NTD}* displayed a decrease in phage titer (PFU/mL) that was restored by *acrIIA1^{NTD} trans*- or *cis*-complementation (Figure 2-4A). The phage expressing only *acrIIA1^{CTD}* (only observed fused to *acrIIA1^{NTD}* in genomes) displayed the strongest lytic defect amongst the ΦA006 phages, while simply separating the two AcrIIA1 domains had no deleterious effect (Figure 2-4A). ΦJ0161aΔ*acrIIA1-2* had the most drastic lytic defect, failing to replicate unless complemented in *trans* with the *acrIIA1^{NTD}* (Figure 2-4A). Moreover, the ΦJ0161aΔ*acrIIA1-2* prophage displayed a Cas9-independent prophage induction deficiency, yielding 25-fold less phage during mitomycin C induction, compared to the

WT prophage or the *acrIIA1*-complemented mutant (Figure 2-4B). Attempts to efficiently induce ΦA006 prophages were unsuccessful, as previously observed (Loessner, 1991; Loessner et al., 1991). Therefore, aside from acting as an anti-CRISPR, AcrIIA1 plays an important Cas9-independent role in the phage life cycle, promoting optimal lytic replication and lysogenic induction.

AcrIIA1^{NTD} contains an HTH motif with strong similarity to transcriptional repressors (Ka et al., 2018). Due to the Cas9-independent growth defects described above, we considered whether regulation of the anti-CRISPR locus is required. Alignments of the anti-CRISPR promoters of ΦA006, ΦJ0161, and ΦA118 revealed a highly conserved palindromic sequence (Figures 2-4C and S4A). An RFP transcriptional reporter assay showed that full-length AcrIIA1 and AcrIIA1^{NTD}, but not AcrIIA1^{CTD}, repress the ΦA006 anti-CRISPR promoter (Figure 2-4E, left). *In vitro* MST binding assays confirmed that AcrIIA1 (K_D = 26 ± 10 nM) or AcrIIA1^{NTD} (K_D = 28 ± 3 nM) bind the anti-CRISPR promoter with high affinity (Figures 2-4D and 2-S4B). Moreover, mutagenesis of the palindromic sequence prevented AcrIIA1-mediated repression of the ΦA006 anti-CRISPR promoter (Figure 2-4E, right) and abolished promoter binding *in vitro* (Figure 2-4D). Alanine scanning mutagenesis of conserved residues predicted to be important for DNA binding and dimerization (Ka et al., 2018) identified AcrIIA1^{NTD} residues L10, T16, and R48 as critical for transcriptional repression, whereas AcrIIA1^{CTD} mutations had little effect (Figure 2-4F). Finally, we observed that Cas9 degradation induced by prophage-expressed AcrIIA1 in *L. monocytogenes* (Figure 2-1A) could be prevented by AcrIIA1^{NTD} overexpression, due to repression of the anti-CRISPR locus (Figure 2-4G). Thus, the AcrIIA1^{NTD}-HTH domain represses anti-CRISPR transcription through a highly conserved operator, which is required for optimal phage fitness.

Transcriptional autoregulation is a general feature of the AcrIIA1 superfamily

Recent studies have reported transcriptional autoregulation of anti-CRISPR loci by HTH-proteins in phages that infect Gram-negative *Proteobacteria,* as a mechanism to limit excessive

transcription and downstream transcriptional conflict (Birkholz et al., 2019; Stanley et al., 2019). To determine whether anti-CRISPR locus regulation is similarly pervasive amongst mobile genetic elements in the Gram-positive *Firmicutes* phylum, we assessed AcrIIA1 homologs for transcriptional repression of their predicted cognate promoters and our model ΦA006 phage promoter. Homologs sharing amino acid sequence identity from 21% (i.e. OrfD) to 72% with AcrIIA1^{NTD} were selected from *Listeria, Enterococcus, Leuconostoc,* and *Lactobacillus* (Figure 2-4H and 2-S4D). All AcrIIA1 homologs repressed transcription of their cognate promoters by 42-99%, except AcrIIA1 from *Lactobacillus parabuchneri,* where promoter expression was undetectable in a foreign host (Figures 2-4H and 2-S4C). Strong repression of the model ΦA006 promoter was seen by *Listeria* orthologues possessing ≥68% protein sequence identity (Figure 2-4H). Likewise, AcrIIA1$_{ΦA006}$ repressed the promoters of AcrIIA1 orthologues that repressed the ΦA006 promoter (Figure 2-4I). Interestingly, the AcrIIA1$_{LMO10}$ homolog, which previously displayed no anti-CRISPR activity despite possessing 85% AcrIIA1^{CTD} sequence identity (Figures 2-2D and 2-S3A), contains an AcrIIA1^{NTD} palindromic binding site overlapping its protein-coding sequence. AcrIIA1$_{LMO10}$ anti-CRISPR function manifested when the AcrIIA1^{NTD} binding site was disrupted with silent mutations (Figure 2-S3A). Altogether, these findings demonstrate that the anti-CRISPR promoter-AcrIIA1^{NTD} repressor relationship is highly conserved.

Host-encoded AcrIIA1^{NTD} blocks phage anti-CRISPR deployment

Given that the AcrIIA1^{NTD} represses anti-CRISPR transcription, we wondered whether bacteria could co-opt this activity and manifest it in *trans*, inhibiting a phage from deploying its anti-CRISPR arsenal. We observed that ΦA006-derived phages encoding anti-CRISPRs were rendered vulnerable to Cas9 targeting when the host expressed anti-CRISPR-deficient AcrIIA1 mutants or AcrIIA1^{NTD} (Figure 2-5A). A panel of distinct anti-CRISPR-encoding phages also became vulnerable to Cas9 targeting when AcrIIA1^{NTD} was expressed from a plasmid (Figure 2-5B) or from an integrated single-copy *acrIIA1^{NTD}* driven by a prophage promoter (Figure 2-S5A).

Each of these phages possesses complete or partial spacer matches to the *Lmo*10403s CRISPR array. In contrast, replication of the non-targeted phage, ΦJ0161a, was unperturbed (Figure 2-5B). This demonstrates that host or mobile elements can use this repressor as an "anti-anti-CRISPR" to block anti-CRISPR synthesis, which may be particularly advantageous, if infecting phages encode other anti-CRISPR proteins (e.g. against the *Listeria* Type I-B CRISPR-Cas system).

The widespread prevalence of AcrIIA1 is driven by AcrIIA1^{NTD}, with orthologues in many *Firmicutes* including *Enterococcus, Bacillus, Clostridium, and Streptococcus.* The AcrIIA1^{NTD} can be found either without a CTD or with a distinct CTD sequence. Diverged AcrIIA1^{CTDs} may represent novel anti-CRISPRs, inhibiting CRISPR-Cas systems in their respective hosts. In *Lactobacillus* sp., for example, there are full-length prophage proteins that lacked anti-SpyCas9 function and contain a novel AcrIIA1^{CTD} (Figures 2-2C, 2-2D and 2-S3A). In other instances, core bacterial genomes encode AcrIIA1^{NTD} orthologues that are short ~70-80 amino acid proteins possessing only the HTH domain. In particular, *Lactobacillus delbrueckii* strains contain an AcrIIA1^{NTD} homolog (35% identical, 62% similar to AcrIIA1$_{\Phi A006}$) with key residues conserved (e.g. L10 and T16). Although there are no known *Lactobacillus* phages that express anti-CRISPRs, this bacterial *acrIIA1^{NTD}* gene may perform an "anti-anti-CRISPR" function. Remarkably, we observe that this AcrIIA1^{NTD} homolog is always a genomic neighbor of either the Type I-E, I-C, or II-A CRISPR-Cas systems in *L. delbrueckii* (Figure 2-5C). This association is supportive of a role that enables these CRISPR-Cas systems to function by repressing the deployment of phage inhibitors against each system. The functions of these diverse AcrIIA1 orthologues found in different bacteria, many of which act as transcriptional repressors (Figure 2-4H), remain to be elucidated.

DISCUSSION

Listeria temperate phages commonly encode the multifunctional AcrIIA1 protein for protection against CRISPR-Cas and autorepression of anti-CRISPR transcription. The broad-spectrum AcrIIA1 is sufficient for Cas9 inactivation during lysogeny, but a nonfunctional anti-CRISPR during lytic growth, perhaps due to slow kinetics of Cas9 cleavage inhibition or degradation. Thus, AcrIIA1 always coexists with a distinct anti-Cas9 protein (e.g. AcrIIA2, AcrIIA4, AcrIIA12) that is much narrower in its inhibitory spectrum, but rapidly inactivates Cas9 during lytic replication. Therefore, *Listeria* temperate phages have evolved multiple anti-CRISPRs with distinct Cas9 binding sites and inactivation mechanisms because they synergistically grant unique advantages in each stage of the temperate phage life cycle (see model, Figure 2-6). While "partner" proteins AcrIIA4 and AcrIIA12 also protected CRISPR-targeted prophages, only AcrIIA1 triggered Cas9 degradation, presumably enhancing the likelihood of long-term stability in lysogeny. *Listeria* lysogens were devoid of Cas9 even when *acrIIA1* was co-encoded with other *acrs*, supporting that Cas9 degradation is the dominant inactivation mechanism in lysogeny. Given that Cas9 is required for selection of functional spacers by recognizing the correct PAM (Heler et al., 2015), eliminating this nuclease could also prevent acquisition of lethal self-targeting spacers.

Notably, this is the first report of an anti-CRISPR that reduces Cas protein levels and is also the first with an additional role integral to the phage life cycle. The highly conserved AcrIIA1^{NTD} plays a general Cas9-independent role by autorepressing *acr* locus transcription to promote phage lytic growth and prophage induction. Engineered phages expressing the AcrIIA1^{CTD} alone had a strong lytic growth defect, perhaps suggesting the AcrIIA1 domains are fused in nature to limit expression of an otherwise problematic anti-CRISPR. Interestingly, when the bacterial host expresses AcrIIA1^{NTD}, an "anti-anti-CRISPR" activity manifests, blocking anti-CRISPR expression from infecting or integrated phages. Thus, the importance of the conserved

anti-CRISPR locus repression mechanism may represent a weakness that can be exploited by the host through the co-opting of this anti-CRISPR regulator.

Many diverse Cas9 orthologues have been identified and AcrIIA1 can inhibit highly distinct II-A and II-C subtypes. This provides a unique advantage to *Listeria* phages, inhibiting a small LivCas9 variant (25% amino acid identity to large LmoCas9) that is also found in *L. monocytogenes* strains. LivCas9 also shares similarity with Type II-C Cas9s, likely explaining the biological basis of AcrIIA1 activity against the II-C subtypes. Broad-spectrum inhibition by AcrIIA1 is likely due to targeting the highly conserved Cas9 HNH domain catalytic site, whereas the DNA binding inhibitors (AcrIIA2, AcrIIA4, AcrIIA12) are far more limited. AcrIIC1 was similarly reported to block various Type II-C orthologues by directly binding Cas9 (Apo or gRNA-bound) via the HNH domain (Harrington et al., 2017). Much like AcrIIA1, AcrIIC1 binds the NmeCas9 HNH domain with strong affinity (K_D = 6.3 nM; Harrington et al., 2017), but it is a rather weak anti-CRISPR in comparison to the DNA binding inhibitors AcrIIC3-5, which have narrow inhibitory spectrums (Lee et al., 2018; Mathony et al., 2019). Therefore, although Cas9 DNA cleavage inhibitors may tend to be weaker anti-CRISPRs, they considerably bolster the phage defense arsenal by targeting a highly conserved, and potentially immutable feature amongst bacterial Cas nucleases. Future engineering of AcrIIA1 could generate a more potent inhibitor, as recently achieved with AcrIIC1 (Mathony et al., 2019). Our attempt to increase anti-CRISPR function in human cells by weakening DNA interactions (AcrIIA1(T16A) mutant, Figure 2-3D) was only modestly successful.

Widespread AcrIIA1^{NTD} conservation also raises the possibility that prophages use this domain to combat phage superinfection, benefitting both the prophage and host cell. Precedent for phage repressors acting in this manner, both in *cis* and in *trans*, is strong. For example, the phage lambda cI protein represses prophage lytic genes and prevents superinfection by related phages during lysogeny (Johnson et al., 1981). Similarly, lysogens could use AcrIIA1 to temper expression of the prophage anti-CRISPR locus while bolstering the activity of a second

CRISPR-Cas system (e.g. Type I-B, which is common in *Listeria*), by preventing incoming phages from expressing their anti-CRISPRs. Given the diversity of anti-CRISPR protein sequences, blocking transcription would be a much more effective strategy than inhibiting individual anti-CRISPRs. Lastly, the widespread nature of the AcrIIA1^{NTD}, its fusion to distinct CTDs, and its shared genetic neighborhood with mechanistically distinct anti-CRISPRs, may be a useful marker for future *acr* discovery.

AUTHOR CONTRIBUTIONS

B.A.O. and J.B.-D. conceived and designed the study. B.A.O., S.Ka., C.M., K.A.C., B.G., and S.Ki. performed experiments. A.R.D., B.P.K., S.Ki., and J.B.-D. supervised experiments. All authors evaluated results. B.A.O. and J.B.-D. wrote the manuscript with input from all authors.

ACKNOWLEDGEMENTS

We would like to thank Daniel A. Portnoy (UC Berkeley) for providing the pLMB3C-pRhamnose plasmid, Jennifer A. Doudna for Cas9 expression plasmids (UC Berkeley), and Jonathan Asfaha (David Morgan Lab, UCSF) and Ujjwal Rathore (Alex Marson Lab, UCSF) for experimental advice and reagents. The J.B.-D lab was supported by the UCSF Program for Breakthrough Biomedical Research funded in part by the Sandler Foundation, the Searle Fellowship, the Vallee Foundation, an NIH Director's Early Independence Award DP5-OD021344, and R01GM127489; S.Ki. by an Ambizione Fellowship (Swiss National Science Foundation, SNF_174108); the B.P.K. lab by NIH R00-CA218870 and P01-HL142494, an A.S.G.C.T. Career Development Award, and the Margaret Q. Landenberger Research Foundation; and the A.R.D. lab by a CIHR Foundation grant FDN-15427.

MATERIALS AND METHODS

Microbes

Listeria monocytogenes strains (10403s) were cultured in brain-heart infusion (BHI) medium at 30°C. All *Lmo* strains containing pPL2oexL-Rhamnose-inducible constructs were cultured in Luria broth (LB) supplemented with 50-150 mM glycerol (neutral carbon source; no induction/repression) and 0-100 mM rhamnose (inducer) as indicated. To ensure plasmid maintenance in *Listeria* strains, BHI or LB was supplemented with tetracycline (2 µg/mL) for the pPL2oexL integrated construct or erythromycin (7.5 µg/mL) for pLEB579. *Escherichia coli* (DH5α, XL1Blue, NEB 10-beta, or NEB Turbo for plasmid maintenance and SM10 for conjugation into *Listeria*) and *Pseudomonas aeruginosa* (PAO1) were cultured in LB medium at 37°C. To maintain plasmids, LB was supplemented with chloramphenicol (25 µg/mL) for pPL2oexL in *E. coli*, erythromycin (250 µg/mL) for pLEB579 in *E. coli,* gentamicin (30 µg/mL) for pHERD30T in *E. coli* and *P. aeruginosa*, or carbenicillin (250 µg/mL for *P. aeruginosa,* 100 µg/mL for *E. coli*) for pMMB67HE. For maintaining pHERD30T and pMMB67HE in the same *P. aeruginosa* strain, media was supplemented with 30 µg/mL gentamicin and 100 µg/mL carbenicillin.

Phages

Listeria phages A006, A118, A502, A620, J0161a, and their derivatives were all propagated at 30°C on *acrIIA1*^{NTD}-expressing *L. monocytogenes* 10403sϕcure (*Δcas9*, *ΔtRNAArg::pPL2oexL-acrIIA1*^{NTD}) to allow optimal lytic growth of phages lacking their own *acrIIA1*^{NTD}. A511 was propagated on *L. ivanovii* WSLC 3009 at 30°C and P35 on *L. monocytogenes* Mack at 20°C. The *Pseudomonas* DMS3m-like phage (JBD30) was propagated on PAO1 at 37°C. All phages were stored in SM buffer (100 mM NaCl, 8 mM $MgSO_4$•$7H_2O$, 50

mM Tris-HCl pH 7.5, 0.01% (w/v) gelatin), supplemented with 10 mM $CaCl_2$ for *Listeria* phages, at 4°C.

Human cell lines

Human HEK 293T cells (ATCC) were cultured in Dulbecco's Modified Eagle Medium (DMEM) supplemented with 10% heat-inactivated FBS (HI-FBS) and 1% penicillin/streptomycin. Media supernatant from cell cultures was analyzed monthly for the presence of mycoplasma using MycoAlert PLUS (Lonza).

METHOD DETAILS

Construction of isogenic ϕA006 anti-CRISPR phages

Isogenic ϕA006 phages encoding distinct anti-CRISPRs from the native anti-CRISPR locus were engineered by rebooting genomic bacteriophage DNA in *L. monocytogenes* L-form cells (EGDe strain variant Rev2) as previously described (Kilcher et al., 2018). Denoted *acr* genes (*) contain the strong ribosomal binding site (RBS) naturally associated with the first gene in the natural ϕA006 anti-CRISPR locus (*orfA*) whereas unmarked genes contain the weaker RBS associated with *acrIIA1*.

***Listeria* phage titering**

A mixture of 150 µl stationary *Listeria* culture and 3 mL molten LC top agar (10 g/L tryptone, 5 g/L yeast extract, 10 g/L glucose, 7.5 g/L NaCl, 10 mM $CaCl_2$, 10 mM $MgSO_4$, 0.5% agar) was poured onto a BHI plate (1.5% agar) to generate a bacterial lawn, 3 µl of phage ten-fold serial dilutions were spotted on top, and after 24 hr incubation at 30°C, plate images were collected using the Gel Doc EZ Documentation system (BioRad) and Image Lab (BioRad) software.

Construction of *Lmo*10403s::ϕA006/ϕA118/ϕJ0161a lysogens

Lysogens were isolated from plaques that emerged after titering phages ϕA006, ϕA118, ϕJ0161a, and their derivatives on a lawn of *Lmo*10403sϕcure*Δcas9* (see "*Listeria* phage titering"). Lysogeny was confirmed by prophage induction with mitomycin C (0.5 µg/mL) treatment as previously described (Estela et al., 1992) and by PCR amplification and Sanger sequencing of the phage anti-CRISPR locus. All *Lmo*10403s strains containing prophages were lysogenized and verified prior to introducing additional constructs (integrated pPL2oexL or episomal pLEB579).

Construction of *L. monocytogenes* and *P. aeruginosa* strains

DNA fragments were PCR-amplified from genomic, plasmid, or synthesized DNA and cloned by Gibson Assembly into *Listeria* plasmids: episomal pLEB579 (Beasley et al., 2004) or the pPL2oexL single-copy integrating plasmid derived from pPL2 (Lauer et al., 2002) or *P. aeruginosa* plasmids: pMMB67HE or pHERD30T. To generate all *Listeria* strains, pPL2oexL plasmids were conjugated (Lauer et al., 2002; Simon et al., 1983) and pLEB579 plasmids were electroporated (Hupfeld et al., 2018; Park and Stewart, 1990) into *Lmo*10403s. For all *Pseudomonas* strains, plasmids were electroporated into PAO1 (Choi et al., 2006).

***Listeria* protein samples for immunoblotting**

Saturated overnight cultures of *Lmo*10403s strains overexpressing FLAG-tagged Cas9 (*Δcas9, ΔtRNAArg::pPL2oexL-LmoCas9-6xHis-FLAG*) were diluted 1:10 in BHI with appropriate antibiotic selection (see "microbes"), grown to log phase (OD_{600} 0.2-0.6), harvested by centrifugation at 8000 g for 5 min at 4°C, and lysed by bead-beating or lysozyme treatment. For bead-beating: 4 OD_{600} units of each culture were harvested, cell pellets were resuspended in 500 µl ice cold lysis buffer (50 mM Tris-HCl pH 8.0, 650 mM NaCl, 10 mM MgCl2, 10% glycerol, 1x cOmplete mini EDTA-free protease inhibitor cocktail [Roche]), combined with ~150 µl 0.1 mm

glass beads, and vortexed for 1 hr at 4°C. Cell debris was cleared by centrifugation at 21000 g for 5 min at 4°C and supernatant was mixed with one-third volume 4X Laemmli Sample Buffer (Bio-Rad). For lysozyme lysis: 1.6 OD_{600} units were harvested, cell pellets were resuspended in 200 µl of TE buffer supplemented with 2.5 mg/mL lysozyme and 1x cOmplete mini EDTA-free protease inhibitor cocktail (Roche), samples were incubated at 37°C for 30 min, quenched with one-third volume of 4X Laemmli Sample Buffer (Bio-Rad), and boiled for 5 min at 95°C.

Immunoblotting

Protein samples were separated by SDS-PAGE using 4-20% Mini-PROTEAN TGX gels (Bio-Rad) and transferred in 1X Tris/Glycine Buffer onto 0.22 micron PVDF membrane (Bio-Rad). Blots were probed with the following antibodies diluted 1:5000 in 1X TBS-T containing 5% nonfat dry milk: rabbit anti-FLAG (Sigma-Aldrich Cat# F7425, RRID:AB_439687), mouse anti-FLAG (Sigma-Aldrich Cat# F1804, RRID:AB_262044), mouse anti-Myc (Cell Signaling Technology Cat# 2276, RRID:AB_331783), rabbit anti-GST (Cell Signaling Technology Cat# 2625, RRID:AB_490796), mouse anti-*E.coli* RNA polymerase β (BioLegend Cat# 663903, RRID:AB_2564524), HRP-conjugated goat anti-Rabbit IgG (Bio-Rad Cat# 170-6515, RRID:AB_11125142), and HRP-conjugated goat anti-mouse IgG (Santa Cruz Biotechnology Cat# sc-2005, RRID:AB_631736). Blots were developed using Clarity ECL Western Blotting Substrate (Bio-Rad) and chemiluminescence was detected on an Azure c600 Imager (Azure Biosystems).

Bacterial growth (OD_{600}) and fluorescence (RFU) measurements

Saturated overnight cultures were diluted 1:100 in 150 µl BHI or LB media with appropriate antibiotic selection (see “microbes”) in a 96-well special optics microplate (Corning). *Listeria* cells were incubated at 30°C and *Pseudomonas* at 37°C with continuous double-orbital rotation for 16-48 hr in the Synergy H1 Hybrid Multi-Mode Reader (BioTeK) and measurements

of OD_{600} and mCherry (excitation 570 nm, emission 610 nm) or RFP (excitation 555 nm, emission 610 nm) relative fluorescence units (RFU) recorded every 5 min with the Gen5 (BioTek) software. For bacterial growth curves, data are displayed as the mean OD_{600} of at least three biological replicates ± SD (error bars) as a function of time (min or hr, as indicated). For Cas9-mCherry or mCherry fluorescence levels, background fluorescence of growth media was subtracted and the resulting RFU values were normalized to OD_{600} for each time point. Data are displayed as the mean normalized fluorescence ($\frac{RFU-background}{OD_{600}}$) of three biological replicates ± SD.

Quantification of Cas9 protein and mRNA reporter levels in *Listeria*

Cas9 (WT or dead; Lmo or Spy) reporters (see Figure 2-1A schematic) designed to measure protein levels contain a single RBS generating a fused Cas9-mCherry protein. Reporters for mRNA levels contain two ribosomal binding sites, one for Cas9 and a second for mCherry, generating two separate proteins. All reporters were conjugated into *Lmo*10403s devoid of endogenous *cas9* generating strains with the genotype *Δcas9, ΔtRNAArg::pPL2oexL-pHyper-Cas9Reporter*. Cells were grown and data collected and processed as in "bacterial growth and fluorescence measurements." Data are shown as the percentage of Cas9 translation and transcription levels (mCherry fluorescence averaged across 6 hr of logarithmic growth) relative to control strains (no prophage (–prophage) or empty vector, as indicated) of at least three biological replicates ± SD (error bars).

RT-qPCR of *cas9* mRNA levels

WT or Cas9-overexpressing *Lmo*10403s (*Δcas9, ΔtRNAArg::pPL2oexL-LmoCas9-6xHis-FLAG*) strains were grown to early (OD_{600} 0.2-0.3) or mid-log (OD_{600} 0.4-0.6) phase and 1.6 OD_{600} units of cells were harvested as in "*Listeria* protein samples." Cell pellets were

resuspended in 100 µl TE buffer supplemented with 0.2 U/µl SUPERase•In RNase Inhibitor (Thermo Fisher Scientific) and 5 mg/mL lysozyme, and incubated at 37°C for 10 min. Each sample was mixed with solutions pre-heated to 65°C for 15 min: 600 µl hot 1.2X lysis buffer (60 mM NaOAc, 1.2% SDS, 12 mM EDTA) and 700 µl hot acid-phenol:chloroform pH 4.5 (with IAA, 125:24:1) (Ambion). After incubating at 65°C for 30 min with shaking at 1500 rpm, followed by centrifugation at 12000 g for 15 min at 4°C, 500 µl aqueous phase was recovered for each sample. RNA was extracted with neutral phenol:chloroform:isoamyl alcohol (25:24:1) (Sigma) three times, precipitated with ethanol, and resuspended in nuclease-free water. Residual DNA was removed using the TURBO DNA-free Kit (Invitrogen). RT-qPCR was conducted in technical triplicate using the Luna Universal One-Step RT-qPCR Kit (New England Biolabs) according to the manufacturer's instructions in 10 µl reaction volumes and reactions were run on a CFX Real-Time PCR Detection System (BioRad). *cas9* mRNA and *16srRNA* were analyzed with the following primers: cas9-FWD: 5′-ATGCCGCGATAGATGGTTAC-3′ and cas9-REV: 5′-CGCCTTCGATGTTCTCCAATA-3′; 16s-FWD: 5′-CCTGGTAGTCCACGCCGT-3′ and 16s-REV: 5′-TGCGTTAGCTGCAGCACTAAG-3′.

Cas9 and anti-CRISPR protein expression and purification

N-terminally 6xHis-tagged Acr proteins were expressed from the pET28 vector whereas WT SpyCas9 and mutants were expressed from 6xHis-MBP-Cas9 constructs (gifts from Jennifer Doudna, UC Berkeley) in *E. coli* Rosetta (DE3) pLysS cells. Recombinant protein expression was induced with 0.25 mM isopropyl β-D-1-thiogalactopyranoside (IPTG) at 18 °C overnight. Cells were harvested by centrifugation and lysed by sonication in buffer A (50 mM Tris-HCl pH 7.5, 500 mM NaCl, 0.5 mM DTT, 20 mM imidazole, 5% glycerol) supplemented with 1 mM PMSF and 0.25 mg/mL lysozyme (Sigma). Cell debris was removed by centrifugation at 20000 g for 40 min at 4 °C and the lysate incubated with Ni-NTA Agarose Beads (Qiagen). After washing, bound proteins were eluted with Buffer A containing 300 mM imidazole and dialyzed

overnight into storage buffer (20 mM HEPES-NaOH pH 7.4, 150mM KCl, 10% glycerol, 2mM DTT). GST-tagged AcrIIA1 and AcrIIA2b.3 were expressed from pGEX-6P-1 plasmids in *E. coli* BL21 (DE3) cells, lysed in buffer (20 mM HEPES-NaOH pH 7.4, 300 mM KCl and 5 mM DTT) supplemented with 1 mM PMSF and 0.25 mg/mL lysozyme, and clarified lysate was incubated with Glutathione Agarose Beads (Pierce). After washing, bound proteins were eluted using 100 mM Tris-HCl pH 8.5, 150 mM KCl, 15 mM reduced glutathione. The GST tag was cleaved with PreScission Protease (Millipore) and proteins were dialyzed overnight in 50 mM HEPES-NaOH pH 7.5, 150 mM KCl, 10% glycerol and 2 mM DTT to remove free glutathione. Cleaved GST was removed from dialyzed proteins with Glutathione Agarose Beads (Pierce).

***in vitro* binding of anti-CRISPRs to SpyCas9**

The binding affinities of anti-CRISPR proteins to SpyCas9 were calculated using microscale thermophoresis (MST) on the Monolith NT.115 instrument (NanoTemper Technologies GmbH, Munich, Germany). For AcrIIA1/AcrIIA2b.3 with WT or mutant Cas9-gRNA complexes, WT and mutant 6xHis-Cas9 proteins were incubated with two-fold molar excess gRNA (Integrated DNA Technologies). The substrate proteins AcrIIA1/AcrIIA2b.3 at 0.09 nM to 3 µM concentrations were incubated with 25 nM RED-tris-NTA-labeled 6xHis-Cas9-gRNA at room temperature (RT) for 10 min in MST buffer (50 mM Tris-HCl pH 7.4, 150 mM NaCl, 15 mM $MgCl_2$, 0.05% Tween-20). For AcrIIA1/AcrIIA2b.3 with apoCas9, the substrate protein apoCas9 (QB3 Macrolab) at 0.61 nM to 10 µM concentrations was incubated with 25 nM NT-647-NHS-labeled AcrIIA1/A2b.3 proteins at RT for 10 min in MST buffer. For AcrIIA1 mutants with WT Cas9-gRNA, the substrate protein Cas9-gRNA (QB3 Macrolab) at 15 pM to 0.5 µM concentrations was incubated with 25 nM RED-tris-NTA-labeled 6xHis-AcrIIA1 mutant proteins at RT for 10 min in MST buffer. Samples were loaded into Monolith NT.115 Capillaries and measurements were performed at 25 °C using 40% LED power and medium microscale

thermophoresis power. All experiments were repeated three times for each measurement. Data analyses were carried out using NanoTemper analysis software.

in vitro pull-downs to verify binding of anti-CRISPRs to SpyCas9

5 µg apoCas9 proteins (WT, dead, D10A, or H840A) were incubated with two-fold molar excess gRNA at 37°C for 15 min. Cas9-gRNA complexes were incubated with 6-fold molar excess AcrIIA1 or AcrIIA2b.3 proteins for 15 min at room temperature in a buffer containing 20 mM HEPES-NaOH pH 7.5, 150 mM KCl, 10% glycerol, and 1 mM DTT. Samples were then incubated with 20 µl Ni-NTA agarose beads (Qiagen) for 15 min at 4°C and washed five times with 1x MST buffer (50 mM Tris-HCl pH 7.4, 150 mM NaCl, 10 mM MgCl2, 0.05 % Tween-20). Beads were boiled in 1X Laemmli Sample Buffer and proteins were analyzed by SDS-PAGE and Bio-Safe Coomassie staining (Biorad).

Limited proteolysis of SpyCas9-AcrIIA1 complex

20 µg purified SpyCas9 (QB3 Macrolab) in Apo form or in complex with gRNA (1.1-fold molar excess) was incubated with 1.5-fold and 4-fold molar excess AcrIIA1 and AcrIIA2b.3, respectively, in protease buffer (10 mM Tris-HCl pH 7.5, 300 mM NaCl) at 25°C for 15 min. Alternatively, ApoSpyCas9 was incubated first with AcrIIA protein followed by gRNA addition. Proteolysis reactions were performed with 20 ng α-chymotrypsin (sequencing grade, Promega) at 25°C and at 0, 10, 30, or 60 min time points, reactions were quenched with 2X SDS Laemmli Buffer and boiled for 10 min at 95°C. Samples were analyzed by SDS-PAGE and staining with Bio-Safe Coomassie (Bio-Rad).

SpyCas9 protein decay measurements in *Listeria*

Saturated overnight cultures of *Lmo*10403s strains devoid of endogenous *cas9* and expressing AcrIIA1 or AcrIIA4 from a tightly regulated rhamnose-inducible promoter (Fieseler et

al., 2012) and SpyCas9-mCherry from the constitutively active pHyper promoter (*Δcas9, ΔtRNAArg::pPL2oexL-pHyper-SpyCas9-mCherry-GyrA_terminator-pRha-AcrIIA*) were diluted 1:100 in fresh LB supplemented with 50 mM glycerol and tetracycline (2 μg /mL) and grown to mid-log (OD_{600} ~0.5). Cultures were then diluted 1:2 in LB containing 50 mM glycerol and tetracycline (2 μg /mL) plus 200 mM rhamnose to induce Acr expression or 200 mM glycerol for uninduced controls (100 mM final concentration rhamnose or glycerol) in a 96-well microplate and treated with gentamicin (5 μg/mL) to inhibit translation or water as a control. Cells were grown and data collected and processed as in "bacterial growth and fluorescence measurements." Data are shown as the mean percentage of SpyCas9-mCherry fluorescence relative to levels measured at "0 hr" (the beginning of translation inhibition or anti-CRISPR induction) of at least three biological replicates ± SD (error bars) as a function of time (min). Data were fitted by nonlinear regression to generate best-fit decay curves.

***Listeria* CRISPRi and self-targeting**

Single-copy integrating CRISPRi and self-targeting constructs (see Figure 2-1E schematics) were designed as follows: pPL2oexL–pHyper-sgRNA [pHELP-spacer] GyrATerminator–pRhamnose-Cas9 (Lmo WT or Lmo dead or Spy dead) LambdaTerminator–pHELP-mCherry-LuxTerminator and conjugated into *Lmo*10403sϕcure*Δcas9* containing pLEB579 plasmids expressing the indicated anti-CRISPRs. Overnight cultures were grown in LB supplemented with 50 mM glycerol (no induction/repression), 2 μg/mL tetracycline, and 7.5 μg/mL erythromycin. Cultures were then diluted 1:100 in LB containing 50 mM glycerol and the aforementioned antibiotics plus 200 mM rhamnose to induce Cas9 expression (and thus, CRISPRi or self-targeting) or 200 mM glycerol for uninduced controls (100 mM final concentration rhamnose or glycerol) in a 96-well microplate. Cells were grown and data collected and processed as in "bacterial growth and fluorescence measurements." For self-targeting, data are displayed as the mean OD_{600} of at least three biological replicates ± SD

(error bars) as a function of time (hr). For CRISPRi, data are shown as the mean percentage mCherry expression (mCherry fluorescence averaged across 6 hr of logarithmic growth) relative to uninduced controls of at least three biological replicates ± SD (error bars).

Plaque forming unit (PFU) quantification of *Listeria* phages

Phage infections were conducted using the soft agar overlay method: 10 µl phage dilution was mixed with 150 µl stationary *Listeria* culture in 3 mL molten LC top agar supplemented with 300 µg/mL Tetrazolium Violet (TCI Chemicals) to generate contrast for plaque visualization (Hurst et al., 1994) and poured onto a BHI-agar plate. After 24 hr incubation at 30°C, phage plaque-forming units (PFU) were quantified.

Efficiency of plaquing of *Listeria* phages

Efficiency of plaquing (EOP) calculations are a ratio of the number of plaque forming units (PFUs) that formed on a *Lmo*10403sϕcure targeting strain (endogenous *cas9* with overexpression of the native CRISPR array spacer #1 that targets ϕA006) divided by the number of PFUs that formed on a non-targeting strain (*Δcas9*). Each PFU measurement was conducted in biological triplicate and all EOP data is displayed as the mean EOP ± SD (error bars).

Construction of self-targeting 10403s::ϕA006 lysogens

*Lmo*10403s*Δcas9*::ϕA006 isogenic self-targeting lysogens encoding no anti-CRISPR or AcrIIA1, AcrIIA4, AcrIIA12 (alone or in combination as indicated) were isolated as in "construction of *Lmo*10403s lysogens." To prevent self-targeting during strain construction, pPL2oexL constructs encoding a tightly regulated rhamnose-inducible LmoCas9 (WT or dead as a control) were conjugated into each lysogen. To assess the stability of each lysogen, cells were cultured, Cas9 induced, and data displayed as described for the self-targeting strain in

"*Listeria* CRISPRi and self-targeting," except erythromycin was omitted from LB media. Each lysogen stability measurement was performed in biological triplicate.

P. aeruginosa anti-SpyCas9 screening platform

The previously described *P. aeruginosa* anti-SpyCas9 screening platform (Jiang et al., 2019) and bacteriophage plaque assays (Borges et al., 2018; Jiang et al., 2019) were utilized to assay the anti-CRISPR activity of AcrIIA1 homologs and mutants. AcrIIA1 homolog genes were synthesized (Twist Bioscience) and cloned into the pMMB67HE-P_{Lac} vector. Protein accession numbers are listed in Table S1. Site directed mutagenesis by Gibson Assembly was used to introduce point mutations into pMMB67HE-P_{Lac}-GST-AcrIIA1. The P_{BAD} promoter driving chromosomally integrated SpyCas9-3xMyc and pHERD30T-sgRNA was induced with 0.1% arabinose and the P_{Lac} promoter driving pMMB67HE-AcrIIA with 1 mM IPTG. Expression of AcrIIA1 mutants was confirmed by harvesting 1 OD_{600} unit of cells and resuspending in 200 µl 1X Laemmli Sample Buffer (Bio-Rad) followed by SDS-PAGE and immunoblotting as described above. The fold reductions in phage titer displayed were qualitatively derived by examining at least three replicates of each experiment. Plate images were acquired as in "*Listeria* phage titering" and a representative picture is shown.

P. aeruginosa self-targeting and CRISPRi

Strains were generated as previously described by Borges et al., 2018 under "construction of PAO1::SpyCas9 expression strain," except the sgRNA was designed to target the PAO1 chromosomal *phzM* gene promoter and was integrated into the bacterial genome using the mini-CTX2 vector (Hoang et al., 2000). Cultures were grown overnight in LB supplemented with 50 µg/mL gentamicin and 0.1% arabinose to pre-induce anti-CRISPR expression and the next day diluted 1:100 with fresh LB containing 50 µg/mL gentamicin, 0.1% arabinose, and IPTG (0, 0.01, 0.1 or 1mM to titrate WT or dead SpyCas9-sgRNA expression) in

a 96-well microplate (150 µl/well) for self-targeting analysis or glass tubes (3 mL) for CRISPRi. Self-targeting experiments were conducted in biological triplicate with cells grown and data collected and processed as in "bacterial growth and fluorescence measurements." For CRISPRi, cells were grown for 8-10 hr with continuous shaking after which CRISPRi was qualitatively assessed by inspecting the culture pigment. Repression of the *phzM* gene by dCas9 generates a yellow culture whereas inhibition of dCas9 (e.g. by an Acr) allows *phzM* expression and pyocyanin production that generates a green culture. Representative pictures of at least three biological replicates are shown.

Co-immunoprecipitation of SpyCas9-3xMyc and GST-AcrIIA

Saturated overnight cultures of *P. aeruginosa* strains were diluted 1:100 in 50 mL of LB supplemented with required antibiotics, grown to OD_{600} 0.3-0.4, and induced with 0.3% arabinose (SpyCas9-gRNA) and 1mM IPTG (anti-CRISPR). Cells were harvested at OD_{600} 1.8-2.0 by centrifugation at 6000 g for 10 min at 4°C, flash frozen on dry ice, resuspended in 1 mL lysis buffer (50 mM Tris-Cl pH 7.4, 150 mM NaCl, 20 mM $MgCl_2$, 0.5% NP-40, 5% (v/v) glycerol, 5 mM DTT, 1 mM PMSF), lysed by sonication (20 sec pulse x 4 cycles with cooling between cycles), and lysate was clarified by centrifugation at 14 000g for 10 min at 4°C. For input samples, 10 µL lysate was mixed with one-third volume 4X Laemmli Sample Buffer. Remaining lysate (~1 mL) was mixed with pre-washed Myc-Tag Magnetic Bead Conjugate #5698 (Cell Signaling Technology) or Glutathione Magnetic Agarose Beads #78601 (Thermo Fisher Scientific) using a lysate to bead slurry volume ratio of 20:1 for Myc or 40:1 for GST. After overnight incubation at 4°C with end-over-end rotation, beads were washed five times with 1 mL cold wash buffer (50 mM Tris-HCl pH 7.4, 150 mM NaCl, 20 mM $MgCl_2$, 5mM DTT) containing decreasing concentrations of NP-40 (0.5%, 0.05%, 0.01%, 0.005%, 0) and glycerol (5%, 0.5%, 0.05%, 0.005%, 0) on a magnetic stand. Bead-bound proteins were resuspended in 100 µl wash buffer without detergent and glycerol. 10 µl bead-bound protein slurry was mixed with

one-third volume 4X Laemmli Sample Buffer, boiled for 5 min at 95°C, and samples were analyzed by SDS-PAGE using 4-20% Mini-PROTEAN TGX gels (Bio-Rad) and staining with Bio-Safe Coomassie (Bio-Rad) or immunoblotting.

Cas9 DNA cleavage assays using immunoprecipitated SpyCas9-3xMyc

Reactions were assembled with bead-bound protein slurry and 1.5 nM DNA substrate, incubated at 25°C with gentle shaking at 1000 rpm, and at 1, 5, 10, and 30 min time points reaction aliquots were mixed with warm Quenching Buffer (50 mM EDTA, 0.02% SDS) and boiled at 95°C for 10 min. DNA cleavage products were analyzed by agarose (1%) gel electrophoresis and staining with SYBR Safe (Thermo Fisher Scientific).

Cas9 DNA cleavage assays using purified proteins

To generate gRNAs, crRNA and tracrRNA were annealed with Nuclease-free Duplex Buffer (Integrated DNA Technologies) according to the manufacturer's instructions. Reactions were assembled in 1X MST Buffer (50 mM Tris-Cl pH 7.4, 150 mM NaCl, 20 mM $MgCl_2$, 5 mM DTT, 5% glycerol, 0.05% (v/v) Tween-20) with 50 nM SpyCas9 and 625 nM AcrIIA, incubated for 5 min on ice, supplemented with 50 nM gRNA, and incubated for an additional 5 min at room temperature. Reactions were initiated by adding 2 nM target DNA substrate and at 1, 2, 5 and 10 min time points reaction aliquots were mixed with warm Quenching Buffer (50mM EDTA, 0.02% SDS) and boiled at 95°C for 10 min. DNA cleavage products were analyzed by agarose (1%) gel electrophoresis and staining with SYBR Safe (Thermo Fisher Scientific).

***E. coli* phage Mu plaquing assays**

Plasmids expressing Type II-A, II-B, and II-C Cas9-sgRNA combinations were previously described (Garcia et al., 2019, *in revision*). Cas9 plasmids containing a spacer targeting phage Mu and a pCDF-1b plasmid expressing the indicated anti-CRISPR proteins were co-

transformed into *E. coli* BB101. After 2 hr of growth in LB at 37°C with continuous shaking, cells were treated with 0.01 mM IPTG to induce anti-CRISPR expression, and incubated for an additional 3 hr. A mixture of cells and LB top agar (0.7% agar) was poured onto an LB plate supplemented with 200 ng/mL aTc, 0.2% arabinose, and 10 mM $MgSO_4$. Ten-fold serial dilutions of phage Mu were spotted on top and plates were incubated overnight. Anti-CRISPR expression after IPTG induction was analyzed by SDS-PAGE on a 15% Tris-Tricine gel followed by Coomassie Blue staining as previously described (Lee et al., 2018).

Inhibition of *LivCas9* by anti-CRISPR proteins

Plaquing assays were conducted as previously described by Hupfeld et al., 2018. Briefly, a pKSV7-derived plasmid expressing AcrIIA1 from the ΦA006 anti-CRISPR promoter or empty vector and pLRSR-crRNA plasmids with a spacer against phage ΦP35, ΦA511, or a non-targeting control were transformed into a *Listeria monocytogenes* Mack strain containing chromosomally-integrated pHelp-LivCas9/tracrRNA or a *Listeria ivanovii* WSLC 30167 strain with an endogenous Type II-A LivCas9 system. A mixture of 200 µl stationary host culture and 4 mL LC top agar was poured onto an agar plate (LC for ΦP35; 1/2 BHI for ΦA511). Ten-fold serial dilutions of phage were spotted on top, plates were incubated at 20°C for ΦP35 and 30°C for ΦA511 for one day, and plate images were subsequently acquired.

Generation of human cell expression plasmids

Descriptions of plasmids used for expression of sgRNAs (including sgRNA/crRNA target sequences), nucleases, and Acr proteins in human cells are available upon request. U6 promoter sgRNA and crRNA expression plasmids were generated by annealing and ligating oligonucleotide duplexes into BsmBI-digested BPK1520, BPK2660, KAC14, KAC27, KAC482, KAC32 and BPK4449 for SpyCas9, SauCas9, St1Cas9, St3Cas9, CjeCas9, and NmeCas9, respectively. New human cell expression plasmids for CjeCas9, St3Cas9, and NmeCas9 were

generated by sub-cloning the nuclease open-reading frames of Addgene plasmids # 89752, 68337, and 119923, respectively (gifts from Seokjoong Kim, Feng Zhang and Erik Sontheimer) into the AgeI and NotI sites of pCAG-CFP (Addgene plasmid 11179; a gift from C. Cepko). Human codon optimized Acr constructs containing a C-terminal SV40 nuclear localization signal were generated by isothermal assembly of synthetic gene fragments (Twist Biosciences) into the NotI and AgeI sites of Addgene plasmid ID 43861. New human expression plasmids described in this study have been deposited with Addgene.

Transfection of human cells

Approximately 20 hours prior to transfection, HEK 293T cells were seeded at $2x10^4$ cells/well in 96-well plates. Cells were transfected using 70 ng of nuclease, 30 ng sgRNA/crRNA, and 110 ng of anti-CRISPR expression plasmids with 1.25 µl of *Trans*IT-X2 (Mirus Bio) in 20 µl Opti-MEM. For control conditions containing no acr plasmid, 110 ng of a pCMV-EGFP plasmid was utilized as filler DNA; for non-targeting sgRNA/crRNA conditions, 30 ng of an empty U6 promoter plasmid was used as filler DNA. Genomic DNA was harvested from cells 72 hours post-transfection by suspending cells in 100 µl of lysis buffer (20 mM Hepes pH 7.5, 100 mM KCl, 5 mM $MgCl_2$, 5% glycerol, 25 mM DTT, 0.1% Triton X-100, and 30 ng/ul Proteinase K (NEB)), followed by incubation at 65°C for 6 minutes and 98°C for 2 minutes. All experiments were performed with at least 3 independent biological replicates.

Assessment of Cas and Acr protein activities in human cells

Genome editing efficiencies were determined by next-generation sequencing using a 2-step PCR-based Illumina library construction method. Briefly, genomic regions were initially amplified using Q5 High-Fidelity DNA Polymerase (NEB), ~100 ng of genomic DNA lysate, and gene-specific round 1 primers. PCR products were purified using paramagnetic beads as previously described (Kleinstiver et al., 2019) and diluted 1:100 prior to the 2nd round of PCR to

add Illumina barcodes and adapter sequences using Q5 polymerase. PCR amplicons were bead purified, quantified and normalized (Qiagen QIAxcel), and pooled. Final libraries were quantified using an Illumina Library qPCR Quantification Kit (KAPA Biosystems) and sequenced on a MiSeq sequencer using a 300-cycle v2 kit (Illumina). Genome editing activities were determined from the sequencing data using CRISPResso2 (Clement et al., 2019) with commands --min_reads_to_use_region 100 and -w 10.

Quantification of prophage induction efficiency

Prophages were induced from *Lmo*10403s::ΦJ0161 lysogens expressing *cis-acrIIA1* from the prophage Acr locus or *trans-acrIIA1* from the bacterial host genome by treating with 0.5 µg/mL mitomycin C as previously described (Estela et al., 1992). After overnight incubation with continuous shaking at 30°C, cells were pelleted by centrifugation at 8000 g for 10 min and phage-containing supernatants were harvested. To quantify the amount of phage induced from each lysogen, phage-containing supernatants were used to infect *Lmo*10403sΦcure lacking *cas9* and expressing AcrIIA1^{NTD} (*Δcas9;IIA1^{NTD}*, to bypass the lytic growth defect of ΦJ0161*ΔacrIIA1-2*) as described in "plaque forming unit (PFU) quantification of *Listeria* phages" and the resulting PFUs were quantified. Data are displayed as the mean PFU/mL after prophage induction of four biological replicates ± SD (error bars).

Transcriptional repression of the *acr* promoter

To generate *acr* promoter transcriptional reporters, the nucleotide sequences (~100-350 base pairs) upstream of putative *acr* loci encoding *acrIIA1* homologs were synthesized (Twist Bioscience) and cloned upstream of an mRFP gene into the pHERD30T vector. Promoter sequences are listed in Table S1. Transcriptional reporters were electroporated into *P. aeruginosa* PAO1 strains containing pMMB67HE-AcrIIA1-variants. Saturated overnight cultures were diluted 1:10 in LB supplemented with 30 µg/mL gentamicin, 100 µg/mL carbenicillin, and 1

mM IPTG to induce AcrIIA1 expression in a 96-well microplate. Cells were grown and data collected as in “bacterial growth and fluorescence measurements.” Data are shown as the mean percentage RFP repression (RFU values at 960 min for AcrIIA1 mutants and 1170 min for homologs, normalized to OD_{600}) in the presence of AcrIIA1 relative to controls lacking AcrIIA1 of at least three biological replicates ± SD (error bars).

in vitro binding of AcrIIA1 to the anti-CRISPR promoter

The affinities of AcrIIA1 and individual domains for DNA were measured in triplicate using MST as described above. Single-stranded complementary oligonucleotides were annealed to generate 40 bp *acr* promoter fragments harboring WT or mutated palindrome. The DNA substrate at 0.15 nM to 5 µM concentrations was incubated with 12.5 nM RED-tris-NTA-labeled AcrIIA1/domains at room temperature for 10 min in 1x buffer (50 mM Tris-HCl pH 7.4, 150 mM NaCl, 10 mM MgCl2, 0.05 % Tween-20). DNA substrate sequences:

5’-AACTATTGAC**TACTACG**TATATT**CGTAGTA**TAATGTGAAT-3’ (Wild-type)

5’-AACTATTGAC**A****AACTACG**TATATT**CGTAGT****T**TAATGTGAAT-3’ (Terminal Mutations)

5’-AACTATTGAC**A****AC****A****AC****C**TATATT**G****GTT****G****TT**TAATGTGAAT-3’ (Six Mutations)

QUANTIFICATION AND STATISTICAL ANALYSIS

All numerical data, with the exception of the microscale thermophoresis (MST) data, were analyzed and plotted using GraphPad Prism 6.0 software. The MST data were analyzed using the NanoTemper analysis software (NanoTemper Technologies GmbH) and plotted using GraphPad Prism 6.0 software. Statistical parameters are reported in the Figure Legends.

REFERENCES

1. Argov, T., Azulay, G., Pasechnek, A., Stadnyuk, O., Ran-Sapir, S., Borovok, I., Sigal, N., and Herskovits, A.A. (2017). Temperate bacteriophages as regulators of host behavior. Curr. Opin. Microbiol. *38*, 81–87.

2. Beasley, S.S., Takala, T.M., Reunanen, J., Apajalahti, J., and Saris, P.E.J. (2004). Characterization and Electrotransformation of Lactobacillus Crispatus Isolated from Chicken Crop and Intestine. Poult. Sci. *83*, 45–48.

3. Birkholz, N., Fagerlund, R.D., Smith, L.M., Jackson, S.A., and Fineran, P.C. (2019). The autoregulator Aca2 mediates anti-CRISPR repression. Nucleic Acids Res.

4. Bondy-Denomy, J. (2018). Protein Inhibitors of CRISPR-Cas9. ACS Chem. Biol. *13*, 417–423.

5. Bondy-Denomy, J., Garcia, B., Strum, S., Du, M., Rollins, M.F., Hidalgo-Reyes, Y., Wiedenheft, B., Maxwell, K.L., and Davidson, A.R. (2015). Multiple mechanisms for CRISPR-Cas inhibition by anti-CRISPR proteins. Nature *526*, 136–139.

6. Bondy-Denomy, J., Qian, J., Westra, E.R., Buckling, A., Guttman, D.S., Davidson, A.R., and Maxwell, K.L. (2016). Prophages mediate defense against phage infection through diverse mechanisms. ISME J. *10*, 2854–2866.

7. Borges, A.L., Davidson, A.R., and Bondy-Denomy, J. (2017). The Discovery, Mechanisms, and Evolutionary Impact of Anti-CRISPRs. Annu. Rev. Virol. *4*.

8. Borges, A.L., Zhang, J.Y., Rollins, M.F., Osuna, B.A., Wiedenheft, B., and Bondy-Denomy, J. (2018). Bacteriophage Cooperation Suppresses CRISPR-Cas3 and Cas9 Immunity. Cell *174*, 917-925.e10.

9. Brouns, S.J.J., Jore, M.M., Lundgren, M., Westra, E.R., Slijkhuis, R.J.H., Snijders, A.P.L., Dickman, M.J., Makarova, K.S., Koonin, E.V., and Oost, J. van der (2008). Small CRISPR RNAs Guide Antiviral Defense in Prokaryotes. Science *321*, 960–964.

10. Chen, Y., Golding, I., Sawai, S., Guo, L., and Cox, E.C. (2005). Population Fitness and the Regulation of Escherichia coli Genes by Bacterial Viruses. PLoS Biol. *3*.

11. Choi, K.-H., Kumar, A., and Schweizer, H.P. (2006). A 10-min method for preparation of highly electrocompetent Pseudomonas aeruginosa cells: Application for DNA fragment transfer between chromosomes and plasmid transformation. J. Microbiol. Methods *64*, 391–397.

12. Clement, K., Rees, H., Canver, M.C., Gehrke, J.M., Farouni, R., Hsu, J.Y., Cole, M.A., Liu, D.R., Joung, J.K., Bauer, D.E., et al. (2019). CRISPResso2 provides accurate and rapid genome editing sequence analysis. Nat. Biotechnol. *37*, 224–226.

13. Deltcheva, E., Chylinski, K., Sharma, C.M., Gonzales, K., Chao, Y., Pirzada, Z.A., Eckert, M.R., Vogel, J., and Charpentier, E. (2011). CRISPR RNA maturation by trans-encoded small RNA and host factor RNase III. Nature *471*, 602–607.

14. Dong, D., Guo, M., Wang, S., Zhu, Y., Wang, S., Xiong, Z., Yang, J., Xu, Z., and Huang, Z. (2017). Structural basis of CRISPR–SpyCas9 inhibition by an anti-CRISPR protein. Nature *546*, 436–439.

15. Estela, L.A., Sofos, J.N., and Flores, B.B. (1992). Bacteriophage Typing of Listeria monocytogenes Cultures Isolated From Seafoods. J. Food Prot. *55*, 13–17.

16. Feiner, R., Argov, T., Rabinovich, L., Sigal, N., Borovok, I., and Herskovits, A.A. (2015). A new perspective on lysogeny: prophages as active regulatory switches of bacteria. Nat. Rev. Microbiol. *13*, 641–650.

17. Fieseler, L., Schmitter, S., Teiserskas, J., and Loessner, M.J. (2012). Rhamnose-Inducible Gene Expression in Listeria monocytogenes. PLOS ONE *7*, e43444.

18. Fuchsbauer, O., Swuec, P., Zimberger, C., Amigues, B., Levesque, S., Agudelo, D., Duringer, A., Chaves-Sanjuan, A., Spinelli, S., Rousseau, G.M., et al. (2019). Cas9 Allosteric Inhibition by the Anti-CRISPR Protein AcrIIA6. Mol. Cell. *Manuscript under review.*

19. Garcia, B., Lee, J., Edraki, A., Hidalgo-Reyes, Y., Erwood, S., Mir, A., Trost, C., Seroussi, U., Stanley, S.Y., Cohn, R.D., et al. (2019). One Anti-CRISPR to Rule Them All: Potent Inhibition of Cas9 Homologs Used for Genome Editing. Cell Rep. *Manuscript under review.*

20. Garneau, J.E., Dupuis, M.-È., Villion, M., Romero, D.A., Barrangou, R., Boyaval, P., Fremaux, C., Horvath, P., Magadán, A.H., and Moineau, S. (2010). The CRISPR/Cas bacterial immune system cleaves bacteriophage and plasmid DNA. Nature *468*, 67–71.

21. Harrington, L.B., Doxzen, K.W., Ma, E., Liu, J.-J., Knott, G.J., Edraki, A., Garcia, B., Amrani, N., Chen, J.S., Cofsky, J.C., et al. (2017). A Broad-Spectrum Inhibitor of CRISPR-Cas9. Cell *170*, 1224-1233.e15.

22. Haurwitz, R.E., Jinek, M., Wiedenheft, B., Zhou, K., and Doudna, J.A. (2010). Sequence- and Structure-Specific RNA Processing by a CRISPR Endonuclease. Science *329*, 1355–1358.

23. Heler, R., Samai, P., Modell, J.W., Weiner, C., Goldberg, G.W., Bikard, D., and Marraffini, L.A. (2015). Cas9 specifies functional viral targets during CRISPR–Cas adaptation. Nature *519*, 199–202.

24. Hoang, T.T., Kutchma, A.J., Becher, A., and Schweizer, H.P. (2000). Integration-Proficient Plasmids for Pseudomonas aeruginosa: Site-Specific Integration and Use for Engineering of Reporter and Expression Strains. Plasmid *43*, 59–72.

25. Hupfeld, M., Trasanidou, D., Ramazzini, L., Klumpp, J., Loessner, M.J., and Kilcher, S. (2018). A functional type II-A CRISPR–Cas system from Listeria enables efficient genome editing of large non-integrating bacteriophage. Nucleic Acids Res. *46*, 6920–6933.

26. Hurst, C.J., Blannon, J.C., Hardaway, R.L., and Jackson, W.C. (1994). Differential Effect of Tetrazolium Dyes upon Bacteriophage Plaque Assay Titers. Appl. Environ. Microbiol. *60*, 3462.

27. Hwang, S., and Maxwell, K.L. (2019). Meet the Anti-CRISPRs: Widespread Protein Inhibitors of CRISPR-Cas Systems. CRISPR J. *2*, 23–30.

28. Hynes, A.P., Rousseau, G.M., Lemay, M.-L., Horvath, P., Romero, D.A., Fremaux, C., and Moineau, S. (2017). An anti-CRISPR from a virulent streptococcal phage inhibits Streptococcus pyogenes Cas9. Nat. Microbiol. *2*, 1374.

29. Hynes, A.P., Rousseau, G.M., Agudelo, D., Goulet, A., Amigues, B., Loehr, J., Romero, D.A., Fremaux, C., Horvath, P., Doyon, Y., et al. (2018). Widespread anti-CRISPR proteins in virulent bacteriophages inhibit a range of Cas9 proteins. Nat. Commun. *9*, 1–10.

30. Jiang, F., Liu, J.-J., Osuna, B.A., Xu, M., Berry, J.D., Rauch, B.J., Nogales, E., Bondy-Denomy, J., and Doudna, J.A. (2019). Temperature-Responsive Competitive Inhibition of CRISPR-Cas9. Mol. Cell *73*, 601-610.e5.

31. Johnson, A.D., Poteete, A.R., Lauer, G., Sauer, R.T., Ackers, G.K., and Ptashne, M. (1981). λ Repressor and cro—components of an efficient molecular switch. Nature *294*, 217–223.

32. Ka, D., An, S.Y., Suh, J.-Y., and Bae, E. (2018). Crystal structure of an anti-CRISPR protein, AcrIIA1. Nucleic Acids Res. *46*, 485–492.

33. Kilcher, S., Studer, P., Muessner, C., Klumpp, J., and Loessner, M.J. (2018). Cross-genus rebooting of custom-made, synthetic bacteriophage genomes in L-form bacteria. Proc. Natl. Acad. Sci. *115*, 567–572.

34. Kleinstiver, B.P., Sousa, A.A., Walton, R.T., Tak, Y.E., Hsu, J.Y., Clement, K., Welch, M.M., Horng, J.E., Malagon-Lopez, J., Scarfò, I., et al. (2019). Engineered CRISPR–Cas12a variants with increased activities and improved targeting ranges for gene, epigenetic and base editing. Nat. Biotechnol. *37*, 276–282.

35. Koonin, E.V., Makarova, K.S., and Zhang, F. (2017). Diversity, classification and evolution of CRISPR-Cas systems. Curr. Opin. Microbiol. *37*, 67–78.

36. Lauer, P., Chow, M.Y.N., Loessner, M.J., Portnoy, D.A., and Calendar, R. (2002). Construction, Characterization, and Use of Two Listeria monocytogenes Site-Specific Phage Integration Vectors. J. Bacteriol. *184*, 4177–4186.

37. Lee, J., Mir, A., Edraki, A., Garcia, B., Amrani, N., Lou, H.E., Gainetdinov, I., Pawluk, A., Ibraheim, R., Gao, X.D., et al. (2018). Potent Cas9 Inhibition in Bacterial and Human Cells by AcrIIC4 and AcrIIC5 Anti-CRISPR Proteins. MBio *9*, e02321-18.

38. Liu, L., Yin, M., Wang, M., and Wang, Y. (2019). Phage AcrIIA2 DNA Mimicry: Structural Basis of the CRISPR and Anti-CRISPR Arms Race. Mol. Cell *73*, 611-620.e3.

39. Loessner, M.J. (1991). Improved procedure for bacteriophage typing of Listeria strains and evaluation of new phages. Appl. Environ. Microbiol. *57*, 882–884.

40. Loessner, M.J., Goeppl, S., and Busse, M. (1991). Comparative inducibility of bacteriophage in naturally lysogenic and lysogenized strains of Listeria spp. by u.v. light and Mitomycin C. Lett. Appl. Microbiol. *12*, 196–199.

41. Makarova, K.S., Wolf, Y.I., Alkhnbashi, O.S., Costa, F., Shah, S.A., Saunders, S.J., Barrangou, R., Brouns, S.J.J., Charpentier, E., Haft, D.H., et al. (2015). An updated evolutionary classification of CRISPR-Cas systems. Nat. Rev. Microbiol. *13*, 722–736.

42. Mathony, J., Harteveld, Z., Schmelas, C., Belzen, J.U. zu, Aschenbrenner, S., Hoffmann, M.D., Stengl, C., Scheck, A., Rosset, S., Grimm, D., et al. (2019). Computational design of anti-CRISPR proteins with improved inhibition potency and expanded specificity. BioRxiv 685032.

43. Mojica, F.J.M., Díez-Villaseñor, C., García-Martínez, J., and Soria, E. (2005). Intervening Sequences of Regularly Spaced Prokaryotic Repeats Derive from Foreign Genetic Elements. J. Mol. Evol. *60*, 174–182.

44. Nakamura, M., Srinivasan, P., Chavez, M., Carter, M.A., Dominguez, A.A., Russa, M.L., Lau, M.B., Abbott, T.R., Xu, X., Zhao, D., et al. (2019). Anti-CRISPR-mediated control of gene editing and synthetic circuits in eukaryotic cells. Nat. Commun. *10*, 1–11.

45. Nuñez, J.K., Kranzusch, P.J., Noeske, J., Wright, A.V., Davies, C.W., and Doudna, J.A. (2014). Cas1–Cas2 complex formation mediates spacer acquisition during CRISPR–Cas adaptive immunity. Nat. Struct. Mol. Biol. *21*, 528–534.

46. Park, S.F., and Stewart, G.S.A.B. (1990). High-efficiency transformation of Listeria monocytogenes by electroporation of penicillin-treated cells. Gene *94*, 129–132.

47. Rabinovich, L., Sigal, N., Borovok, I., Nir-Paz, R., and Herskovits, A.A. (2012). Prophage Excision Activates Listeria Competence Genes that Promote Phagosomal Escape and Virulence. Cell *150*, 792–802.

48. Rauch, B.J., Silvis, M.R., Hultquist, J.F., Waters, C.S., McGregor, M.J., Krogan, N.J., and Bondy-Denomy, J. (2017). Inhibition of CRISPR-Cas9 with Bacteriophage Proteins. Cell *168*, 150-158.e10.

49. Shin, J., Jiang, F., Liu, J.-J., Bray, N.L., Rauch, B.J., Baik, S.H., Nogales, E., Bondy-Denomy, J., Corn, J.E., and Doudna, J.A. (2017). Disabling Cas9 by an anti-CRISPR DNA mimic. Sci. Adv. *3*.

50. Simon, R., Priefer, U., and Pühler, A. (1983). A Broad Host Range Mobilization System for In Vivo Genetic Engineering: Transposon Mutagenesis in Gram Negative Bacteria. Bio/Technology *1*, 784–791.

51. Stanley, S.Y., Borges, A.L., Chen, K.-H., Swaney, D.L., Krogan, N.J., Bondy-Denomy, J., and Davidson, A.R. (2019). Anti-CRISPR-Associated Proteins Are Crucial Repressors of Anti-CRISPR Transcription. Cell *0*.

52. Thavalingam, A., Cheng, Z., Garcia, B., Huang, X., Shah, M., Sun, W., Wang, M., Harrington, L., Hwang, S., Hidalgo-Reyes, Y., et al. (2019). Inhibition of CRISPR-Cas9 ribonucleoprotein complex assembly by anti-CRISPR AcrIIC2. Nat. Commun. *10*, 1–11.

53. Trasanidou, D., Gerós, A.S., Mohanraju, P., Nieuwenweg, A.C., Nobrega, F.L., and Staals, R.H.J. (2019). Keeping crispr in check: diverse mechanisms of phage-encoded anti-crisprs. FEMS Microbiol. Lett. *366*.

54. Yang, H., and Patel, D.J. (2017). Inhibition Mechanism of an Anti-CRISPR Suppressor AcrIIA4 Targeting SpyCas9. Mol. Cell *67*, 117-127.e5.

55. Yao, R., Liu, D., Jia, X., Zheng, Y., Liu, W., and Xiao, Y. (2018). CRISPR-Cas9/Cas12a biotechnology and application in bacteria. Synth. Syst. Biotechnol. *3*, 135–149.

56. Yosef, I., Goren, M.G., and Qimron, U. (2012). Proteins and DNA elements essential for the CRISPR adaptation process in Escherichia coli. Nucleic Acids Res. *40*, 5569–5576.

57. Zhu, Y., Gao, A., Zhan, Q., Wang, Y., Feng, H., Liu, S., Gao, G., Serganov, A., and Gao, P. (2019). Diverse Mechanisms of CRISPR-Cas9 Inhibition by Type IIC Anti-CRISPR Proteins. Mol. Cell *74*, 296-309.e7.

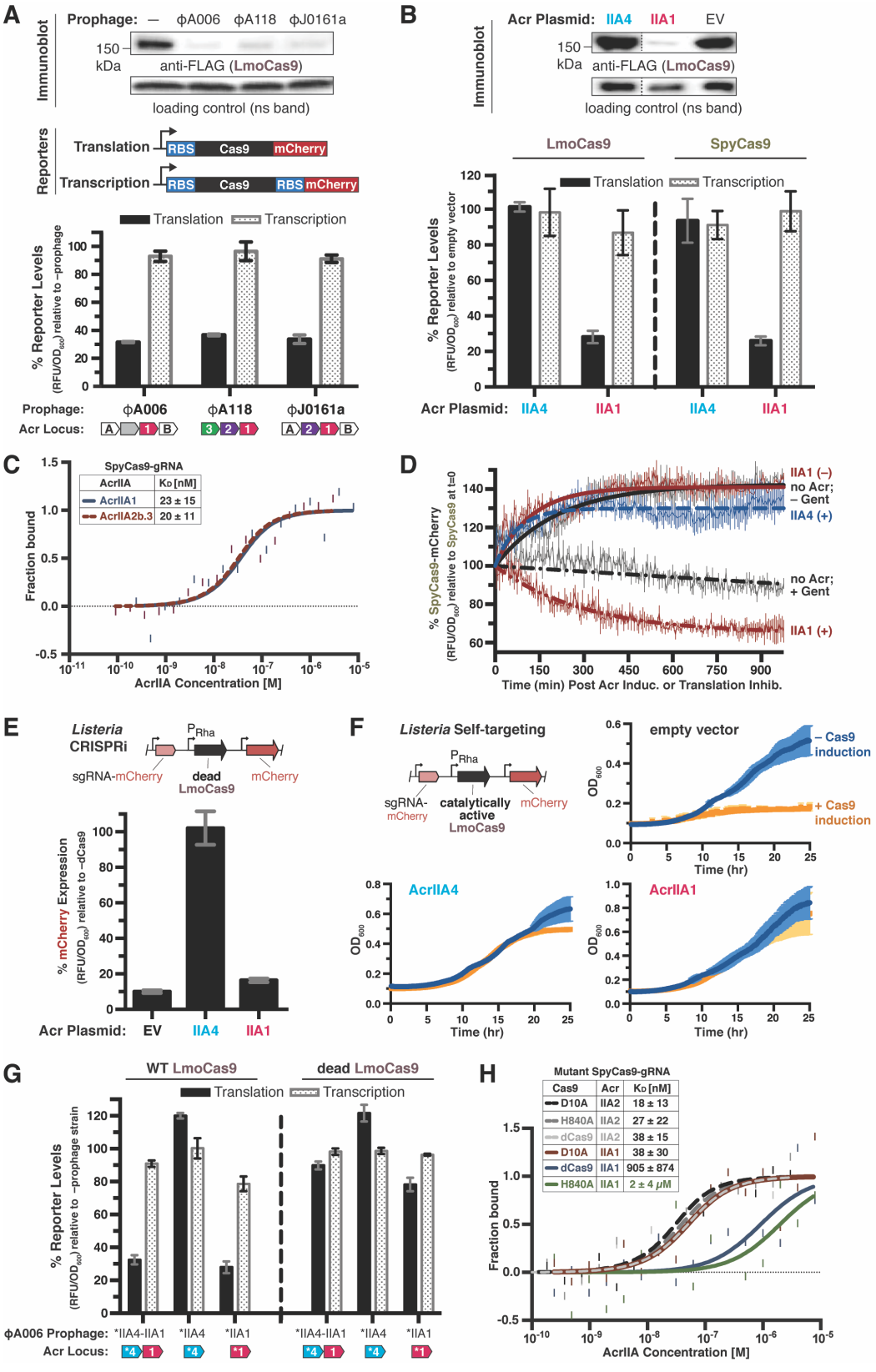

Figure 2-1. AcrIIA1 Binds Catalytically Active Cas9 to Trigger its Degradation in *Listeria*
(A and B) Immunoblots detecting FLAG-tagged LmoCas9 protein and a non-specific (ns) protein

loading control in *Listeria monocytogenes* strain 10403s (*Lmo*10403s) lysogenized with the indicated wild-type prophages (A, top) or *Lmo*10403s containing Acr-expressing plasmids (B, top). Dashed lines indicate where intervening lanes were removed for clarity (B, top). Representative blots of at least three biological replicates are shown (A and B). Schematics of translational and transcriptional reporters used to measure Lmo or Spy Cas9 protein and mRNA levels in *Lmo*10403s (A, middle). Cas9 translational (black bars) and transcriptional (gray shaded bars) reporter measurements reflect the mean percentage mCherry relative fluorescence units (RFU normalized to OD_{600}) in the indicated lysogens (A, bottom) or strains with Acr-expressing plasmids (B, bottom) relative to the control strain lacking a prophage (– prophage) (A, bottom) or containing an empty vector (B, bottom). Error bars represent the mean ± SD of at least three biological replicates. (C) Quantification of the binding affinities (K_D; boxed inset) of AcrIIA1 and AcrIIA2b.3 for WT SpyCas9-gRNA using microscale thermophoresis. Data shown are representative of three independent experiments. (D) SpyCas9-mCherry protein levels post anti-CRISPR induction or translation inhibition. *Lmo*10403s strains expressing SpyCas9-mCherry from the constitutively active pHyper promoter and AcrIIA1 or AcrIIA4 from an inducible promoter were grown to mid-logarithmic phase and treated with 100 mM rhamnose to induce Acr expression (+, thick dashed lines) or 100 mM glycerol as a neutral carbon source control (–, thick solid lines) and 5 µg/mL gentamicin (Gent) to inhibit translation (+) or water (–) as a control. SpyCas9-mCherry protein measurements reflect the mean percentage fluorescence (RFUs normalized to OD_{600}) relative to the SpyCas9-mCherry levels at the time (0 min) translation inhibition was initiated (thin solid lines). Error bars (vertical lines) represent the mean ± SD of at least three biological replicates. Data were fitted by nonlinear regression to generate best-fit decay curves (thick lines). See Figure 2-S1D for additional controls and S1E for data showing tight repression of the pRhamnose promoter under non-inducing conditions. (E and F) Anti-CRISPR inhibition of CRISPRi (E) or self-targeting (F) in *Listeria*. *Lmo*10403s strains contain chromosomally-integrated constructs expressing dead (E) or catalytically active (F) LmoCas9 from the inducible pRha-promoter and a sgRNA that targets the pHelp-promoter driving mCherry expression. For CRISPRi, mCherry expression measurements reflect the mean percentage fluorescence (RFU normalized to OD_{600}) in deadCas9-induced cells relative to uninduced (–dCas9) controls of three biological replicates ± SD (error bars) (E). For self-targeting, bacterial growth was monitored after LmoCas9 induction (orange lines) or no induction (blue lines) and data are displayed as the mean OD_{600} of three biological replicates ± SD (error bars) (F). See Figure 2-S1F for CRISPRi data with *Lmo*10403s expressing dead SpyCas9. (G) Translational (black bars) and transcriptional (gray shaded bars) reporter levels of catalytically active (left) and dead LmoCas9 (right) in *Lmo*10403s lysogenized with engineered isogenic ΦA006 prophages encoding the indicated anti-CRISPRs. Measurements were normalized and graphed as in (A, bottom) with error bars representing the mean ± SD of at least three biological replicates. (*) Indicates the native orfA RBS (strong) in ΦA006 was used for Acr expression. See Figure 2-S1H for equivalent data with *Lmo*10403s expressing SpyCas9. (H) Quantification of the binding affinities (K_D; boxed inset) of AcrIIA1 (IIA1, solid lines) and AcrIIA2b.3 (IIA2, dashed lines) for catalytically dead (dCas9) and nickase (D10A or H840A) SpyCas9-gRNA complexes using microscale thermophoresis. Data shown are representative of three independent experiments.

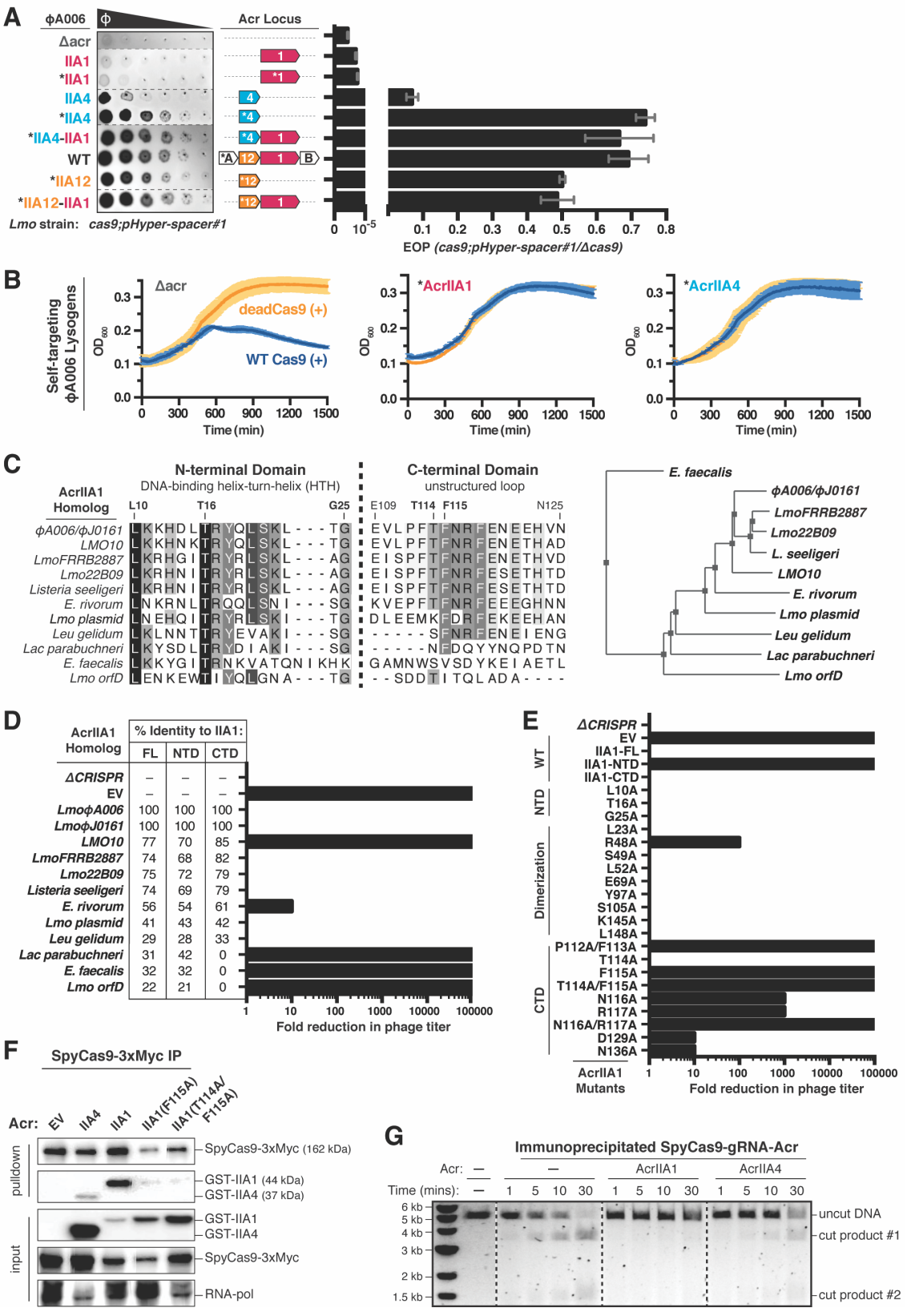

Figure 2-2. AcrIIA1 Inhibits Cas9 DNA Cleavage to Protect Prophages During Lysogeny

(A) Left: Representative image of plaquing assays where isogenic ΦA006 phages are titrated in

ten-fold serial dilutions (black spots) on a lawn of *Lmo*10403s (gray background). Dashed lines indicate where intervening rows were removed for clarity. Right: Efficiency of plaquing (EOP) of isogenic ΦA006 phages (expressing the indicated anti-CRISPRs) on *Lmo*10403s. Plaque forming units (PFUs) were quantified on *Lmo*10403s overexpressing the first spacer in the native CRISPR array that targets ΦA006 (*cas9;pHyper-spacer#1*) and normalized to the number of PFUs measured on a non-targeting *Lmo*10403s-derived strain (*Δcas9*). Data are displayed as the mean EOP of at least three biological replicates ± SD (error bars). See Figure 2-S2A for EOP measurements of additional ΦA006 phages. (B) Bacterial growth curves of self-targeting *Lmo*10403s::ΦA006 isogenic lysogens expressing the indicated anti-CRISPRs and rhamnose-induced (+) WT or dead LmoCas9. WT LmoCas9 induction (blue lines), but not dead LmoCas9 (orange lines) is lethal in an Acr-deficient (Δacr) strain because the *Lmo*10403s CRISPR array contains a spacer targeting the ΦA006 prophage integrated in the bacterial genome. Data are displayed as the mean OD_{600} of at least three biological replicates ± SD (error bars) as a function of time (min). (*) Indicates the native orfA RBS (strong) in ΦA006 was used for Acr expression. (C) Left: Alignment of AcrIIA1 homolog protein sequences denoting key residues. Right: Phylogenetic tree of the protein sequences of AcrIIA1 homologs. See Figure 2-S4D for a complete alignment of the AcrIIA1 homolog protein sequences. (D and E) Fold reduction in phage titer in response to SpyCas9 targeting of a *P. aeruginosa* DMS3m-like phage in the presence of AcrIIA1 homologs (D) or mutants (E). The percent protein sequence identities of each homolog to the full-length (FL) or domains (NTD or CTD) of $AcrIIA1_{ΦA006}$ (IIA1) are listed in (D). The displayed fold reductions in phage titer were qualitatively determined by examining three biological replicates of each phage-plaquing experiment. See Figure 2-S3A for representative pictures of the corresponding phage-plaquing experiments. (F) Immunoblots detecting GST-tagged anti-CRISPR proteins that co-immunoprecipitated with Myc-tagged SpyCas9 in a *P. aeruginosa* strain heterologously expressing Type II-A SpyCas9-gRNA and the indicated Acrs. For input samples, one-hundredth lysate volume was analyzed to verify tagged protein expression and RNA-polymerase was used as a loading control. Representative blots of at least three biological replicates are shown. See Figure 2-S2F for the reciprocal GST-Acr pulldown. (G) Time courses of SpyCas9 DNA cleavage reactions in the presence of the indicated anti-CRISPRs conducted with SpyCas9-gRNA-Acr (or no Acr, –) complexes immunoprecipitated from *P. aeruginosa*. Dashed lines indicate where intervening lanes were removed for clarity. Data shown are representative of three independent experiments. See Figure 2-S2H for reactions with AcrIIA1 mutants.

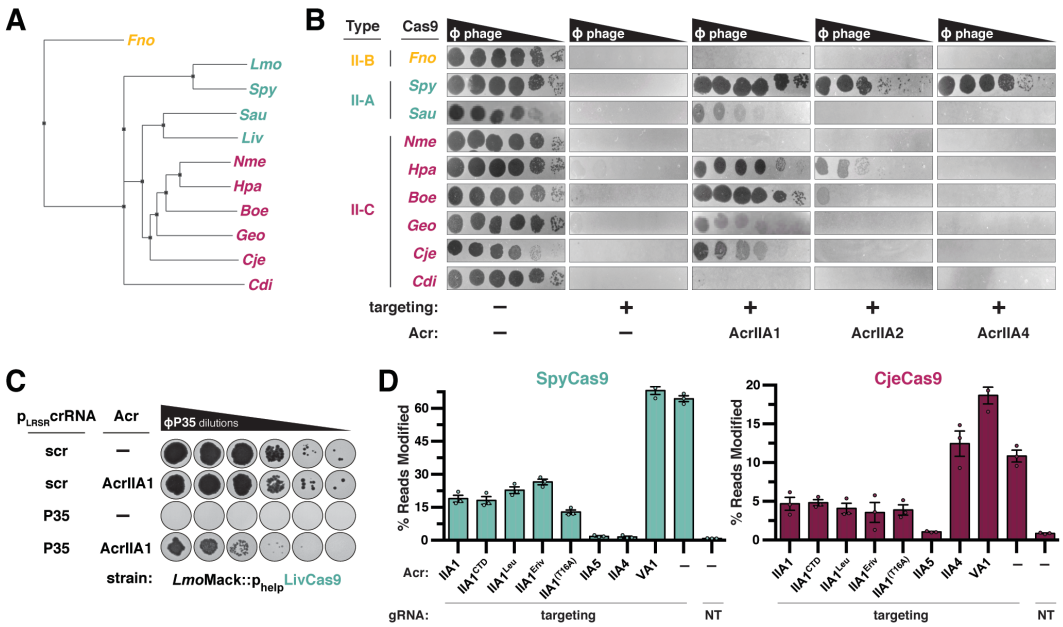

Figure 2-3. AcrIIA1 is a Broad-Spectrum Cas9 Inhibitor

(A) Phylogenetic tree of the protein sequences of Cas9 orthologues: *Francisella novicida (Fno), Listeria monocytogenes (Lmo), Streptococcus pyogenes (Spy), Staphylococcus aureus (Sau), Listeria ivanovii (Liv), Neisseria meningitidis (Nme), Haemophilus parainfluenzae (Hpa), Brackiella oedipodis (Boe), Geobacillus stearothermophilus (Geo), Campylobacter jejuni (Cje), Corynebacterium diphtheriae (Cdi).* (B) Plaquing assays where the *E. coli* phage Mu is titrated in ten-fold serial dilutions (black spots) on lawns of *E. coli* (gray background) expressing the indicated anti-CRISPR proteins and Type II-A, II-B and II-C Cas9-sgRNA combinations programmed to target phage DNA. Representative pictures of at least 3 biological replicates are shown. (C) Plaquing assays where the *Listeria* phage ΦP35 is titrated in ten-fold serial dilutions (black spots) on lawns of *L. monocytogenes* Mack (gray background) expressing episomal AcrIIA1 or no Acr (–), chromosomally-integrated LivCas9/tracrRNA, and episomal (pLRSR) crRNA that targets ΦP35 phage DNA or a non-targeting control (scr). (D) Gene editing activities of Cas9 orthologues in human cells in the presence of AcrIIA1 variants and orthologues. AcrIIA4 is a known inhibitor of SpyCas9, AcrIIA5 is a broad-spectrum inhibitor (Garcia et al., 2019, *in revision*), and AcrVA1 as a known non-inhibiting control for SpyCas9 orthologues. NT, no-sgRNA control condition. Error bars indicate SEM for three independent biological replicates. See Figure 2-S3F for editing experiments with additional Cas9 orthologues.

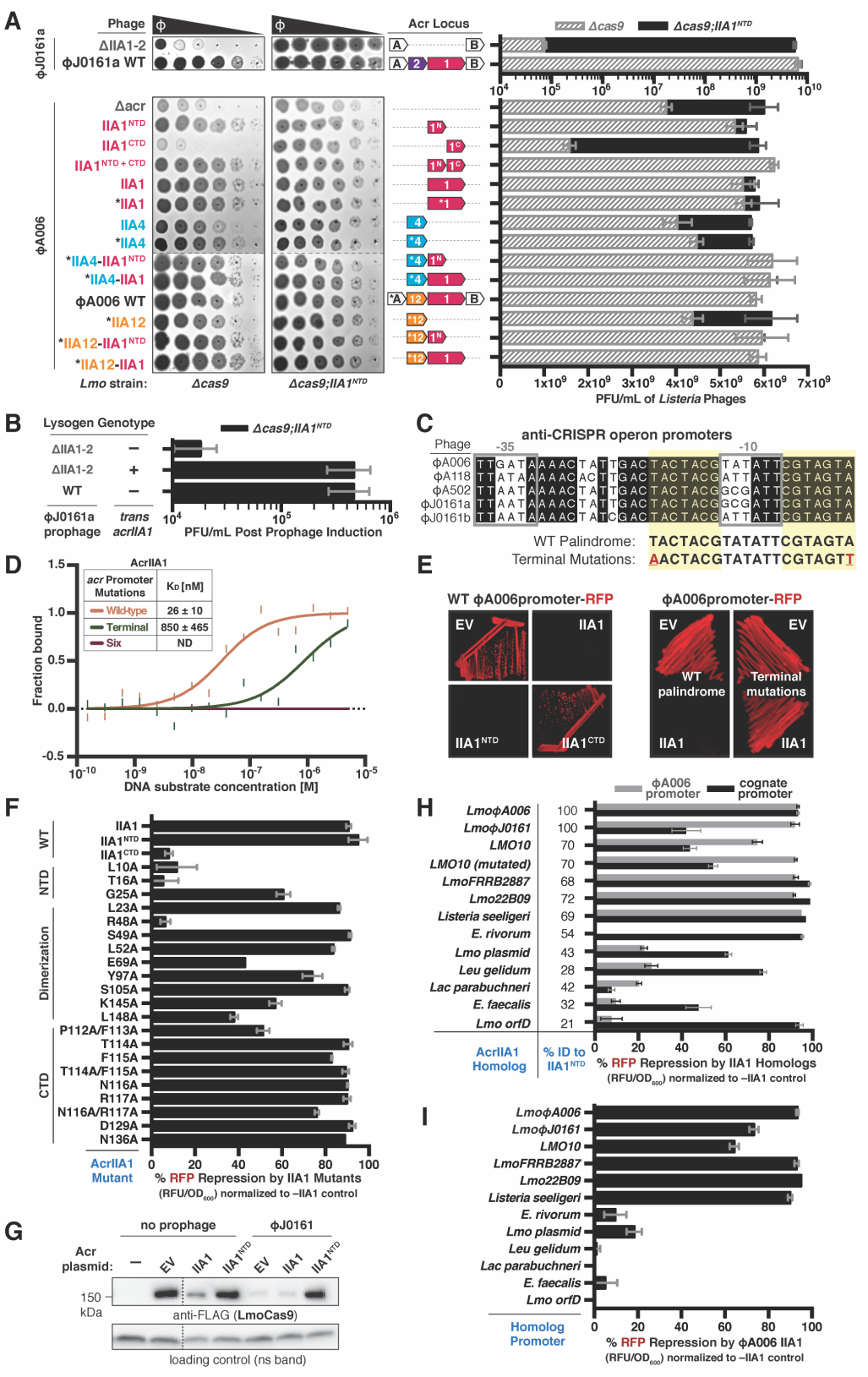

Figure 2-4. The AcrIIA1 N-terminal Domain Autorepresses the Anti-CRISPR Promoter

(A) Left: Representative images of plaquing assays where the indicated *Listeria* phages were

titrated in ten-fold serial dilutions (black spots) on lawns of *Lmo*10403s (gray background) lacking Cas9 and encoding AcrIIA1^{NTD} (*Δcas9;IIA1^{NTD}*) or not (*Δcas9*). Dashed lines indicate where intervening rows were removed for clarity. Right: Cas9-independent replication of isogenic ΦJ0161a or ΦA006 phages in *Listeria*. Plaque forming units (PFUs) were quantified on *Lmo*10403s lacking *cas9* (*Δcas9*) and expressing AcrIIA1^{NTD} (black bars) or not (gray shaded bars). Data are displayed as the mean PFU/mL of at least three biological replicates ± SD (error bars). (B) Induction efficiency of ΦJ0161 prophages. Prophages were induced with mitomycin C from *Lmo*10403s::ΦJ0161 lysogens expressing *cis-acrIIA1* from the prophage Acr locus (WT) or not (ΔIIA1-2) and *trans-acrIIA1* from the bacterial host genome (+) or not (–). Plaque forming units (PFUs) were quantified on *Lmo*10403s lacking *cas9* and expressing AcrIIA1^{NTD} (*Δcas9;IIA1^{NTD}*). Data are displayed as the mean PFU/mL after prophage induction of four biological replicates ± SD (error bars). (C) Alignment of the phage anti-CRISPR promoter nucleotide sequences denoting the -35 and -10 elements (gray boxes) and conserved palindromic sequence (yellow highlight). Terminal palindrome mutations (red letters) were introduced for the binding assay in (D). See Figure 2-S4A for a complete alignment of the promoters. (D) Quantification of the binding affinity (K_D; boxed inset) of AcrIIA1 for the palindromic sequence within the *acr* promoter using microscale thermophoresis. ND indicates no binding detected. Data shown are representative of three independent experiments. (E) Expression of RFP transcriptional reporters containing the wild-type (left) or mutated (right) ΦA006-Acr-promoter in the presence of AcrIIA1 (IIA1) or each domain (IIA1^{NTD} or IIA1^{CTD}). Representative images of three biological replicates are shown. (F and H-I) Repression of RFP transcriptional reporters containing the ΦA006-Acr-promoter (black bars in F; gray bars in H) or the cognate-AcrIIA1-homolog-promoters (black bars in H and I) by AcrIIA1$_{ΦA006}$ (mutants in F; wild-type in I) or AcrIIA1 homolog (H) proteins. Data are shown as the mean percentage RFP repression in the presence of the indicated AcrIIA1 variants relative to controls lacking AcrIIA1 of at least three biological replicates ± SD (error bars). The percent protein sequence identities of each homolog to the ΦA006 AcrIIA1^{NTD} are listed in (H). (G) Immunoblots detecting FLAG-tagged LmoCas9 protein and a non-specific (ns) protein loading control in *Lmo*10403s::ΦJ0161a lysogens or non-lyosgenic strains containing plasmids expressing AcrIIA1 (IIA1) or AcrIIA1^{NTD} (IIA1^{NTD}). Dashed lines indicate where intervening lanes were removed for clarity. Representative blots of at least three biological replicates are shown.

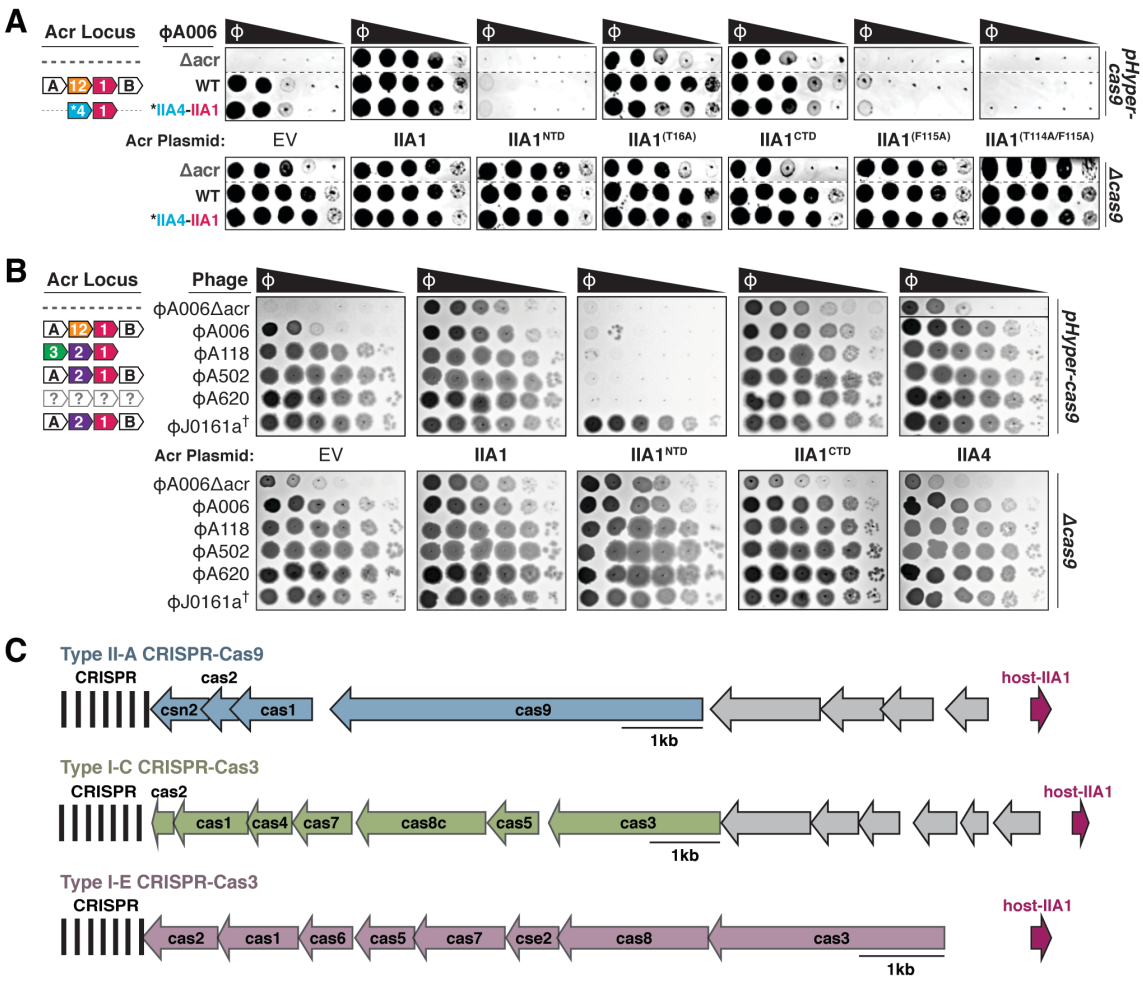

Figure 2-5. AcrIIA1^{NTD} Encoded from a Bacterial Host Displays "anti-anti-CRISPR" Activity

(A-B) Plaquing assays where engineered (A) or wild-type (B) *L. monocytogenes* phages are titrated in ten-fold dilutions (black spots) on lawns of *L. monocytogenes* (gray background) expressing anti-CRISPRs from plasmids, LmoCas9 from a strong promoter (*pHyper-cas9*) or lacking Cas9 (*Δcas)*, and the natural CRISPR array containing spacers with complete or partial matches to the DNA of each phage. (†) Denotes the absence of a spacer targeting the ΦJ0161a phage. Representative pictures of at least 3 biological replicates are shown. Dashed lines indicate where intervening rows were removed for clarity (A). Solid lines indicate where separate images are shown. (C) Schematic of bacterial (host) AcrIIA1^{NTD} homologs encoded next to Type II-A, I-C, and I-E CRISPR-Cas loci in *Lactobacillus delbrueckii* strains.

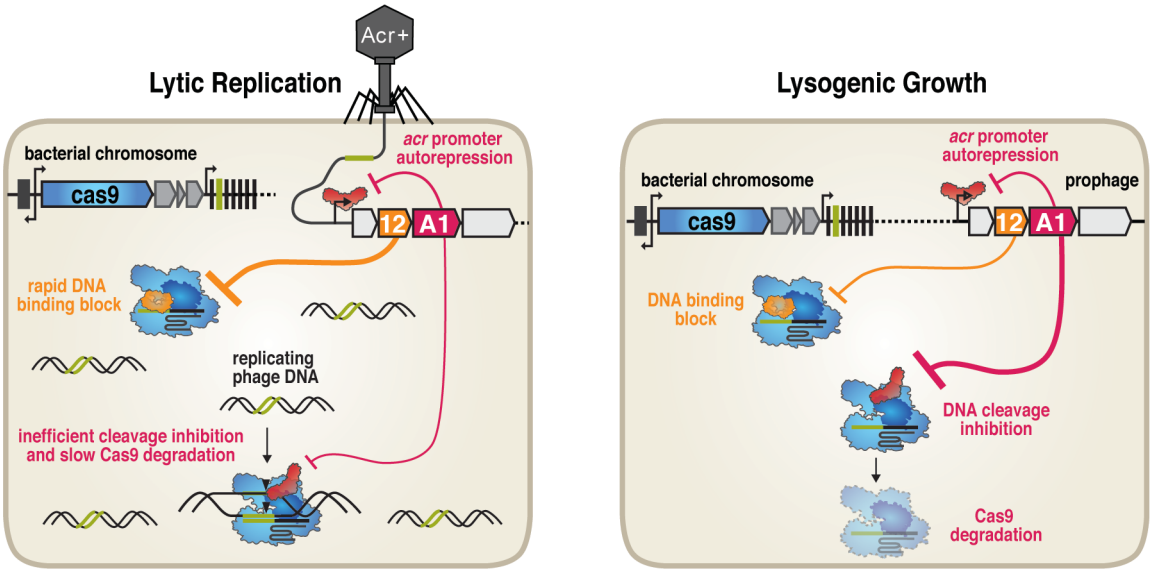

Figure 2-6. Model for *Listeria* Phage Anti-CRISPR Functions in Lysogenic & Lytic Growth

Listeria temperate phages encode the multifunctional AcrIIA1 (red) for protection against CRISPR-Cas in lysogeny (AcrIIA1^{CTD}) and autorepression of anti-CRISPR transcription (AcrIIA1^{NTD}). In lysogeny (right), AcrIIA1 binds the Cas9 HNH domain (dark blue in Cas9) to prevent DNA cleavage and triggers Cas9 degradation. For replication in lytic growth (left), AcrIIA1 is slow or inefficient, thus a distinct coexisting anti-Cas9 protein (like AcrIIA12, orange) is necessary to rapidly inactivate Cas9.

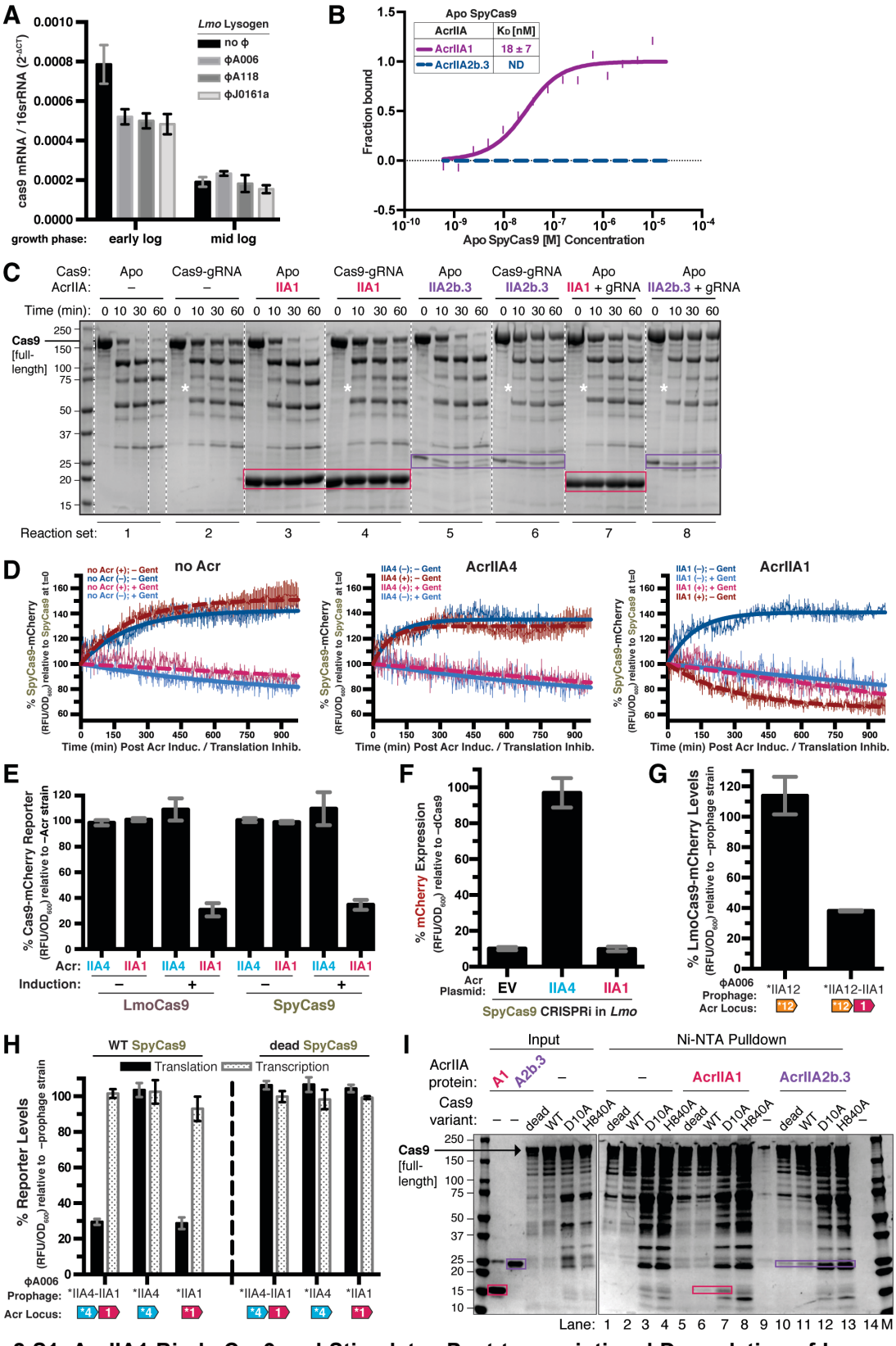

Figure 2-S1. AcrIIA1 Binds Cas9 and Stimulates Post-transcriptional Degradation of Lmo and Spy Cas9 in *Listeria*, Related to Figure 2-1

(A) Cas9 mRNA levels of *Lmo*10403s lysogens containing the indicated prophages during early

or mid-logarithmic growth as quantified by qRT-PCR. Transcript measurements were conducted in technical triplicate and data are shown as the mean $2^{-\Delta CT}$ values normalized to the 16S rRNA endogenous control gene ± SD (error bars). (B) Quantification of the binding affinities (K_D; boxed inset) of AcrIIA1 and AcrIIA2b.3 for Apo SpyCas9 using microscale thermophoresis. ND indicates no binding was detected. Data shown are representative of three independent experiments. (C) Limited α-chymotrypsin proteolysis of SpyCas9-Acr complexes. Proteolysis of Apo SpyCas9 (set 1) or SpyCas9-gRNA (set 2) without anti-CRISPR (–) or in the presence of AcrIIA1 (sets 3, 4, 7; magenta boxes) or AcrIIA2b.3 (sets 5, 6, 8; purple boxes). For reaction sets 7 and 8, Apo Cas9 was first incubated with anti-CRISPR followed by addition of gRNA. (*) Denotes a proteolysis product that appears in all Cas9-gRNA reactions but not Apo Cas9 reactions. Dashed lines indicate where intervening lanes were removed for clarity. (D) SpyCas9-mCherry protein levels post anti-CRISPR induction or translation inhibition. *Lmo*10403s strains expressing SpyCas9-mCherry from the constitutively active pHyper promoter and AcrIIA1 or AcrIIA4 from an inducible promoter were grown to mid-logarithmic phase and treated with 100 mM rhamnose to induce Acr expression (+, thick dashed lines) or 100 mM glycerol as a neutral carbon source control (–, thick solid lines) and 5 µg/mL gentamicin (Gent) to inhibit translation (+) or water (–) as a control. SpyCas9-mCherry protein measurements reflect the mean percentage fluorescence (RFUs normalized to OD_{600}) relative to the SpyCas9-mCherry levels at the time (0 min) translation inhibition was initiated (thin solid lines). Error bars (vertical lines) represent the mean ± SD of at least three biological replicates. Data were fitted by nonlinear regression to generate best-fit decay curves (thick lines). (E) Lmo or Spy Cas9-mCherry protein levels (black bars) in *Lmo*10403s expressing Lmo or Spy Cas9-mCherry from the constitutively active pHyper promoter and AcrIIA1 or AcrIIA4 from an inducible promoter. Cas9-mCherry measurements reflect the mean percentage mCherry (RFU normalized to OD_{600}) in cells treated with 100 mM rhamnose (+, induced Acr expression) or 100 mM glycerol (–, non-induced Acr expression), relative to a control strain lacking an anti-CRISPR (–Acr). Error bars represent the mean ± SD of at least three biological replicates. (F) Anti-CRISPR inhibition of CRISPRi in a *Listeria Lmo*10403s strain containing a chromosomally-integrated construct expressing dead SpyCas9 from the inducible pRha-promoter and a sgRNA that targets the pHelp-promoter driving mCherry expression. mCherry expression measurements reflect the mean percentage fluorescence (RFU normalized to OD_{600}) in deadCas9-induced cells relative to uninduced (–dCas9) controls of three biological replicates ± SD (error bars). (G) Catalytically active LmoCas9-mCherry protein levels in *Lmo*10403s lysogenized with isogenic ΦA006 prophages encoding AcrIIA12 alone or in combination with AcrIIA1. LmoCas9-mCherry (black bars) measurements reflect the mean percentage mCherry (RFUs normalized to OD_{600}) in the indicated lysogens relative to the control strain lacking a prophage (–prophage). Error bars represent the mean ± SD of at least three biological replicates. (*) Indicates the native orfA RBS (strong) in ΦA006 was used for Acr expression. (H) Translational (black bars) and transcriptional (gray shaded bars) reporter levels of catalytically active and dead SpyCas9 in *Lmo*10403s lysogenized with isogenic ΦA006 prophages encoding the indicated anti-CRISPRs. Measurements were normalized and graphed as in (G) with error bars representing the mean ± SD of at least three biological replicates. (*) Indicates the native orfA RBS (strong) in ΦA006 was used for Acr expression. (I) Differential interactions of SpyCas9 nickases with AcrIIA1. Partially purified 6xHis-tagged SpyCas9 (WT, dead, D10A, H840A) proteins (input) were incubated with 2-fold molar excess gRNA and subjected to Ni-NTA pull-down in the presence or absence (lanes 1-4; –) 6-fold molar excess AcrIIA1 (lanes 5-8) or AcrIIA2b.3 (lanes 10-13). AcrIIA1 (magenta boxes) co-purifies with WT and D10A (lanes 6 and 7) but not dead and H840A Cas9-gRNA (lanes 5 and 8). AcrIIA2b.3 (purple boxes) co-purifies with all four Cas9-gRNA complexes (lanes 10-13). AcrIIA1 and A2b.3 were incubated with Ni-NTA beads in the absence of Cas9-gRNA to test for non-specific binding to Ni-NTA beads (lanes 9 and 14).

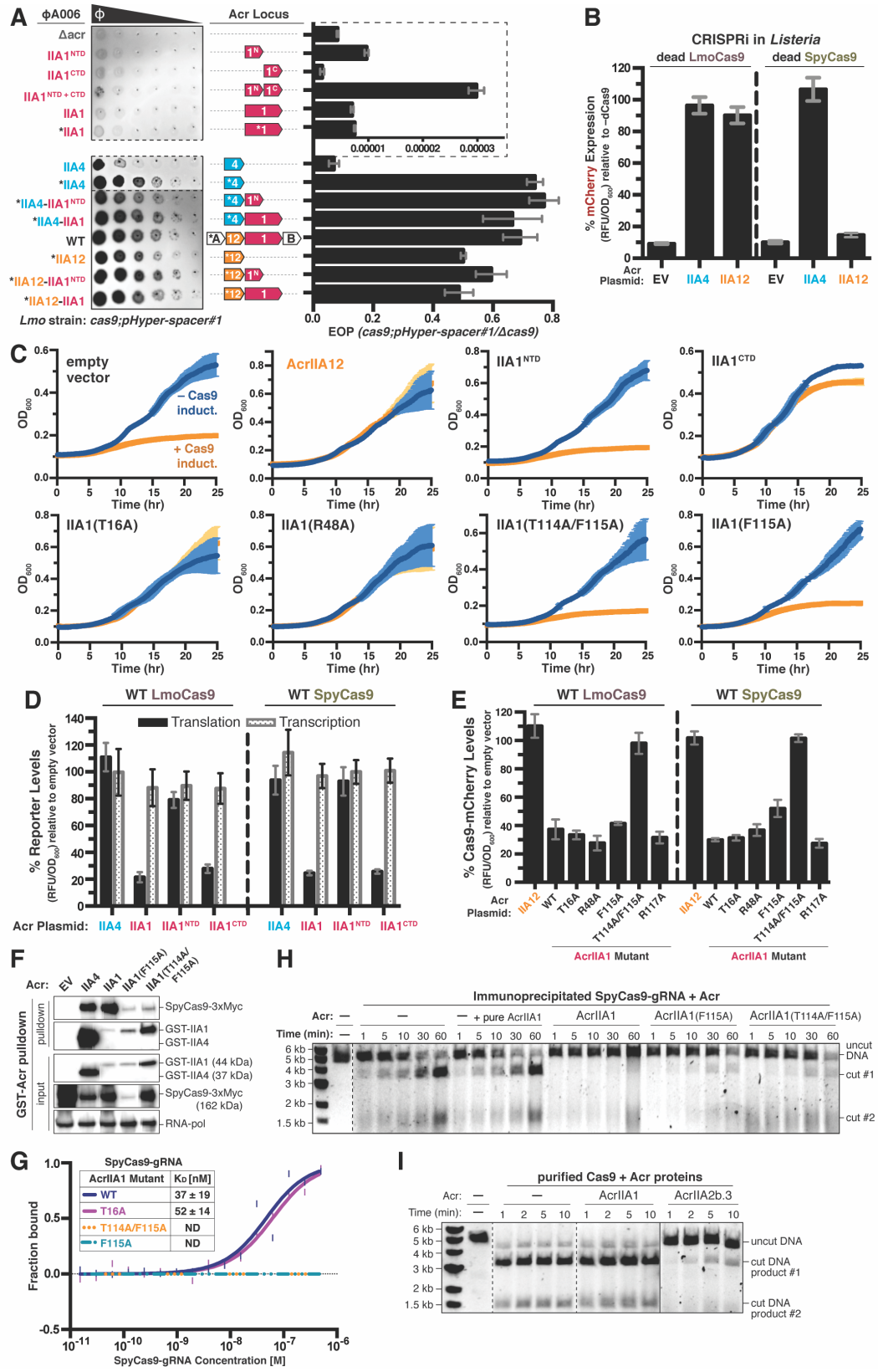

Figure 2-S2. AcrIIA1^{CTD} Mutants Cannot Bind Cas9 or Trigger its Degradation, Related to Fig 2-2
(A) Left: Representative image of plaquing assays where isogenic ΦA006 phages are titrated in

ten-fold serial dilutions (black spots) on a lawn of *Lmo*10403s (gray background). Dashed lines indicate where intervening rows were removed for clarity. Right: Efficiency of plaquing (EOP) of isogenic ΦA006 phages (expressing the indicated anti-CRISPRs) on *Lmo*10403s. Plaque forming units (PFUs) were quantified on *Lmo*10403s overexpressing the first spacer in the native CRISPR array that targets ΦA006 (*cas9;pHyper-spacer#1*) and normalized to the number of PFUs measured on a non-targeting *Lmo*10403s-derived strain (*Δcas9*). The dashed lines boxing the first 6 phages show a zoomed in view of the graph with a distinct x-axis scale. Data are displayed as the mean EOP of at least three biological replicates ± SD (error bars). Note that this figure contains the same subset of data displayed in Figure 2-2A. (B) AcrIIA12 anti-CRISPR activity in a *Lmo*10403s CRISPRi strain expressing Lmo or Spy deadCas9 from the inducible pRha-promoter and a sgRNA that targets the pHelp-promoter driving mCherry expression. mCherry expression measurements reflect the mean percentage RFU in deadCas9-induced cells relative to uninduced (–dCas9) controls of three biological replicates ± SD (error bars). Note that AcrIIA12 inhibits Lmo but not Spy deadCas9-based CRISPRi, indicating its specificity against LmoCas9. (C) Anti-CRISPR activity in *Lmo*10403s self-targeting strains containing chromosomally-integrated constructs expressing LmoCas9 from the inducible pRha-promoter and a sgRNA that targets the pHelp promoter driving mCherry expression. Bacterial growth was monitored after LmoCas9 induction (orange lines) or no induction (blue lines) and data are displayed as the mean OD_{600} of at least three biological replicates ± SD (error bars). (D) Translational (black bars) and transcriptional (gray shaded bars) reporter levels of catalytically active Lmo and Spy Cas9 in *Lmo*10403s containing plasmids expressing anti-CRISPRs. Reporter measurements reflect the mean percentage mCherry (RFU normalized to OD_{600}) in the presence of the indicated anti-CRISPRs relative to the control strain containing an empty vector of three biological replicates ± SD (error bars). (E) Catalytically active Lmo and Spy Cas9-mCherry protein levels in *Lmo*10403s containing plasmids expressing anti-CRISPRs. Cas9-mCherry measurements (black bars) reflect the mean percentage mCherry (RFU normalized to OD_{600}) in the presence of the indicated anti-CRISPRs relative to the control strain containing an empty vector of three biological replicates ± SD (error bars). (F) Immunoblots detecting 3xMyc-tagged SpyCas9 protein that co-immunoprecipitated with GST-tagged anti-CRISPR proteins in a *P. aeruginosa* strain heterologously expressing the Type II-A SpyCas9-gRNA system and the indicated Acrs. For input samples, one-hundredth lysate volume was analyzed to verify tagged protein expression and RNA-polymerase was used as a loading control. Representative blots of at least three biological replicates are shown. (G) Quantification of the binding affinities (K_D; boxed inset) of WT and mutant AcrIIA1 proteins with SpyCas9-gRNA using microscale thermophoresis. ND indicates no binding detected. Data shown are representative of three independent experiments. (H-I) Time courses of SpyCas9 DNA cleavage reactions in the presence of the indicated anti-CRISPR proteins conducted with SpyCas9-gRNA-Acr complexes immunoprecipitated from *P. aeruginosa* (H) or recombinant proteins purified from *E. coli* (I). Where indicated, the reaction with SpyCas9-gRNA immunoprecipitated without an Acr (–) was supplemented with recombinant WT AcrIIA1 protein purified from *E. coli* (+ pure AcrIIA1) (H). Dashed lines indicate where intervening lanes were removed for clarity. Solid lines indicate a separate image. Data shown are representative of three independent experiments.

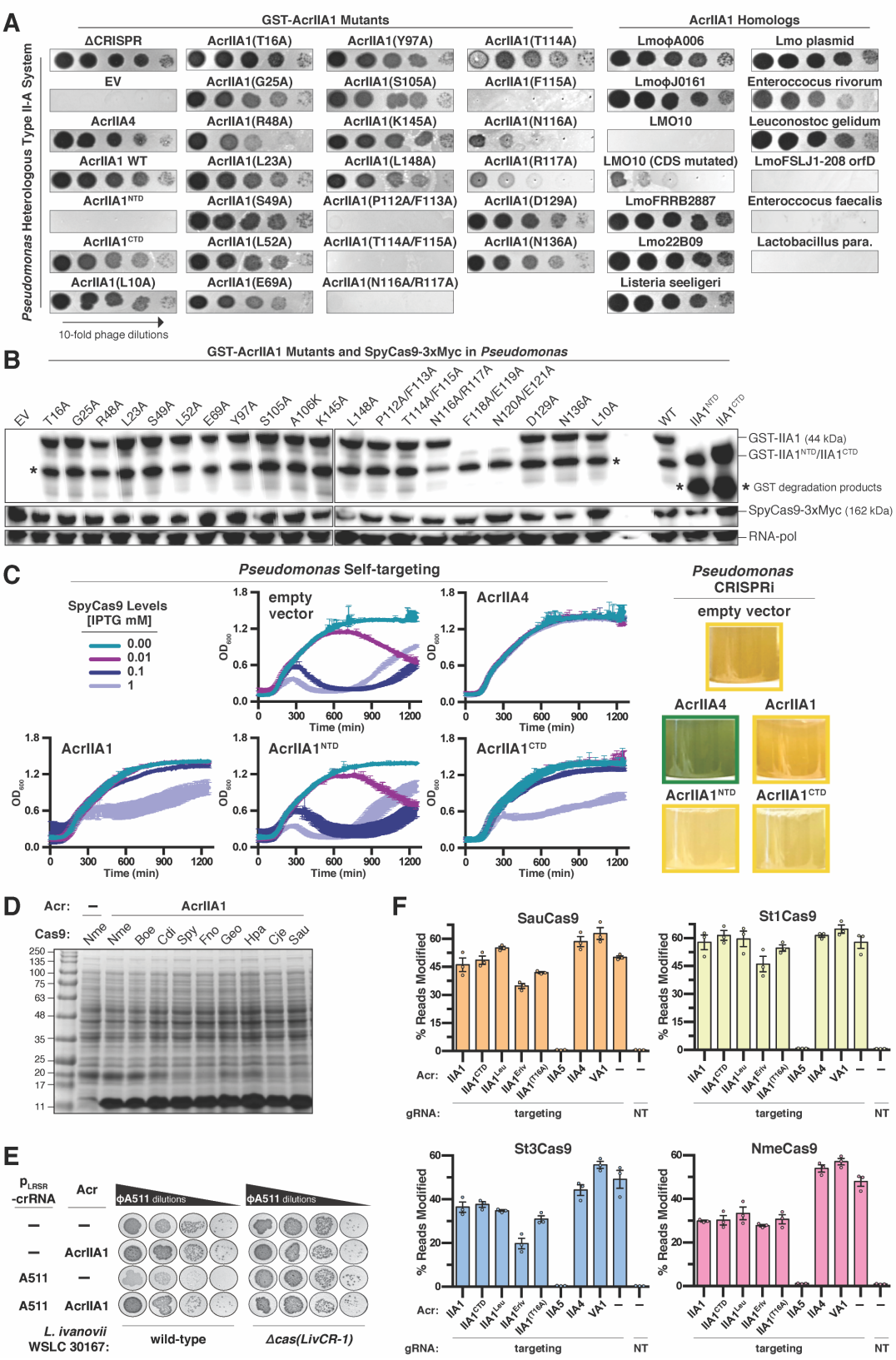

Figure 2-S3. AcrIIA1 Inhibition of Cas9 Orthologues in Heterologous Hosts, Related to Fig 2-2–2-3
(A) Plaquing assays where the *P. aeruginosa* DMS3m-like phage is titrated in ten-fold dilutions

(black spots) on a lawn of *P. aeruginosa* (gray background) expressing the indicated anti-CRISPR proteins and Type II-A SpyCas9-sgRNA programmed to target phage DNA. Representative pictures of at least 3 biological replicates are shown. (B) Immunoblots detecting GST-tagged AcrIIA1 (mutants or individual domains) proteins, Myc-tagged SpyCas9 protein, and RNA-polymerase as a protein loading control in a *P. aeruginosa* strain heterologously expressing the Type II-A SpyCas9-gRNA system and the indicated Acrs. (*) Denotes GST degradation products derived from GST-tagged Acr proteins. AcrIIA1 mutants that failed to express were not analyzed further. (C) Anti-CRISPR activity in *P. aeruginosa* self-targeting (left) and CRISPRi (right) strains containing plasmids expressing anti-CRISPRs and chromosomally-integrated SpyCas9-sgRNA programmed to target the *phZM* gene promoter. For self targeting, SpyCas9 expression from the inducible pLAC-promoter was titrated using the indicated IPTG concentrations (mM) and bacterial growth curves display the mean OD_{600} of at least three biological replicates ± SD (error bars) measured over time (left). CRISPRi was qualitatively assessed by inspecting the culture pigment. Transcriptional repression of the *phzM* gene by dCas9 generates a yellow culture whereas inhibition of dCas9 (e.g. by an Acr) allows *phzM* expression and pyocyanin production that generates a green culture. Representative pictures of at least three biological replicates are shown (right). (D) SDS-PAGE and Coomassie Blue staining analysis of AcrIIA1 expression after IPTG induction in *E. coli* strains containing the indicated Cas9 orthologues. (E) Plaquing assays where the *Listeria* phage ΦA511 is titrated in ten-fold serial dilutions (black spots) on lawns of the *Listeria ivanovii* WSLC 30167 (gray background) strain with an endogenous Type II-A LivCas9 system or lacking this system (*Δcas*), plasmid-expressed AcrIIA1 or no Acr (–), and crRNA that targets ΦA511 phage DNA or a non-targeting control (–) expressed from the pLRSR plasmid. (F) Gene editing activities of Cas9 orthologues in human cells in the presence of AcrIIA1 variants and orthologues. AcrIIA4 is a known selective inhibitor of SpyCas9, AcrIIA5 is a broad-spectrum inhibitor (Garcia et al., 2019, *in revision*), and AcrVA1 as a known non-inhibiting control for SpyCas9 orthologues. NT, no-sgRNA control condition. Error bars indicate SEM for three independent biological replicates.

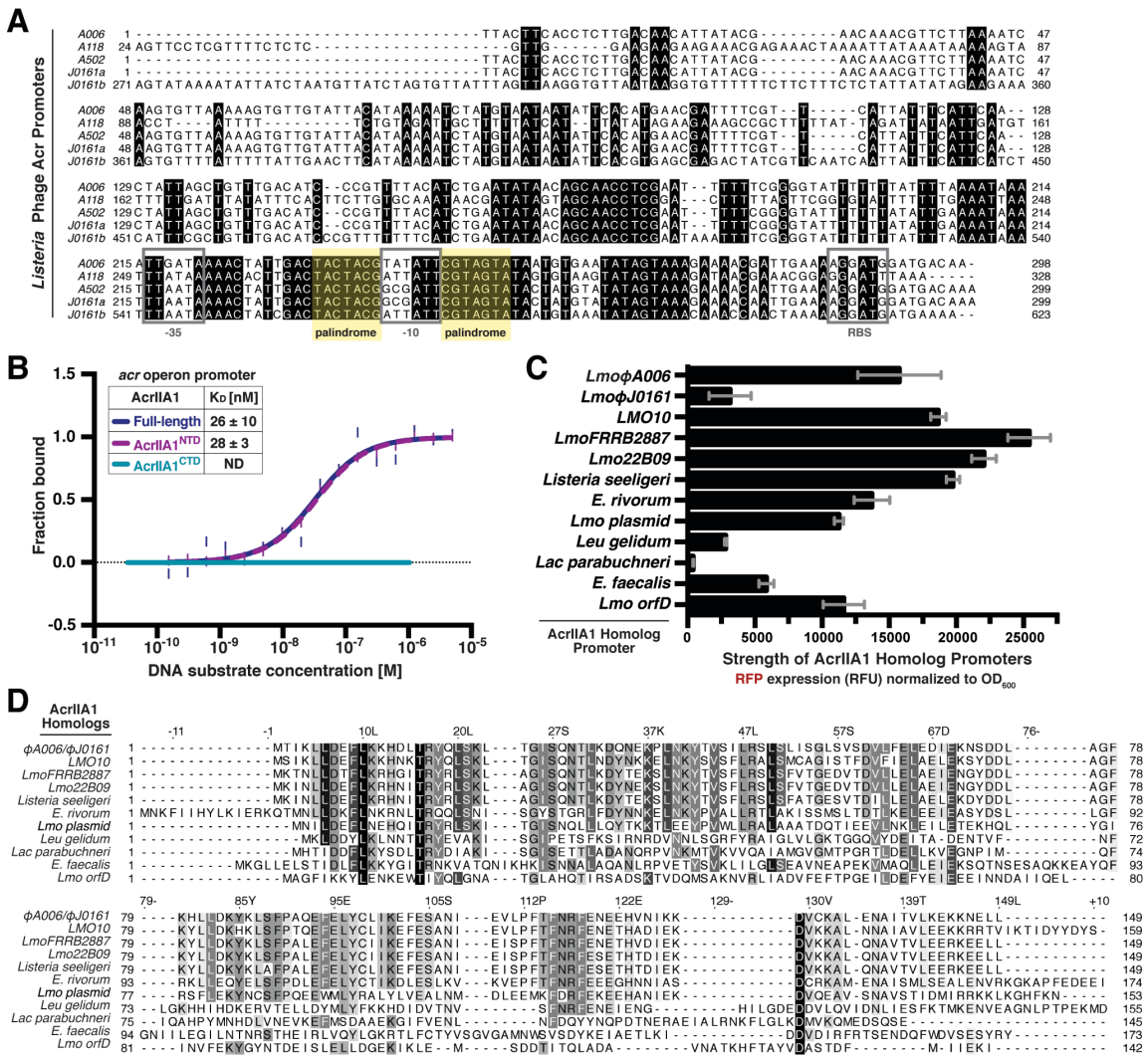

Figure 2-S4. Acr Promoters in Mobile Genetic Elements Across the *Firmicutes* Phylum are Autoregulated by AcrIIA1 Homologs, Related to Figures 2-2 and 2-4

(A) Alignment of the phage anti-CRISPR promoter nucleotide sequences denoting the -35 and -10 elements and ribosomal binding site (RBS) (gray boxes) and conserved palindromic sequence (yellow highlight). (B) Quantification of DNA binding abilities (K_D; boxed inset) of full-length AcrIIA1 and each domain ($AcrIIA1^{NTD}$ and $AcrIIA1^{CTD}$) using microscale thermophoresis. Data shown are representative of three independent experiments. ND indicates no binding detected. (C) Expression strength of the AcrIIA1 homolog promoters. Data are shown as the mean RFP expression (RFU normalized to OD_{600}) driven by each AcrIIA1 homolog promoter of at least three biological replicates ± SD (error bars). (D) Alignment of AcrIIA1 homolog protein sequences.

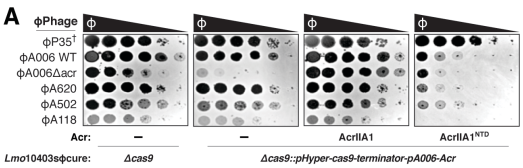

Figure 2-S5. Bacterial expression of AcrIIA1^{NTD} blocks phage anti-CRISPR deployment, Related to Figure 2-5

(A) Plaquing assays where wild-type *L. monocytogenes* phages are titrated in ten-fold dilutions (black spots) on lawns of *L. monocytogenes* (gray background) containing single-copy integrated constructs expressing AcrIIA1 or AcrIIA1^{NTD} from the ΦA006 anti-CRISPR promoter (pA006), LmoCas9 from a constitutive promoter (pHyper-Cas9), and the natural CRISPR array containing spacers with complete or partial matches to the DNA of each phage. (†) Denotes the absence of a spacer targeting the virulent phage ΦP35. Representative pictures of at least 3 biological replicates are shown.

Table 2-S1. AcrIIA1 homolog protein accession numbers and associated promoter sequences

Strains Containing AcrIIA1 Homologs	Designated Homolog Name	Protein Accession #	Associated Promoter Sequence (5' to 3')
Listeria monocytogenes J0161	LmoϕA006/ ϕJ0161	WP_003722518.1	tttacttcacctcttgacaacattatacgaacaaacgttcttaaaatcaagtgttaaaaagtgtt gtattacataaaaatctatgtaataatattcacatgaacgattttcgttcattatttcattcaactatt agctgtttgacatcccgttttacatctgaatataacagcaacctcgaatttttcggggtatttttttat attgaaaataaatttaataaaaactattgactactacggcgattcgtagtatactatgtatatagt aaagaaaacaattgaaaaggatggatgacaaa
Listeria monocytogenes strain LMO10	LMO10	KUG37233.1	ttttgttgacgctttcacaaagacatgttattatatattcaagaacttaataagttctagcgctgttt cggcgcgttttaattacgcattgtgcaatgtaaatttctatgtatttaattttatttagcacgaaaag aagctacaaattttaactacttactatgaaatgtaaggaaaaaaacatcagacttcggtttgat gttttttactgtaaaaaaattaatccaataaaaaccattgactactacgattattcgtagtataat atgtatatagtaaaggaacgggaggaaaataca
Listeria monocytogenes strain FRRB 2887	LmoFRRB2887	WP_085696370.1	aataaaaagtaacctgtttttctatagattgctttttatcatatatatagaagaaagccgcttttatt agattataattgatgtttttgatttatatttcactccctgtgcaaataacgatatagtagcaacctc gaacttttttgttcggggtatttttttgaaattaatttataaaaacactgactactacgaatttacgt agtatactttaaatatagtaaagataacgaaacggaggaacttaaaa
Listeria monocytogenes isolate 22B09	Lmo22B09	WP_077316628.1	ttttatcagttatttttaaaaaaggttatctttcgtaaaacgcctatatgtagccgttttatagatagat agccttttttctttctgtttgaatcggtatattccagaaaagttttgccacgaatttgccacaaaattt gccgttgaataattctttataaatatagtagtgcctcggactttatggttcggggtatttttttgaaat taatttataaaaacacttgactactacgaatttacgtagtatactttaaatatagtaaagataac gaaacggaggaacttaaaa
Listeria seeligeri FSL S4-171	Listeria seeligeri	EFS02359.1	ttgaaatgatgtacacgaacttgttcgctttagtagaaatagaccctcgcgacgaaaaaaga tattacttttccgacttaactcgtgatgaagtatttacaatgctgcaaaatatcaaaaataaata atgaatatagttgactaatacgaaaaatcgtagtatactgtgtatatagtaaagaaacgggaa ggagcttaaaa
Enterococcus rivorum strain LMG 258993	E. rivorum	WP_069698591.1	tgttcgtatttaggactataccgtaaaatttcgtacaactgatctggagataatcgcttattaaat gagaagattataataataaaaattgaaaacgttgatttaacagagttttcaaaaaaatataag aaaatataccgtaaaatttcgttccactgatacgtggaccccaaaaattgaagtaaattgag cgaaactcttgatttcttccgatttcggaagtataatagtgttataaggttgggataaggaaata gcacttccgcttaatcttaaataaattaaaagaggatgaatgaa
Listeria monocytogenes CFSAN026587 plasmid	Lmo plasmid	WP_061665673.1	aacttacaatagtataggagcgttgctaatcattgctgtatgcttaaagaagtgcagatttaaa attagatatctttataacttattaaattatagttgactattaaattatatatttagtataataaaggtat agagataagacataaaaatagaacaaatgaggtgcaatgac
Leuconostoc gelidum subsp. gasicomitatum KG16-1	Leu gelidum	CUR63869.1	tattattttccctctaaaataatagtacgtattaaacaagatgaactcttaatgttatttgccattag atataactgtaacacaatcgtaacattaatctattgcacactgcttaattaagcggtatacttaa ttcaaggttaaggaagaggtaaacgac
Lactobacillus parabuchneri strain FAM23166	Lac parabuchneri	WP_084975236.1	aacccctgtatagcataaaggttgcaatcctgccgagtgcataatcgcggtaaatcatcgat tccgcatattcgttaatgtgatgcctccagtctctttagatgagagattggaggcatttttgcttttt aaaaaccgatgttttatattgcatacttcgctgtaacgtagtaatattttaaaacatgaagttgcg acacacagttaacttcgttattatttaacagtaaattcatggaggaaaaaca
Enterococcus faecalis strain plasmid Efsorialis-p2	E. faecalis	WP_002401838.1	ctaccataagttactgatagaaaagaaccaacagagtatgcctgttggttcttttctttgtccag ttgttaccaggtcagtagtaggacattcaaattgggcatacgtcatttgtgttaattttgagtacg ctttaaatttacatgtaatgaataaagtaatgggtattcgttttccactaactggccaaacagat agataggtgaagaacaaatttaacgcaaatggtaatgattgtgtttacatttaccttatatgtga tataatataagtgtaatcaaagaagcctactcttgaaaattcaagaataggcaggtcgctaa acctctttgattataccatatatcaaaggaagaaggaatgaaa
Listeria monocytogenes SLCC2540, serotype 3b	Lmo orfD	WP_012951927.1	acaaagaacatgcaaattatttaaaaagccgttcagctgcgcgatcttttattaagaaaaaa gccacttagaagacttggaagaactagaaattgcagtaaagcaaagaaaaactgaaata atttcattagacaatagccctgaatgaaaaatttcggggcatttttttattttataatcaaatataa ttgactaatcaaatatatcgtgttatactatatatagtaaagaaacgggaggcgtacata
Lactobacillus delbrueckii strains	*L. delbrueckii*	OOV09772.1	not applicable; AcrIIA1^{NTD} homolog in core bacterial genomes found next to Type I-E, I-C, or II-A CRISPR-Cas systems

Publishing Agreement

It is the policy of the University to encourage the distribution of all theses, dissertations, and manuscripts. Copies of all UCSF theses, dissertations, and manuscripts will be routed to the library via the Graduate Division. The library will make all theses, dissertations, and manuscripts accessible to the public and will preserve these to the best of their abilities, in perpetuity.

Please sign the following statement:

I hereby grant permission to the Graduate Division of the University of California, San Francisco to release copies of my thesis, dissertation, or manuscript to the Campus Library to provide access and preservation, in whole or in part, in perpetuity.

DocuSigned by:
36A053876B55448...

Author Signature

11/8/2019

Date